Comparison of methods to determine the carbonation depth in fly ash blended cement mortars

by:

Ricardo Herrera

A thesis presented to Lakehead University

in fulfillment of the

thesis requirement for the degree of

Master of Science in

Environmental Engineering

Thunder Bay, Ontario, Canada, 2011

I hereby declare that I am the sole author of this thesis. This is the true copy of the thesis, including any required final revisions, as accepted by my examiners.

I understand that my thesis may be made electronically available to the public.

Abstract

Carbonation negatively affects the durability of steel-reinforced concrete structures by causing a decrease in pore solution pH, thus facilitating corrosion which eventually leads to cracking and spalling. Different analytical methods for assessing carbonation depth were compared on carbonated cement mortar samples, including blended samples in which up to 40% of the ordinary portland cement (OPC) were substituted by Type C coal fly ash (FA). The methods included the measurement of $CaCO_3$ concentrations by FTIR, the dust digestion method which provided an apparent pH profile, the traditional phenolphthalein method, and computerized image-processing methods based on the use of different pH indicators (thymolphthalein, phenolphthalein, and alizarin) or changes in mortar colour due to carbonation. The traditional phenolphthalein method, which measures the average advancement of the carbonation front, significantly underestimated the carbonation depth when compared with the FTIR, dust digestion, and all the image-processing methods, which measure the maximum advancement of the carbonation front. The dust digestion method provided carbonation depths which were essentially equivalent to those provided by the FTIR method. The diffusion-limited unreacted core model generally fitted well the carbonation depth versus time data measured by all analytical methods. When used in conjunction with the model, all analytical methods, except the traditional phenolphthalein method, gave consistent estimates of the times required for total sample carbonation. By contrast, the traditional phenolphthalein method significantly underestimated times for total carbonation. Partial replacement of cement by FA caused the carbonation front to advance faster and decreased the time required for complete carbonation of the mortar samples.

Acknowledgements

I would like to thank my supervisor, Dr. Lionel J.J. Catalan, for his support and guidance. He gave me the opportunity to join the Master's program in Environmental Engineering which has been, undoubtedly, one of the best experiences of my entire life. There are no words to describe the gratitude I have for him.

Also, I want to acknowledge Dr. Stephen D. Kinrade, my co-supervisor, for the ideas that enriched the content of this work.

The experimental part of this project would not have been possible to complete without the training and help kindly provided by the staff of both the Instrumentation and the Geology laboratories: Mr. Allan MacKenzie, Mr Ain Raitsakas, Mr. Keith Pringnitz, Mr Grzegorz Kepka, Dr. Shannon Zurevinski and Ms. Anne Hammond.

Similarly, I would like to thank Mr. Garry Rathje for his hard work and warm personality.

I deeply appreciate the advice, contributions and moral support made by my classmates and lab mates. Among them, Andrea Johnson, Jatin Sharma, Chadi Badour, Jaclyn Donald, Daniel Hamilton, Bhishan Pandey and Hassan HajiEsmaeili.

Finally, I want to thank my beloved family who, regardless of the distance, has always been there for me. I appreciate the huge sacrifices they have made to support my journey and the trust that they have put on me. I have been blessed to have such a loving supportive family. Mom and Dad, this is for you.

Table of Contents

Declaration..... ii

Abstract..... iii

Acknowledgements..... iv

Table of Contents..... v

List of Figures..... viii

List of Tables..... x

Glossary..... xi

1. Introduction..... 1

1.1 Steel Corrosion in Concrete Structures..... 1

1.2 The Traditional Phenolphthalein Method..... 1

1.3 The FTIR Method..... 2

1.4 The Dust Digestion Method..... 2

1.5 The Effect of Cement Replacement by Fly Ash..... 2

1.6 Models to Describe the Advancement of the Carbonation Front..... 3

1.7 Opportunities for Further Studies and Research Objectives 4

2. Materials and Methods..... 5

2.1 Materials 5

2.2 Preparation of Mortar Specimens..... 5

2.3 Carbonation of Mortar Samples 7

2.4 Measurement of Carbonation Depth 7

2.4.1 Fourier Transform Infrared Sprectroscopy (FTIR)..... 7

2.4.2 Dust Digestion (DD) Method ……..……..... 13

2.4.3 Traditional Phenolphthalein (Trad-P) Method ……... 14

2.4.4 Image Processing Methods...…… 15

3. Experimental Results and Discussion…....…… 19

3.1 Comparison of Analytical Methods……... 19

3.1.1 FTIR…....…… 19

3.1.2 Dust Digestion...…….…….. 20

3.1.3 Traditional Phenolphthalein Method…….……... 21

3.1.4 Image Processing Methods……... 23

4. Modeling the Advancement of the Carbonation Front…….……..... 29

5. Conclusions……... 34

6. References……. 35

Appendices…..……..….. 43

Appendix A Water Requirement Testing ……... 43

Appendix B Measurement of CO_2 Concentration in the Carbonation Chamber……. 45

B1 Gas Sampling…..……..……... 45

B2 GC Calibration Curve ……..……...…… 45

B3 Assessment of CO_2 vol%. Sample Calculations..……...……. 46

B4 Summary of GC Analyses Over Time.....……...……. 46

Appendix C FTIR Method……...…….…... 47

Appendix D Dust Digestion Method…..…….……. 79

D1 pH-meter Calibration…….…….. 79

D2 Environmental Conditions…..…….. 79

D3 Assessment of Carbonation Depth. Sample Calculations……..... 79

D4 Experimental Data….…….. 80

Appendix E Traditional Phenolphthalein Method (Trad-P)……...…….. 107

Appendix F Image Processing Methods…...….……... 108

F1 Image Processing Method on Unsprayed Samples (IM-U). Sample Calculations…….……... 108

F2 Image Processing Method for Phenolphthalein, Thymolphthalein and Alizarin pH Indicators……... 111

Appendix G Reaction-limited UR-core Model…….…. 113

G1 Model Equations…….. 113

G2 Calculation of τ…….…….…….. 113

List of Figures

Figure 2-1 Split mortar cylinders showing grooves from material removed by the drill press for the FTIR and dust digestion methods..…….…... 9

Figure 2-2 Diagram showing the consecutive steps of the powder collection method. Upper and front views…...……...……..... 10

Figure 2-3 Particle size distribution of a ground carbonated mortar sample……..……. 10

Figure 2-4 FTIR spectra of mortar, sand and pure $CaCO_3$ samples…….....…….. 11

Figure 2-5 Integration method for the two $CaCO_3$ peaks in FTIR spectra of carbonated mortar samples……...…….. 12

Figure 2-6 Variation of $CaCO_3$ concentration along the depth of a 7-day carbonated 20%-FA mortar sample….....……...……. 13

Figure 2-7 Apparent pH profile of a 21-day carbonated 20%-FA mortar sample..……. 14

Figure 2-8 Image of a carbonated split cylinder sprayed with thymolphthalein showing the rectangular area “a” considered for image analysis……... 17

Figure 2-9 Profiles of average pixel values along the direction parallel to the diameter of the carbonated sample sprayed with thymolphthalein ……..……. 17

Figure 2-10 Difference between blue and red average pixel values versus location along the direction parallel to the diameter of the carbonated sample sprayed with thymolphthalein shown in Figure 8.....……..... 18

Figure 3-1 Depth of carbonation determined by the FTIR method versus carbonation time for mortars having various substitutions by FA…… 19

Figure 3-2 Depths of carbonation determined by the DD method versus carbonation time for mortars having various cement substitutions by FA ……..... 20

Figure 3-3 Comparison between DD and FTIR carbonation depths……...……... 21

Figure 3-4 Depth of carbonation determined by the Trad-P method versus carbonation time for mortars having various cement substitutions by FA…. 23

Figure 3-5 Comparison between Trad-P and FTIR carbonation depths..…….... 23

Figure 3-6 Carbonation depths versus carbonation time determined by imaging methods…..…… 24

Figure 3-7 Comparison of carbonation depths determined by imaging and FTIR Methods…...……..... 27

Figure 4-1 Schematic showing the conceptual basis of the UR-core model ….……. 30

Figure 4-2 RHS of equation 2 versus time and best fit lines..……. 31

List of Tables

Table 2-1 Proportioning of mortar mixes…..…….…..…. 6

Table 3-1 Values of slope *s* and intercepts *i* of linear relationships between carbonation depths determined by various methods……...…… 28

Table 4-1 Estimated times for total carbonation using the diffusion-limited UR-Core Model…….……..……... 32

Glossary

Carbonation Reaction Compounds:

Calcium-silicate-hydrate (C-S-H)	$x\text{CaO}\cdot\text{SiO}_2\cdot n\text{H}_2\text{O}$
Calcium hydroxide (Portlandite)	Ca(OH)_2
Carbon dioxide	CO_2
Calcium carbonate	CaCO_3

Other Terms:

A	Alizarin pH indicator
ASTM	American Society for Testing and Materials
ATR	Attenuated Total Reflectance
DD	Dust digestion method
FA	Fly ash
FTIR	Fourier-transform infrared spectroscopy method
IM	Imaging method
OPC	Ordinary portland cement
P	Phenolphthalein pH indicator
RH	Relative humidity
τ	Time for total carbonation
T	Thymolphthalein pH indicator

Trad-P method	Traditional phenolphthalein pH indicator method
U	Unsprayed sample
UR-Core model	Unreacted-core model
w/c	Water/cement ratio

1. Introduction

1.1 Steel Corrosion in Concrete Structures

Among durability requirements, resistance to carbonation is especially important for steel-reinforced concrete. Corrosion of the commonly used steel reinforcement is normally inhibited because the protective oxide film on the surface of the steel is chemically stable in the usual, alkaline environment within concrete. However, the oxide film can be destroyed if the concrete pore solution becomes less alkaline. Calcium hydroxide, $Ca(OH_2)$, one of the main products of the hydration of cement, buffers the pH of the concrete pore solution and is consumed during the carbonation reaction with environmental carbon dioxide. As a result, the pH of pore solution drops from approximately 13 to less than 9. If the carbonation front reaches the reinforcement and there is adequate moisture present around the steel surface, then corrosion is likely to be initiated *(Parrot, 1990)*. When steel corrodes, the resulting rust occupies a greater volume than steel. The expansion creates tensile stresses in the concrete, which can eventually cause cracking and spalling *(Portland Cement Association, 2010)*. Spalling, in its most general form, is defined as the breaking off of layers or pieces of concrete from the surface of a structural element (Khoury and Anderberg, 2000).

1.2 The Traditional Phenolphthalein Method

The traditional method for assessing carbonation depth in hardened concrete is based on a visual inspection of a broken sample sprayed with the pH indicator phenolphthalein which gives a pink color to the surface area whose pore solution pH is higher than approximately pH 9, whereas the area whose pH is lower than 9 remains gray *(Chang and Chen, 2004; Anstice et al., 2005)*. The carbonation depth is determined by measuring the distance from the edge of the sample to the color boundary. It has been widely reported, however, that the phenolphthalein method significantly underestimates the

carbonation depth due to the presence of a partially carbonated zone which has a pore solution pH between 9 and 13 and is undetectable by this method *(Jung et al. 2004; Chang et al., 2004)*. Underestimating the carbonation depth can lead to an overestimation of the lifespan of concrete structures which contain steel reinforcements.

1.3 The FTIR Method

Fourier transform infrared spectroscopy (FTIR) can detect the $CaCO_3$ formed during the carbonation reaction by virtue of its two C-O bond characteristic absorption peaks at 1420 and 850 cm^{-1}. Previous studies have shown that FTIR is more sensitive than the phenolphthalein method for detecting the advancement of carbonation fronts *(Lo and Lee, 2002; Chang and Chen, 2006).* Because the FTIR method directly detects the carbonation product $CaCO_3$, it can be considered an accurate method for measuring carbonation depth and can provide early warnings of $CaCO_3$ formation. However, the main problem associated with the FTIR method is its high cost due to equipment and specialized training. Hence, more affordable methods to assess the carbonation depth are needed.

1.4 The Dust Digestion Method

The dust digestion method determines the apparent-pH profile of carbonated samples by assessing the pH of slurries made with powder collected from consecutive layers of the sample. The resulting pH profiles depend on both the type of binder and the duration of exposure to environmental CO_2. The dust digestion method is an inexpensive and simple method for establishing the effect of carbonation on concrete *(McPollin et al, 2007)*.

1.5 The Effect of Cement Replacement by Fly Ash

Fly ash (FA) is a finely divided residue from the combustion of pulverized coal in electric power generation plants (Kosmatka SH *et al.*, 2002). FA belongs to the class of pozzolan materials defined as siliceous or aluminosiliceous materials that, in finely divided form and in the presence of moisture, chemically react with the calcium hydroxide released by the hydration of portland cement to form calcium silicate hydrate (CSH) and other cementing compounds. FA is the most widely used supplementary cementing material in concrete. For blended concretes containing FA, the resistance to carbonation decreases as cement replacement by FA increases *(Papadakis, 2000; Burden, 2006)*. When cement is replaced by FA, the calcium hydroxide content of concrete is reduced due to the pozzolanic reaction, thereby reducing the pH buffering capacity of concrete and causing the carbonation front to advance faster. On the other hand, aggregate replacement by FA slows down carbonation because the total amount of carbonatable constituents (calcium hydroxide and CSH) remains approximately the same while permeability decreases. *(Papadakis, 2000; Bouzoubaa and Foo, 2005)*.

1.6 Models Describing the Advancement of the Carbonation Front

Modeling the carbonation process is relevant in terms of lifespan estimations for concrete structures. The advancement of the carbonation front is often described as a function of the square root of time: $D = C\ t^{0.5}$, where D is the carbonation depth, C is the carbonation coefficient and t is the period of exposure *(McPolin et al., 2007; Khunthongkeaw et al., 2006)*. Empirical exponents smaller than 0.5 (power model) have, however, been found to describe the process more accurately *(Sisomphon and Franke, 2007)*. More complex theoretical models such as the unreacted core model *(Levenspiel, 1999)* have been applied to the carbonation of concrete. Several studies found that the diffusion-limited unreacted core (UR-Core) model fits experimental data from a number of mortars relatively well including binders such as OPC and OPC-FA (*Bernal et al.,2010; Castellote and Andrade, 2008 and 2009).* A description of the UR-Core model is provided in Section 4.

1.7 Opportunities for Further Studies and Research Objectives

Previous studies have been published regarding the use of different pH indicators to assess the carbonation depth in concrete. *Jung et al. (2003)* conducted a field study on five different bridges in South Korea. They sprayed four different pH indicators (phenolphthalein, thymolphthalein, alizarin and tropaeolin) on core samples cut by means of an autodrill from different sections of the bridges. The results showed that pH indicators with a higher pH threshold detected larger carbonation depths. The carbonation depths ranged between 3.7 and 28.6 mm using phenolphthalein, between 6.6 and 32.5 mm using thymolphthalein, between 7.5 and 35.7 mm using alizarin, and between 8.3 and 39.2 mm using tropaeolin. No comparisons were made, however, with other analytical methods such as FTIR or dust digestion. The present work is the first to provide a thorough comparison between several pH indicator methods and other analytical methods.

To date, the visual inspection of samples sprayed with pH indicators has been done manually by using a ruler. Because the carbonation front is irregular, this technique requires averaging several carbonation depths measured at various locations and suffers from lack of precision and the possibility of human error. In this study, an imaging-based technique is used for the first time to deal with both issues. Moreover, because the carbonation reaction itself results in a slight colour change, the imaging technique can also be applied without the use of pH indicators.

Most of the previous studies on modeling of the advancement of the carbonation front in cement mortars have relied on the simplistic square-root or power models. In the present work, the diffusion-limited UR-Core model has been used to fit the time dependence of carbonation depths obtained by several methods and to estimate the times required for total carbonation of cylindrical mortar samples. The UR-Core model was selected because it accounts for the cylindrical geometry of our mortar samples, unlike the square-root or power model.

2. Materials and Methods

2.1 Materials

Ordinary portland cement (OPC) type 10 (Lafarge, Calgary, Alberta) was used in all mortar admixtures. All the cement used in this study was taken from the same bag, which was sealed in a plastic container after each use. All mortar samples were prepared within a period of 14 days. The Type C fly ash was derived from lignite coal and was provided by the Atikokan Generating Station (AGS), Atikokan, Ontario, Canada. A full characterization of this fly ash is given in Johnson et al. (2010). Graded sand (Hoskin Scientific, Burlington, Ontario) was used in all mortar samples and met the sieve passing requirements of ASTM C778 (2003). A detailed characterization of the sand is also provided in Johnson et al. (2010). Nanopure water (18.2 MΩ, Barnstead D11911 Nanopure Diamond) was used to prepare all mortar samples.

Three different pH indicators solutions were prepared: 0.2 wt% phenolphthalein; 0.5 wt% thymolphthalein; and 0.2 wt% alizarin. The transition pH ranges over which colour changes are 8.1–10.0 for phenolphthalein, 9.5–10.5 for thymolphtalein, and 11.1–12.4 for alizarin (*Zumdahl and Zumdahl, 2007*). All indicator solutions had an ethanol-water volume ratio of 70-30.

2.2 Preparation of Mortar Specimens

All mortar samples were prepared according to ASTM C109 (2003) using a five quart Hobart mixer (Hobart Corporation, Troy, Ohio). Three different mortar mixes were prepared containing 0%, 20% or 40% cement substitution by FA. Nanopure water was placed in the mixing bowl, followed by either OPC or a blend of OPC and FA. The mixture was mixed at slow speed for 30 seconds and at medium speed for another 30 seconds. Then, mixing was stopped for 90 seconds;

the first 15 seconds were used to scrape down the wall and base of the bowl to enhance homogeneity, and the admixture was left alone for the last 75 seconds. Next, mixing was resumed for 60 seconds at medium speed.

Flow table tests were performed according to ASTM C1437 (2003) to determine the amount of water needed to achieve constant consistency for the different mixes. Additional details on flow table testing are provided in Appendix A. Table 2-1 shows the proportions of OPC, FA, sand and water used in each mix. The water requirement decreased with increasing FA content because the lower reactivity of FA compared with cement results in more free residual water for flow. Moreover, the flow of mixes containing FA is enhanced by the spherical and smooth shape of fly ash particles, while cement particles have more angular shapes.

Table 2-1 Proportioning of mortar mixes

Mix	OPC (g)	FA (g)	Sand (g)	Water (g)
0% FA	500	0	1375	242
20% FA	400	100	1375	228
40% FA	300	200	1375	206

Immediately after mortar was prepared, it was placed in 2-in x 4-in cylindrical molds capped at the base. Molds were filled to one third of their height and then tamped 20 times to get rid of air bubbles. This step was repeated two more times until the mold was completely filled. Excess mortar was cut off from the top of the cylinder with a straight edge. The open molds were cured in a humidity chamber (ESL-3CA, ESPEC Corp., USA) for 24 hours at 23 °C and 100% relative humidity (RH). Then, the samples were demolded and submerged in saturated lime water for 27 days further curing at room temperature.

2.3 Carbonation of Mortar Samples

After 28 days of curing, the mortar cylinders were put in a sealed chamber and exposed to a controlled environment of 50 ± 5 vol% CO_2 concentration and 61.7 ± 3.4% RH. The CO_2 flow to the chamber was regulated by a needle valve and bubbled through a saturated NaCl solution which maintained a stable RH *(*Anstice *et al.,* 2005*)*. According to ASTM R104-02 (2007), saturated NaCl solution in a temperature range of 25 to 30 °C provides 75.2 ± 0.3% RH at equilibrium; however, equilibrium was likely not reached in the carbonation chamber due to the difficulty of achieving a perfect seal. To measure the CO_2 concentration, gas samples were taken from inside the chamber and analyzed by gas chromatography on a daily basis. The calibration curves and results pertaining to the gas chromatography measurements are shown in Appendix B. Two portable fans were put inside the chamber to enhance homogeneity of the CO_2-air admixture. The heat released by the fans maintained a temperature ranging from 26.2 to 30.7 °C. An environmental station (Vantage Pro, Davis Instruments, Hayward, California) measured both RH and temperature values on a daily basis inside the chamber. Mortar samples were carbonated for six different times: 1; 3; 7; 14; 21; and 28 days.

2.4 Measurement of Carbonation Depth

After carbonation, the mortar cylinders were cut in half along their length, and the carbonation depth was assessed by various methods.

2.4.1 Fourier Transform Infrared Spectroscopy (FTIR)

IR spectra were obtained with a Bruker Tensor 37 FTIR spectrophotometer (Bruker Optics Inc, Billerica, Massachusetts) equipped with the OPUS 3.1 software. Mixtures containing various proportions of pure $CaCO_3$ (Sigma-Aldrich, St. Louis, Missouri) and sand were prepared to determine calibration curves relating the area of the characteristic $CaCO_3$ absorption peaks obtained by attenuated Total Reflectance (ATR) to the concentration of $CaCO_3$. The pure $CaCO_3$ and sand were ground together for 50 minutes using an automatic mortar and pestle (Geoscience Pulverit comminution equipment type RP-202, Geoscience Corp, New York). To ensure a uniform particle size distribution, the grinding process was done in four steps, two of 15 minutes each and two more of 10 minutes each, where 1 minute was taken between steps to scrape down the pestle and the wall and base of the mortar. Each calibration sample was analyzed eight times and the replicate peak areas were averaged and plotted versus the $CaCO_3$ content in the range 0 – 50 wt%. Calibration data for the characteristic absorption peaks at 1420 and 850 cm^{-1} showed linear behavior with R^2 values higher than 0.98. Calibration curves determined at various dates throughout the research are shown in Appendix C1.

To measure the $CaCO_3$ content of mortar cylinders as a function of depth (measured from the cylinder surface), a drill press was used to sample consecutive layers of material (Figure 2-1). Each sample channel measured approximately 80 mm in length, 10 mm in width, and 2 mm in depth. The cylinders were kept in plastic bags during the drilling process to collect most of the powder that was released. Once the powder from a single layer was collected and stored in an air-tight 20 mL plastic container, the groove was extended by approximately 4 mm in width and length to prevent cross-contamination from upper layers during collection of the next deeper layer. The amount of powder collected per layer ranged from 1.0 to 1.7 g. Figure 2-2 illustrates the basic steps of the collection method. The powders were ground using the same procedure as

described above for calibration mixtures. Figure 2-3 shows the particle size distribution of the ground material taken from a carbonated mortar sample, as determined using a laser particle size analyzer (Mastersizer 2000, Malvern Instruments Ltd., Malvern, UK). The particle sizes ranged from 0.5 to 77 µm with a mode at 4.5 µm.

Figure 2-1 Split mortar cylinders showing grooves from material removed by the drill press for the FTIR and dust digestion methods.

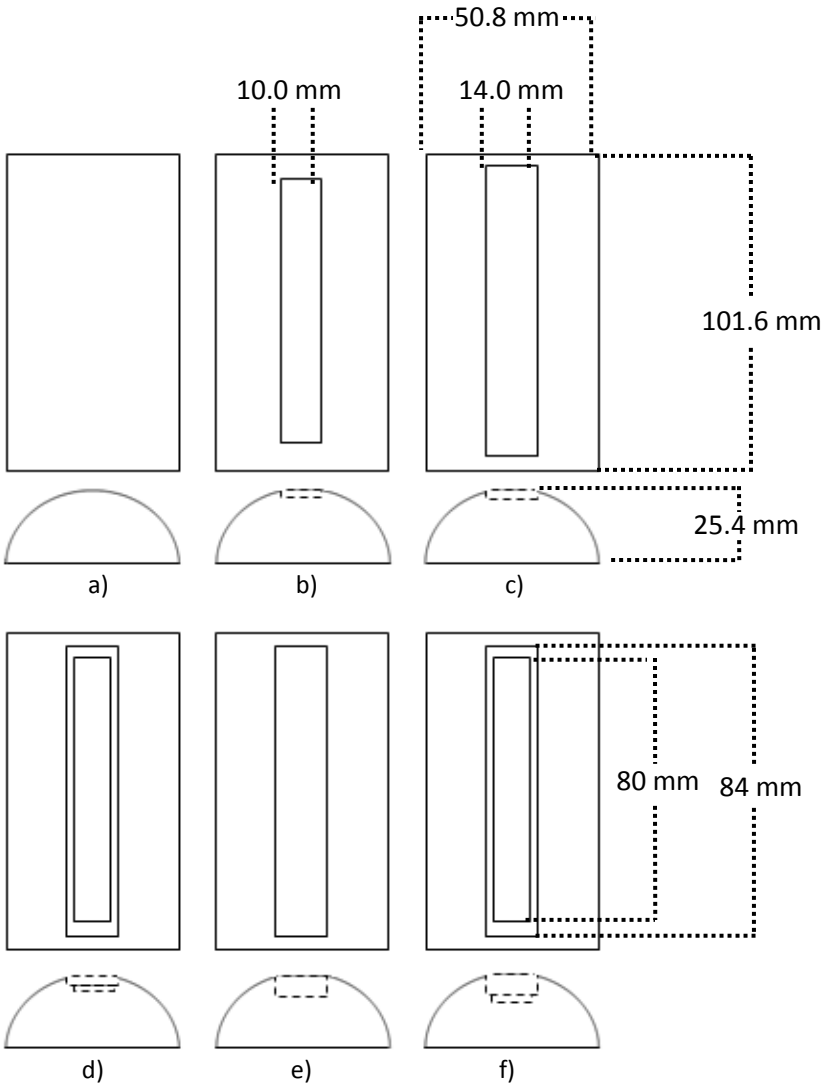

Figure 2-2 Diagram showing the consecutive steps of the powder collection method. Upper and front views: a) split cylinder; b) first layer is collected; c) width and length of groove from first layer are increased; d) second layer is collected; e) width and length of groove from second layer are increased; f) third layer is collected.

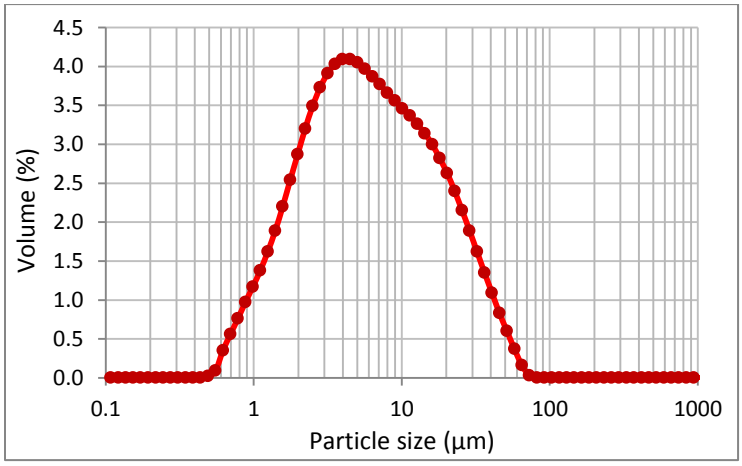

Figure 2-3 Particle size distribution of a ground carbonated mortar sample.

Figure 2-4a shows the FTIR spectrum of a 7-day carbonated mortar sample containing no fly ash. Based on the spectra of graded sand and pure calcium carbonate (Figure 2-4b), it was possible to identify the three main peaks in Figure 2-4a. The silica peak at 1100 cm^{-1} overlaps to some extent with the $CaCO_3$ peaks at 1420 and 875 cm^{-1}. The integration method for the two $CaCO_3$ peaks is graphically represented in Figures 2-5a and b.

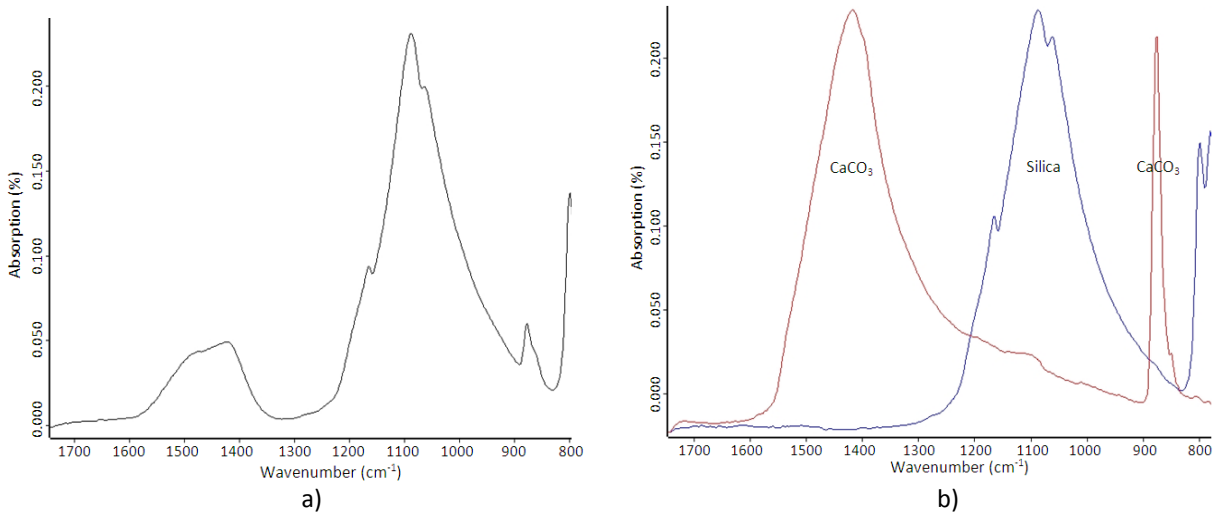

Figure 2-4 a) FTIR spectrum of a 7-day carbonated 0%-FA mortar sample showing $CaCO_3$ characteristic peaks at 1420 and 875 cm^{-1}; b) FTIR spectra of 100% sand and 100% $CaCO_3$ samples.

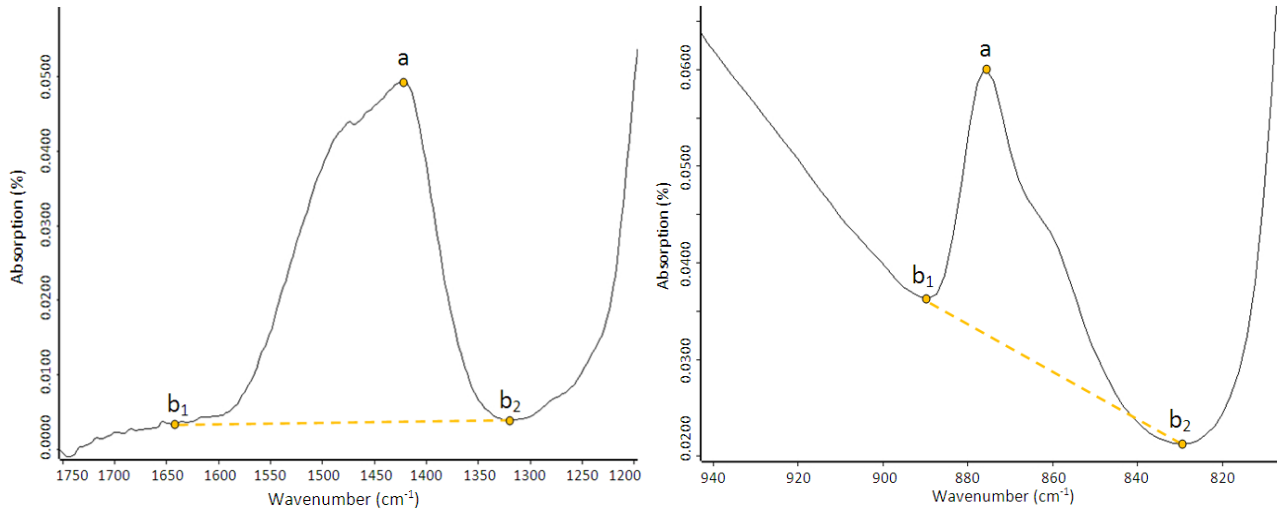

Figure 2-5 Integration method for the two $CaCO_3$ peaks in FTIR spectra of carbonated mortar samples: a) Peak at 1420 cm^{-1}; b) Peak at 875 cm^{-1}. Maxima and minima are determined within the wavenumber ranges of 1650–1300 and 900–820 cm^{-1}, respectively. Maxima are denoted as "a" while minima are denoted as "b_1" and "b_2". Baselines are drawn between points "b_1" and "b_2"

Each powder sample representing a layer of carbonated mortar sample was analyzed eight times by FTIR. The average integrated area of each $CaCO_3$ absorption peak was then calculated and converted to a $CaCO_3$ concentration using the appropriate calibration curve. A new calibration curve was determined for each new batch of mortar samples to compensate for the drift in FTIR measurements happening over time.

The method for determining the depth of carbonation is illustrated in Figure 2-6, which shows the $CaCO_3$ concentration versus depth for a 7-day carbonated mortar sample containing 20 wt% cement substitution by fly ash. The x-axis represents the depth corresponding to the middle of each removed mortar layer. Hence, the average $CaCO_3$ concentration in the 0-2 mm layer was assigned to a depth of 1 mm. Calcium carbonate concentrations were as high as 15 wt% in the outer layers and decreased as a function of depth. Material taken from layers at

depths larger than 10 mm had low $CaCO_3$ concentrations ranging from 0.11 to 0.52 wt%, which represent the baseline. Hence, the carbonation depth was estimated to be 10 mm for this particular sample. Additional examples of $CaCO_3$ concentration profiles and determination of carbonation depths are presented in Appendix C2.

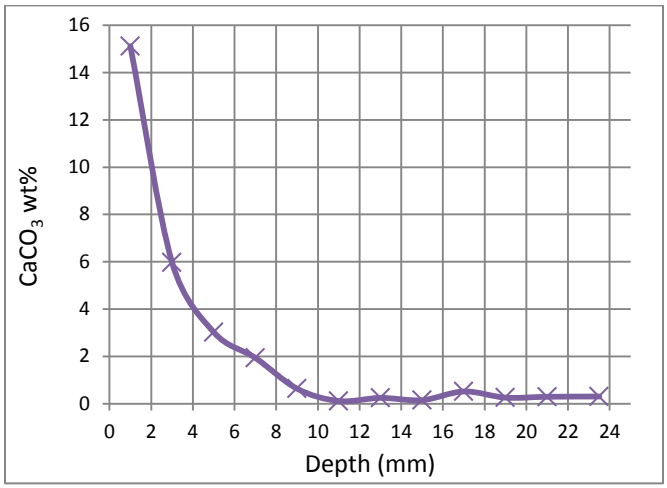

Figure 2-6 Variation of $CaCO_3$ concentration along the depth of a 7-day carbonated 20%-FA mortar sample.

2.4.2 Dust Digestion (DD) Method

Ground mortar powder samples collected at 2 mm depth intervals of by the methods described above were placed in 50 mL polyethylene centrifuge tubes along with nanopure water at a 1:20 ratio. Air in the containers was replaced with nitrogen gas to avoid the reaction of environmental CO_2 with the alkaline slurry. Next, the slurries were placed in a water bath and agitated at a constant temperature of 25 °C for 24 hours. The slurry pH at equilibrium was measured with an Accumet Research AR25 pH meter and a Fluka high-pH electrode. The pH meter was calibrated with buffer solutions at pH 7, 9 and 13 at 25 °C. The pH 13 buffer solution was prepared by mixing 50 mL of 0.2 M KCl and 132 mL of 0.2 M NaOH (Robinson and Stokes, 1970).

The equilibrium pH of mortar slurries depends mainly on the concentration of alkaline compounds such as $Ca(OH)_2$ and CSH in the mortar. Because carbonation partly converts these compounds into calcium carbonate, slurries containing carbonated mortar powder have a lower pH than those made with non-carbonated mortar. Profiles of slurry pH versus mortar depth were used to determine the depth of carbonation, as illustrated in Figure 2-7 for a 21-day carbonated mortar sample having a cement substitution by FA of 20 wt%. The slurry pH increased with depth up to 12 mm. At larger depths, the slurry pH was nearly constant at 12.1, which is therefore taken as the baseline pH for non-carbonated material. Hence, the carbonation depth was estimated to be 12 mm for this particular sample. Further details on the dust digestion method as well as examples of pH profiles and determinations of carbonation depth are provided in Appendix D.

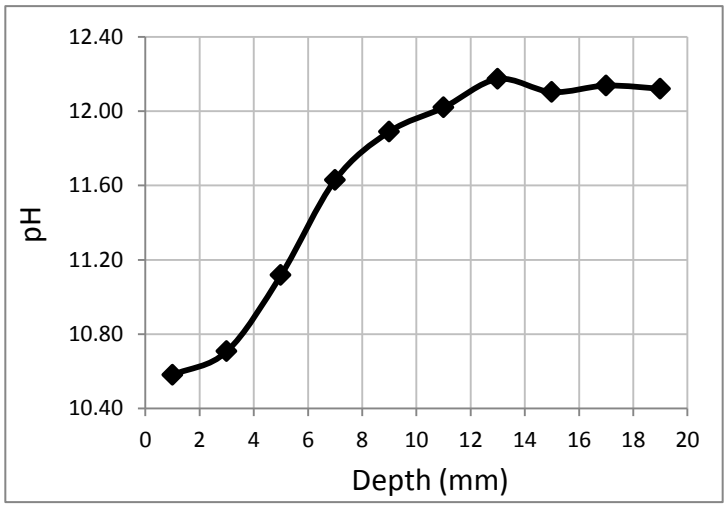

Figure 2-7 Apparent pH profile of a 21-day carbonated 20%-FA mortar sample.

2.4.3 Traditional Phenolphtalein (Trad-P)Method

In accordance to RILEM (1988), depths of carbonation were measured approximately 24 hours after spraying phenolphthalein pH indicator on the freshly exposed surface of a split cylinder. The part of the surface that remained gray was considered to be carbonated while the pink surface was considered to be uncarbonated. An average carbonation depth for a given cylinder was determined from 10 individual measurements done every 2 cm along the length and on both sides of the exposed surface of the split cylinder. Additional details on the Trad-P method are provided in Appendix E.

2.4.4 Image Processing Methods

The exposed surfaces of split cylinders were sprayed with different pH indicators, imaged with a digital camera, and analysed with the image analysis software MaximDL (Diffraction Limited, Ottawa, ON). The pH indicators were thymolphthalein, phenolphthalein, and alizarin. Images of samples that had not been sprayed with pH indicator were also analyzed. Figure 2-8 shows a carbonated split cylinder sprayed with thymolphthalein. The digital image is formed of an array of red, green and blue pixels having values between 0 and 255 which represent the light intensity at red, green, and blue wavelengths. Figure 2-9 shows the average values of red, green, and blue pixels along the X-axis parallel to the diameter of the cylinder. The X coordinate measures distance in number of pixels along the width of the split cylinder. Average pixel values were obtained by averaging the values of all pixels of a given colour for a given X value within the rectangle denoted as "r" in Figure 2-8. The top and bottom ends of the samples were purposely excluded from the analysis to avoid edge effects. Sudden changes in average pixel values at $X \approx 340$ and $X \approx 1675$ correspond to transitions between the dark image background and the edge of the mortar sample. The non-carbonated material near the centre of the sample ($X \approx 1000$) has

lower pixel values than the carbonated material near the surface. The difference is more pronounced for red and green pixels than for blue pixels because of the bluish colour of thymophtalein in the non-carbonated part of the sample.

Average pixel values are affected not only by the colour of the pH indicator but also by uneven illumination of the split cylinder. Because uneven illumination affects all three elementary colours to a similar extent, plotting the difference between blue and red pixel values (Figure 2-10) allows a more accurate determination of carbonation depth. The sudden drop in blue-red pixel values occurring between points a_1 and b_1 on one side, and between points a_4 and b_2 on the other correspond to the edges of the mortar sample. The precise X coordinate of the edges was taken to coincide with the middle points m_1 and m_2, respectively. Pixels between the local minimum b_1 and the local maximum a_2 belong to the carbonated zone on the left side of the sample. Similarly, positions between the local minimum b_2 and the local maximum a_3 correspond to the carbonated zone on the right side of the sample. Since the split cylinder measures exactly 2 inches in diameter, the relationship between the X-axis scale and distances in millimetres can be accurately established. The depth of carbonation is calculated as the average of the distances from m_1 to a_2 and from a_3 to m_2 along the X-axis. An example of application of the image processing method on unsprayed samples (IM-U) is given in Appendix F.

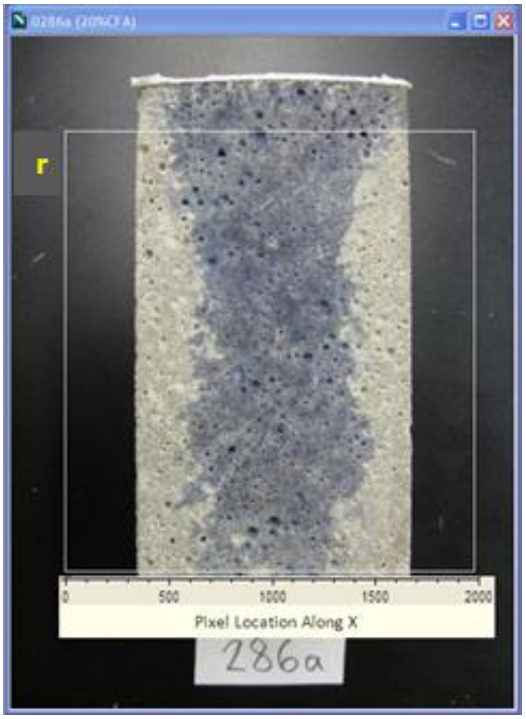

Figure 2-8 Image of a carbonated split cylinder sprayed with thymophthalein showing the rectangular area "r" considered for image analysis.

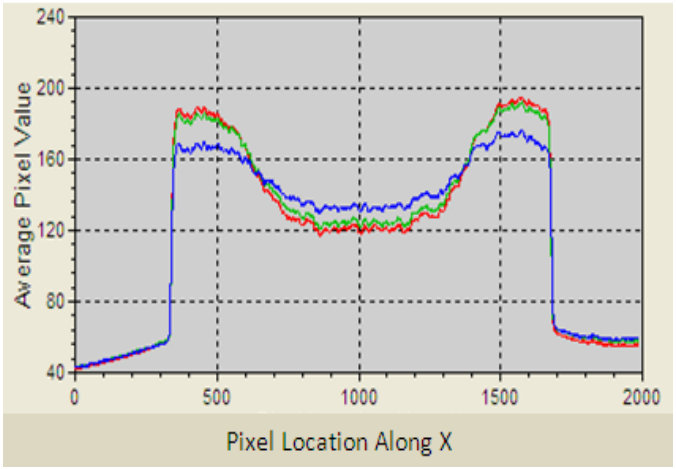

Figure 2-9 Profiles of average pixel values along the direction parallel to the diameter of the carbonated sample sprayed with thymolphthalein shown in Figure 2-8.

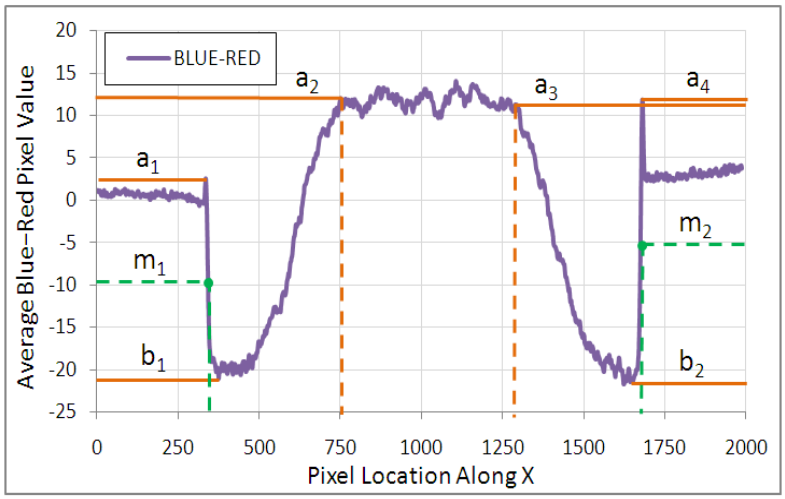

Figure 2-10 Difference between blue and red average pixel values versus pixel location along the direction parallel to the diameter of the carbonated sample sprayed with thymophthalein shown in Figure 2-8. The depth of carbonation is the average of the distances from m_1 to a_2 and from a_3 to m_2 along the X-axis.

3. Experimental Results and Discussion

3.1 Comparison of Analytical Methods

3.1.1 FTIR

The FTIR technique showed that the carbonation depth increased with carbonation time and with percent cement substitution by fly ash (Figure 3-1). Samples with fly ash have less $Ca(OH)_2$ available to react with CO_2 for two reasons. First, less CaO is added to the concrete as the CaO content of fly ash is substantially lower than that of cement; second, some of the $Ca(OH)_2$ formed during cement hydration reacts with fly ash to form CSH *(Lin and Fu, 1987)*. The FTIR data used to determine carbonation depths were obtained by integrating the $CaCO_3$ peak at 1420 cm^{-1} because the reproducibility of $CaCO_3$ concentrations was found to be higher at this wavelength than at 875 cm^{-1}. Carbonation depths estimated using both wavelengths were comparable, but data scatter was minimized at 1420 cm^{-1}.

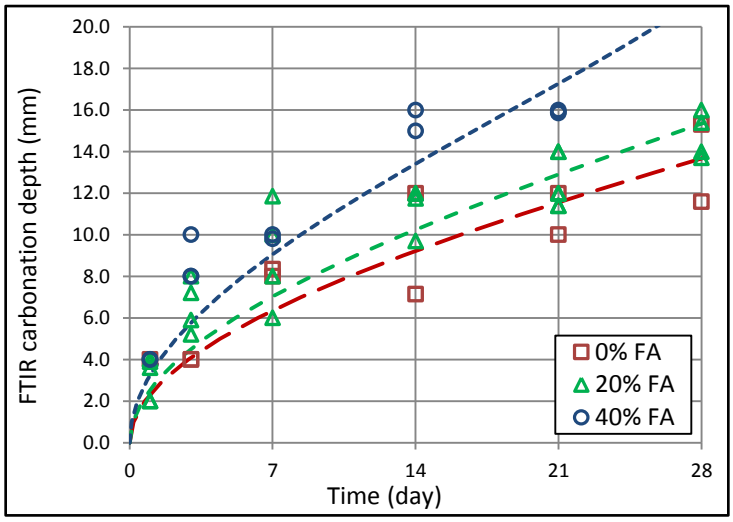

Figure 3-1 Depths of carbonation determined by the FTIR method versus carbonation time for mortars having various cement substitutions by FA. Mortars with 40% cement substitution by FA and carbonated for 28 days were not included because of lack of sufficient measurements to define the baseline. Best fit lines were determined using the diffusion-limited UR-Core model.

3.1.2 Dust digestion

Depths of carbonation measured by the DD method are shown in Figure 3-2. Data scattering was relatively high for samples carbonated for 14 days. This may be explained by a higher uncertainty in the pH baseline of uncarbonated material, which was estimated over only 2 consecutive mortar layers for these samples. By contrast, the pH baseline of the other samples was estimated over 3 to 5 mortar layers.

Figure 3-3 compares the depths of carbonation measured by the DD and FTIR methods for the same samples. They are related by a linear relationship of the form $d_{DD} = s\ d_{FTIR} + i$, where the slope s and intercept i are reported in Table 3-1. The value of s, which is statistically indistinguishable from unity ($s = 0.94 \pm 0.07$), and the value of i, which is very close to zero ($i = 0.79 \pm 0.71$), reflect a very good agreement between the two methods.

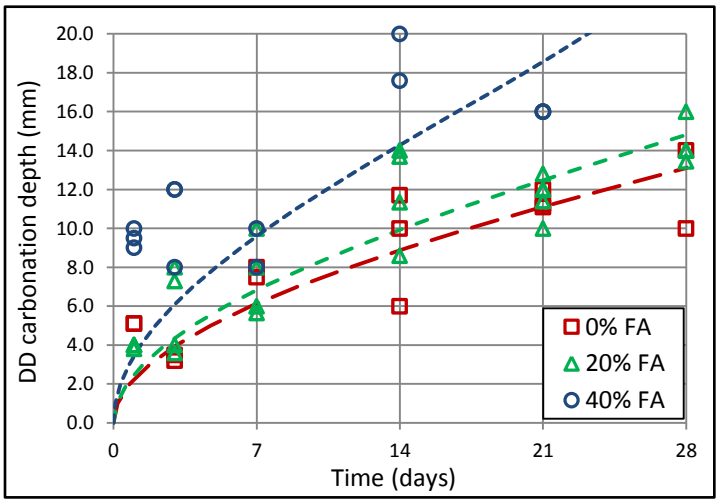

Figure 3-2 Depths of carbonation determined by the DD method versus carbonation time for mortars having various cement substitutions by FA. Mortars with 40% cement substitution by FA and carbonated for 28 days were not included because of lack of sufficient measurements to define the baseline. Best fit lines were determined using the diffusion-limited UR-Core model.

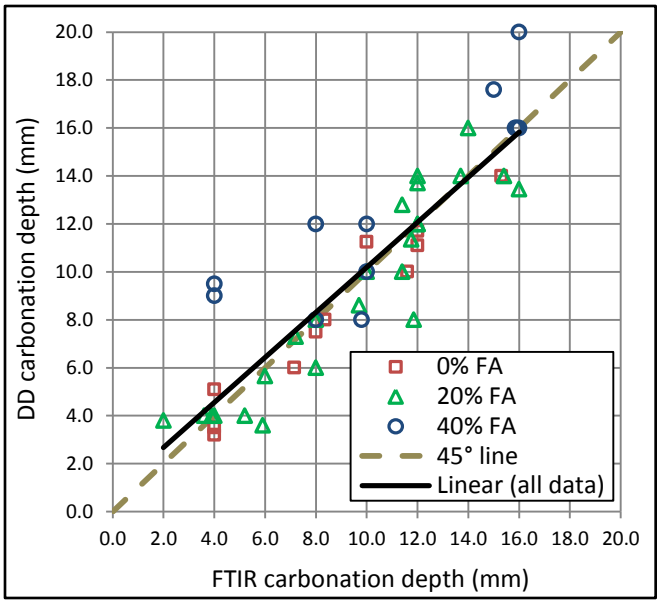

Figure 3-3 Comparison between DD and FTIR carbonation depths.

3.1.3 Traditional Phenolphtalein Method

Figure 3-4 shows carbonation depths versus carbonation time determined by the Trad-P method, and Figure 3-5 compares these depths to those obtained by the FTIR method. The carbonation depths obtained by these methods can be related by a linear relationship such as $d_{Trad\text{-}P} = s_{FTIR} + i$, where the slope s and intercept i are reported in Table 3-1. Although the two methods are in fair agreement for small carbonation depths of 2 to 3 mm, the Trad-P method underestimates the carbonation depth by comparison with the FTIR method at larger carbonation depths, and the amount of underestimation increases as the carbonation depth increases. This is reflected in the slope s being much lower than unity (0.50 ± 0.05). These results are consistent with previous reports that the phenolphthalein method significantly underestimates the carbonation depth due to the presence of a partially carbonated zone having a pore solution pH between 9 and 13 (Broomfield, 1997; Lo and Lee, 2002; Jung et al., 2004; Chang et al., 2004). This partially

carbonated zone is detected by FTIR but not by the Trad-P method since the pH must drop below 10 for phenolphthalein to change color.

The value of *s* lower than unity would suggest that the size of the partially carbonated zone increases with carbonation depth and, hence, with time (since carbonation depth increases with time). There is, however, a compounding reason for the observed difference between the carbonation depths determined by the Trad-P and FTIR methods which is independent of the existence of a partially carbonated zone. Because of mortar heterogeneity, the carbonation front does not advance as a flat front, as is readily apparent in Figure 2-8. The Trad-P method provides a measurement of the *average* carbonation depth as it averages 10 individual depth measurements along the length of the sample. On the other hand, the FTIR method measures $CaCO_3$ concentrations in powder samples representative of the almost entire length of the sample (excluding the first and last centimeters) at a given depth (see Figure 2-2). Because the FTIR method defines the carbonation depth as the depth were the $CaCO_3$ concentration is elevated with respect to the baseline, the FTIR measures the *maximum* advancement of the carbonation front rather than the average carbonation depth. This difference between the two methods contributes to the lower estimates of carbonation depth provided by the Trad-P method.

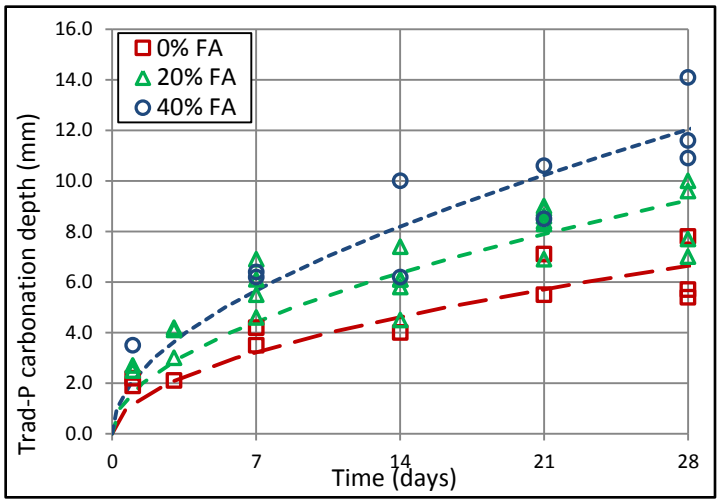

Figure 3-4 Depths of carbonation determined by the Trad-P method versus carbonation time for mortars having various cement substitutions by FA. Best fit lines were determined using the diffusion-limited UR-Core model.

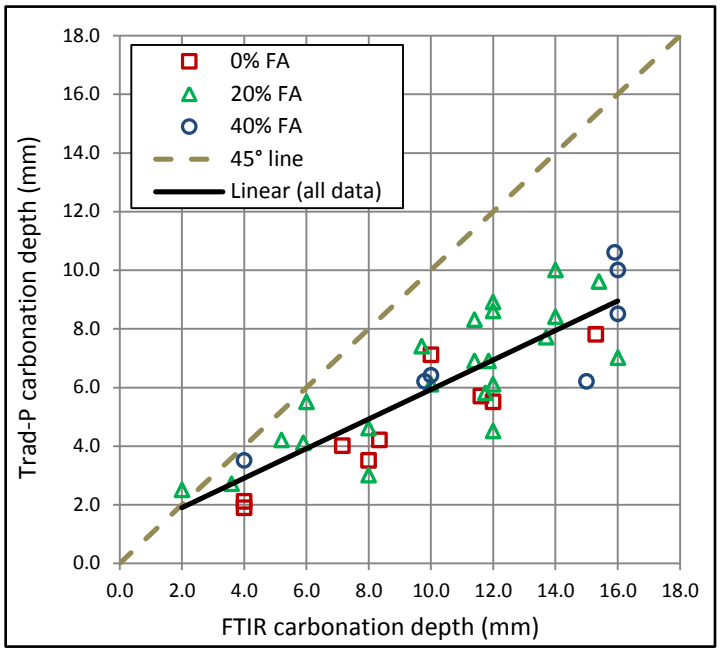

Figure 3-5 Comparison between Trad-P and FTIR carbonation depths.

3.1.4 Image Processing Methods

Even without spraying pH indicator solution, carbonated mortar has a distinctly lighter gray color than non-carbonated material. The imaging method to determine carbonation depth was

applied to digital images of unsprayed split cylinders (IM-U method), as well as split cylinders sprayed with phenolphthalein (IM-P method), thymolphthalein (IM-T method), and alizarin (IM-A method). Carbonation depths versus carbonation time determined by these methods are shown in Figures 3-6a-d. All image processing methods consistently show that the depth of carbonation increases with carbonation time and percent substitution cement by FA.

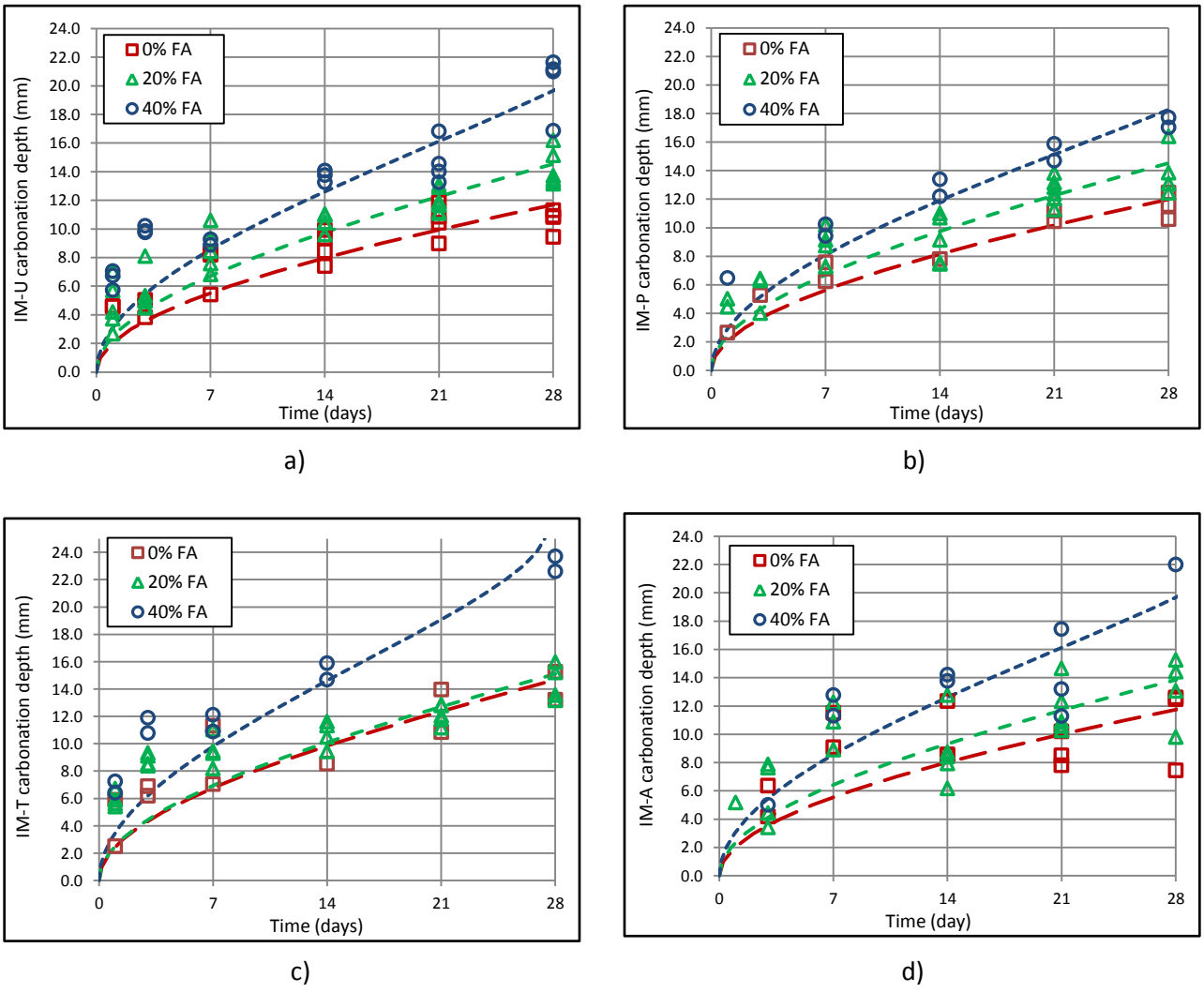

Figure 3-6 Carbonation depths versus carbonation time determined by image processing methods: a) unsprayed mortar samples; b) phenolphthalein; c) thymolphthalein; d) alizarin. Best fit lines were determined using the diffusion-limited UR-Core model.

Figures 3-7a to d compare the carbonation depths determined by the imaging methods with different pH indicators to those determined by FTIR. These depths are related by linear relationships of the form $d_{IM} = s\ d_{FTIR} + i$, where the slopes s and intercepts i are reported in Table 3-1. All the imaging methods consistently provide slopes s less than unity that correlate with the upper end of the transition pH range where color change occurs for each indicator. Thus, the lowest slope (s = 0.75 ± 0.07) corresponds to phenolphthalein (transition pH range = 8.1 – 10) and the largest slope (s = 0.81 ± 0.09) corresponds to alizarin (transition pH range = 11.1 – 12.4). Thymolphtalein provides an intermediate slope (0.77 ± 0.05) as it has an intermediate pH transition range of 9.5 – 10.5. This correlation suggests that the difference between the slope s and unity is related to the presence of a partially carbonated zone having pore solution pH intermediate between that of uncarbonated mortar (approx. 13) and that of fully carbonated mortar (approx. 9). The higher the pH at which the pH indicator starts to change color, the least sensitive it is to the effect of the partially carbonated zone, and the closer s is to unity.

Image processing methods, similar to the FTIR and the dust digestion methods, but unlike the traditional phenolphthalein method, measure the maximum advancement of the carbonation front rather than the average carbonation depth. This is because the pixel values (color intensities) are averaged over the almost entire length of the cylinders for each given depth. Hence, a change in color at any position along the cylinder length affects the positions of the local maxima a_2 and a_3 in Figure 2-10, and hence the depth of carbonation determined by the image processing methods. This explains why the carbonation depths measured by the IM-P method are generally much larger than those determined by the Trad-P method and therefore in better agreement with the FTIR method.

All imaging methods overestimate the carbonation depth compared with the FTIR method at low carbonation depths (i.e., when the carbonation time is small). The value of the intercept i in the linear relationship $d_{IM} = s\ d_{FTIR} + i$ reflects the amount by which the imaging methods overestimate the carbonation depth at small carbonation times. This overestimation is smallest for alizarin ($i = 1.54 \pm 1.05$) and largest for thymolphtalein ($i = 3.19 \pm 0.46$).

As noted before, although FTIR can be considered the most accurate method for measuring carbonation depth since it directly measures the carbonation product $CaCO_3$, its cost and complexity limit its practical applicability. The other methods tested in this study are both more affordable and easier to apply. The goodness of the fit of the linear relationship between carbonation depths determined by various methods and those determined by FTIR is quantified by the coefficient of determination R^2 in the last column of Table 3-1. The dust digestion method and all the image processing methods, except that based on alizarin (IM-A), have R^2 values ranging from 0.78 to 0.88, indicating that any of these methods can effectively predict the depth of carbonation that would be determined by FTIR, given the linear regression coefficients s and i. On the other hand, the traditional phenolphthalein and the alizarin-based imaging method have lower R^2 values equal to 0.73 and 0.69, which makes them be less reliable. The DD method has an advantage over the image processing methods in that its s and i values are very close to unity and zero, respectively, making the DD method essentially equivalent to the FTIR method.

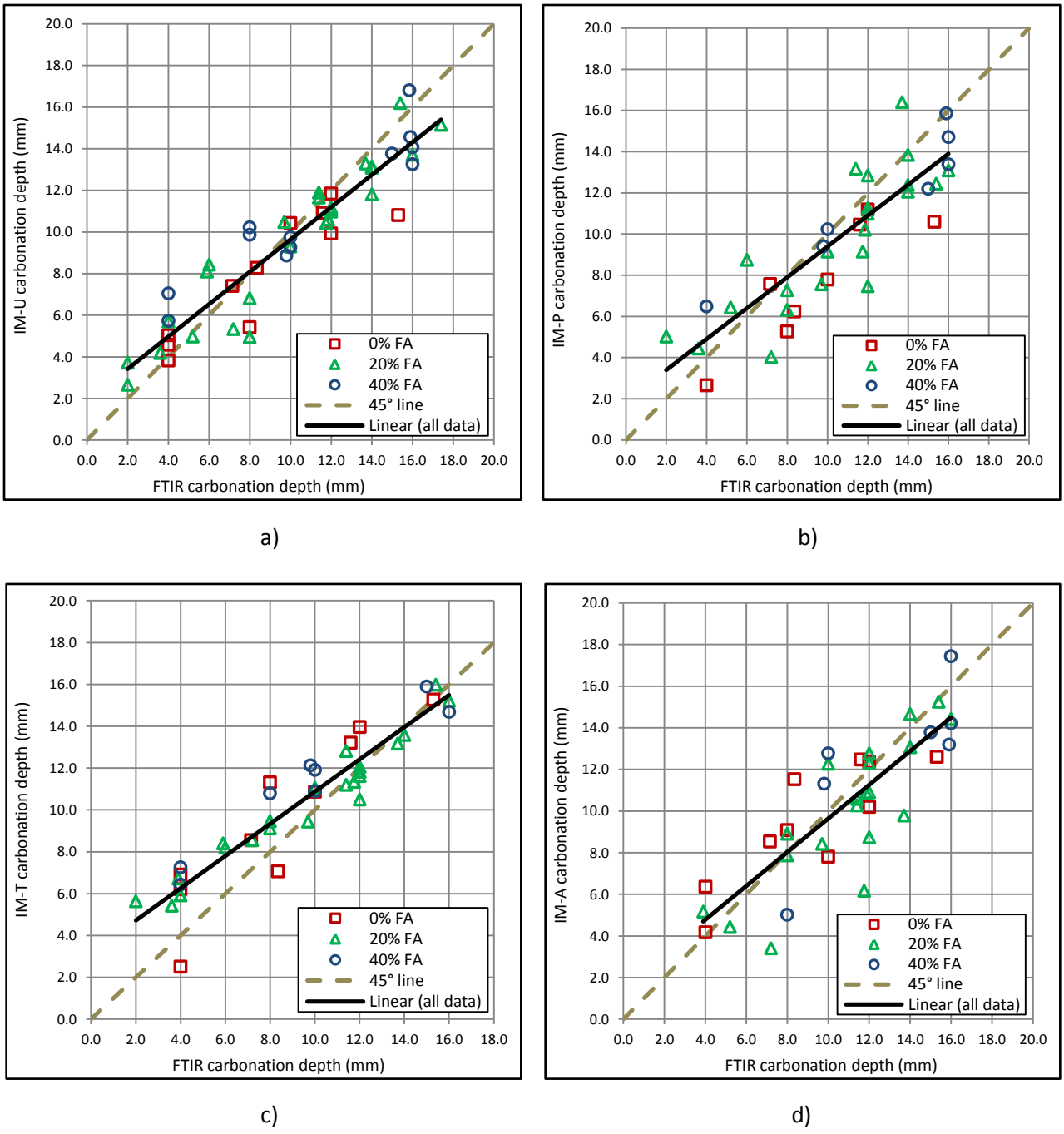

Figure 3-7 Comparison of carbonation depths determined by image processing and FTIR methods: a) IM-U vs FTIR; b) IM-P vs FTIR; c) IM-T vs FTIR; d) IM-A vs FTIR.

Table 3-1 Values of slope *s* and intercepts *i* of linear relationships between carbonation depths determined by various methods.

	s	*i*	R^2
DD vs FT-IR	0.94 ± 0.07	0.79 ± 0.71	0.81
Trad-P vs FT-IR	0.50 ± 0.05	0.89 ± 0.57	0.73
IM-U vs FT-IR	0.78 ± 0.04	1.87 ± 0.46	0.87
IM-P vs FT-IR	0.75 ± 0.07	1.89 ± 0.75	0.78
IM-T vs FT-IR	0.77 ± 0.05	3.19 ± 0.46	0.88
IM-A vs FT-IR	0.81 ± 0.09	1.54 ± 1.05	0.69

4. Modeling the advancement of the carbonation front

In this chapter, we evaluate how well the carbonation depth versus time data provided by each analytical method can be fitted by the diffusion-limited UR-core model. Also, we compare the methods with respect to the predicted time for complete carbonation of the cylindrical mortar samples.

Figure 4-1 *(Castellote and Andrade, 2008)* is a schematic showing the conceptual basis of the UR-Core model for the advancement of the carbonation front and the concentration profile of solid reactant (material susceptible to be carbonated) in a cylindrical sample at three consecutive times. Equations describing the advancement of the carbonation front can be derived by assuming that the process is controlled by either 1) the diffusion rate of CO_2 through the pore space of carbonated material or 2) the carbonation reaction rate. *Castellote and Andrade (2008)* found that their experimental carbonation data for OPC, OPC-FA and OPC-Micro silica samples was better fitted by the diffusion-limited model than by the reaction-limited model. We reached the same conclusion with our carbonation data (see Appendix G for the results of chemical reaction-limited UR-Core modeling); hence, only results pertaining to the diffusion-limited UR-Core model are discussed in the following. The model equations describing the radial position of the carbonation front, r, are as follows:

$$X_s = 1 - \left(\frac{r}{R}\right)^2 \qquad (1)$$

$$\frac{t}{\tau} = X_s - (1 - X_s)ln(1 - X_s) \qquad (2)$$

where R is the radius of the cylinder, X_s is the fractional conversion of the solid reactant, t is carbonation time, and τ is the time required for complete conversion of the reactant.

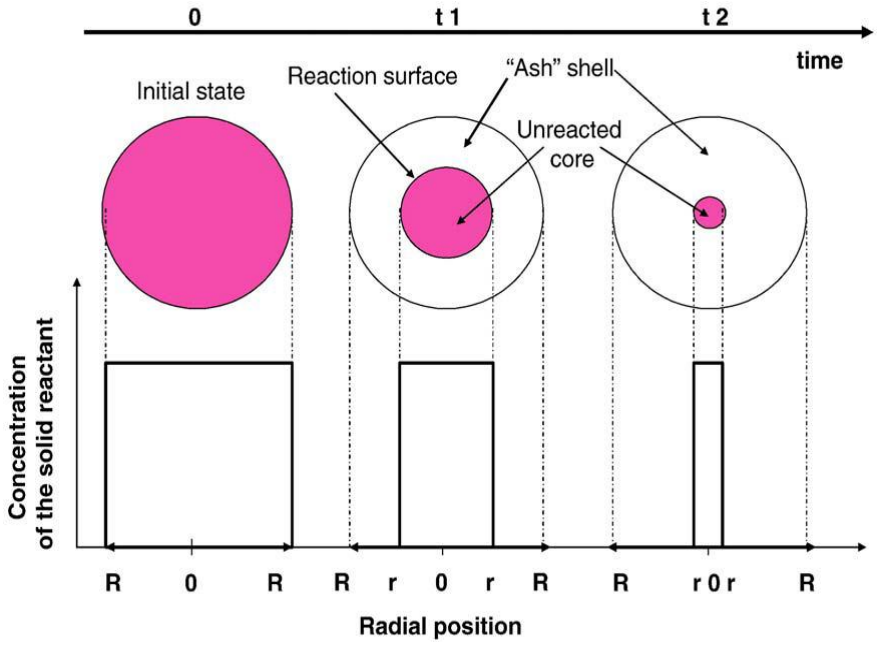

Figure 4-1 Schematic showing the conceptual basis of the UR-core model. *(from Castellote and Andrade, 2008).*

The time for complete carbonation, τ, can be estimated by plotting the right hand side of equation 2 as a function of t. The inverse of the slope of the best fit line is τ. Experimental values of X_s are obtained from measured carbonation depths, D, noting that $r = R - D$. Figures 4-2a to g show the fit of equation 2 to carbonation data obtained with various experimental methods and mortars containing 0, 20, and 40% cement substitution by fly ash. The corresponding values of τ are given in Table 4-1.

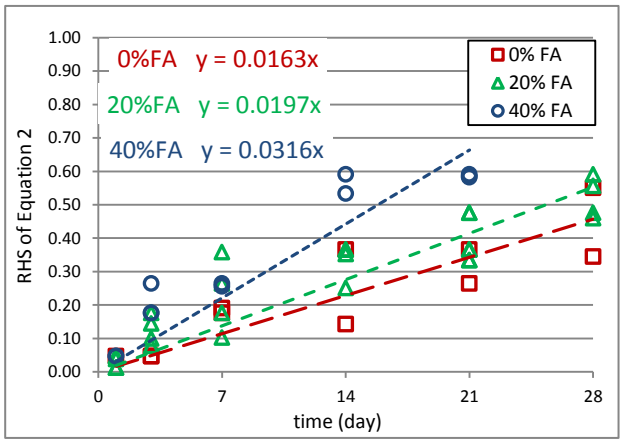
0%FA y = 0.0163x
20%FA y = 0.0197x
40%FA y = 0.0316x
0% FA
20% FA
40% FA
RHS of Equation 2
time (day)

a)

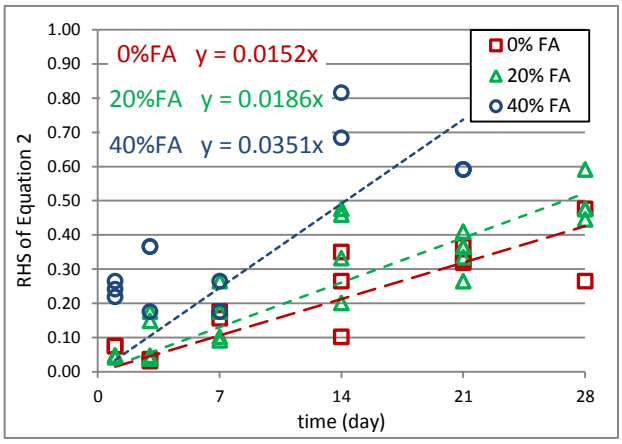
0%FA y = 0.0152x
20%FA y = 0.0186x
40%FA y = 0.0351x
0% FA
20% FA
40% FA
RHS of Equation 2
time (day)

b)

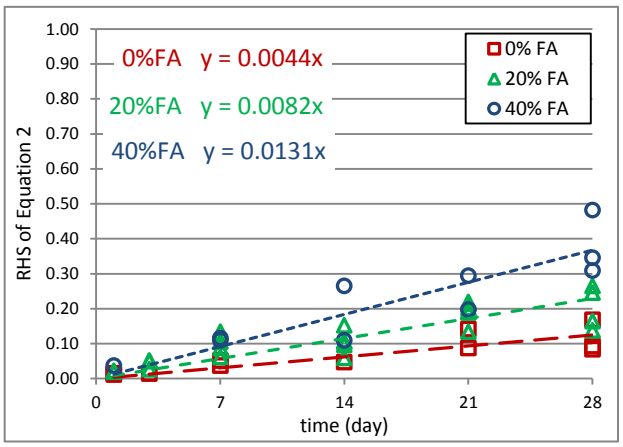
0%FA y = 0.0044x
20%FA y = 0.0082x
40%FA y = 0.0131x
0% FA
20% FA
40% FA
RHS of Equation 2
time (day)

c)

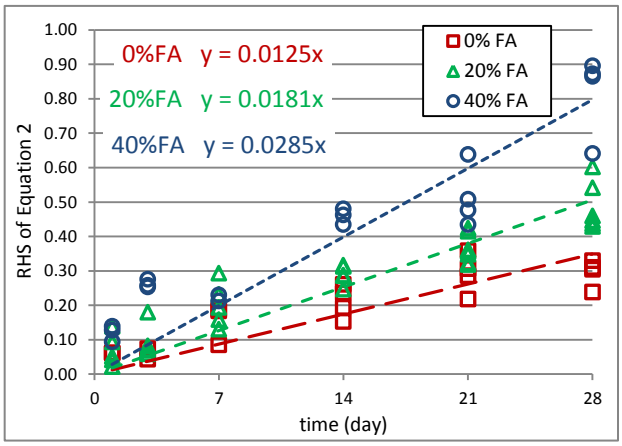
0%FA y = 0.0125x
20%FA y = 0.0181x
40%FA y = 0.0285x
0% FA
20% FA
40% FA
RHS of Equation 2
time (day)

d)

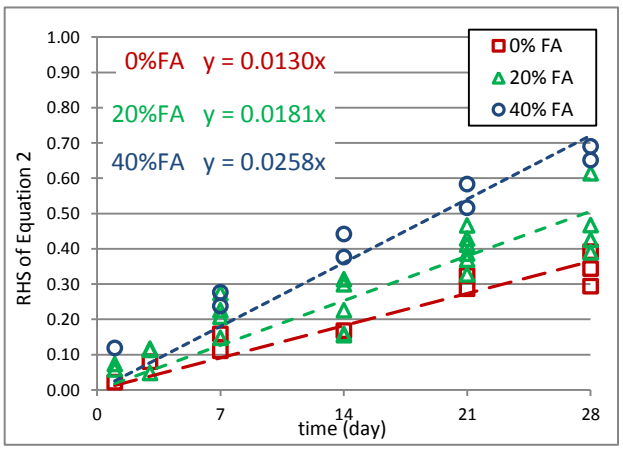
0%FA y = 0.0130x
20%FA y = 0.0181x
40%FA y = 0.0258x
0% FA
20% FA
40% FA
RHS of Equation 2
time (day)

e)

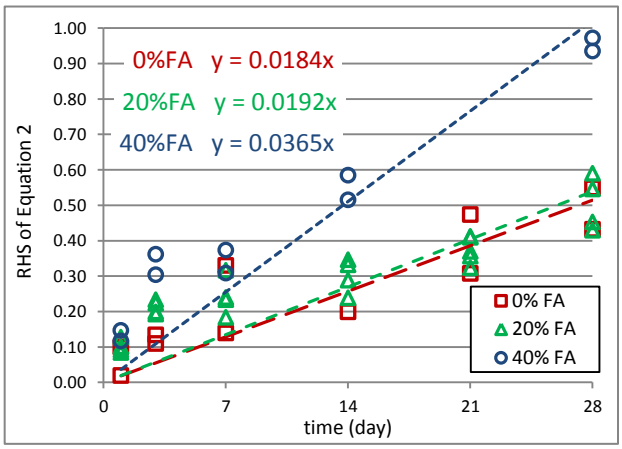
0%FA y = 0.0184x
20%FA y = 0.0192x
40%FA y = 0.0365x
0% FA
20% FA
40% FA
RHS of Equation 2
time (day)

f)

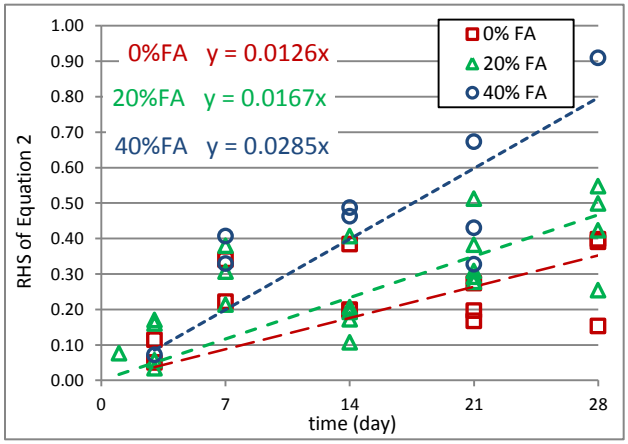

g)

Figure 4-2 RHS of equation 2 versus time and best fit lines for a) FTIR; b) DD; c) Trad-P; d) IM-U; e) IM-P; f) IM-T; g) IM-A carbonation data.

Table 4-1 Estimated times for total carbonation using the diffusion-limited UR-Core model.

Method	*FA content (%)*	*Time for total carbonation τ (day)*
Trad-P	*0*	*225 ± 23*
	20	*122.2 ± 7.2*
	40	*76.2 ± 6.1*
FTIR	*0*	*61.3 ± 5.6*
	20	*50.7 ± 2.4*
	40	*31.6 ± 2.2*
DD	*0*	*65.8 ± 5.6*
	20	*53.7 ± 3.1*
	40	*28.5 ± 3.8*
IM-U	*0*	*80.2 ± 5.1*
	20	*55.3 ± 2.0*
	40	*35.1 ± 1.9*
IM-P	*0*	*76.8 ± 4.1*
	20	*55.4 ± 2.7*
	40	*38.8 ± 1.9*
IM-T	*0*	*54.5 ± 5.1*
	20	*52.0 ± 3.3*
	40	*27.4 ± 2.1*
IM-A	*0*	*79 ± 12*
	20	*60.0 ± 5.2*
	40	*35.1 ± 3.7*

The value of τ decreases as a function of increasing cement replacement by fly ash, which is consistent with faster carbonation as more cement is substituted by fly ash. The τ values obtained with the Trad-P method were at least twice as long as those obtained with the other methods, confirming that the traditional phenolphthalein method underestimates the advancement of the carbonation front. All the other methods provide compatible values of τ when considering statistical uncertainty.

5. Conclusions

Several analytical methods were compared for measuring the advancement of the carbonation front and predicting the time required for total carbonation of cylindrical mortar samples. These methods were the measurement of $CaCO_3$ concentrations by FTIR, the dust digestion method which provided an apparent pH profile, the traditional phenolphthalein method, and computerized image-processing methods based on the use pH indicators or changes in mortar colour due to carbonation. The following conclusions can be made.

1. The traditional phenolphthalein method, which measures the average advancement of the carbonation front, significantly underestimates the carbonation depth when compared with the FTIR, dust digestion, and all the image processing methods, which measure the maximum advancement of the carbonation front.
2. The dust digestion method provides carbonation depths which are essentially equivalent to those provided by the FTIR method.
3. The diffusion-limited UR-core model generally fits well the carbonation depths versus time data measured by all analytical methods.
4. When used in conjunction with the diffusion-limited UR-core model, all analytical methods, except the traditional phenolphthalein method, give consistent estimates of the times required for total sample carbonation. By contrast, the traditional phenolphthalein method significantly overestimates times for total carbonation.
5. Partial replacement of cement by FA causes the carbonation front to advance faster and decreases the time required for complete carbonation of the mortar samples.

6. References

American Society for Testing and Materials (ASTM), Concrete and Aggregates, West Conshohocken, PA, USA, Section 04, Vol. 04.01, 2003:

C109/C109M-02 Standard test for compressive strength of hydraulic cement mortars (using 2-in or [50mm] cube specimens).

C778-03 Standard specification for standard sand.

C1437-01 Standard test method for flow of hydraulic cement mortar.

Anstice DJ, Page CL, Page MM, *The pore solution phase of carbonated cement pastes*, Cement and Concrete Research, 35, 377-383, 2005.

Atis CD, *Accelerated carbonation and testing of concrete made with fly ash*, Construction and Building Materials, 17, 147-152, 2003.

Bernal SA, Mejia de Gutierrez R, Pedraza AL, Provis JL, Rodriguez ED, Delvasto S, *Effect of binder content on the performance of alkali-activated slaf concretes*, Cement and Concrete Research, 41, 1-8, 2010.

Berry EE, MalhotraVM, *Fly ash in concrete,* V.M. Malhotra (Ed), Supplementary Cementing Materials for Concrete, Ottawa, CANMET SP-86-8E, 35-163, 1987.

Bouzoubaa N, Foo S, *Use of Fly Ash and Slag in Concrete: A Best Practice Guide,* Materials and Technology Laboratory, MTL 2004-16 (TR-R), Minerals and Metals Program of the Government of Canada Action Plan 2000 on Climate Change, 2005.

Broomfield JP, *Corrosion and residual life in concrete structures. An overview*, Bulletin of Electrochemistry, 11, 121-128, 1995.

Broomfield JP, *Corrosion of steel in concrete,* E&FN SPON, London, UK, pp. 52-72, 1997.

Broomfield JP, *Carbonation and its effects in reinforced concrete,* Materials Performance 1, Wilson Applied Science & Technology Abstracts, 2000.

Burden D, *The durability of concrete containing high levels of fly ash,* Masters of Science in Engineering Thesis, Research and Development Information, PCA R&D Serial No. 2989, Portland Cement Association, 2006.

Butler WB, *Discussion on the paper: carbonation and chloride-induced corrosion of reinforcement in fly ash concretes,* ACI Materials Journal Disc 89-M5, pp. 602, 1992.

Cabrera JG, Claisee PA, Hunt DN, *A statistical analysis of the factors which contribute to the corrosion of steel in Portland cement and silica fume concrete*, Constructions and Building Materials, 9, 105-113, 1995.

Castellote M, Andrade C, *Modelling the carbonation of cementitious matrixes by means of unreacted-core model, UR-CORE,* Cement and Concrete Research, 38, 1374-1384, 2008.

Castellote M, Andrade C, *Modelling the carbonation of concrete (UR-CORE) from fractional conversion data obtained through in situ monitored neutron diffraction experiments,* Revista Ingeniería de Construcción, 24, 245-258, 2009.

Cement Association of Canada, website (2009):
http://www.cement.ca/index.php/en/Cement_Manufacturing/Cement_Manufacturing.html

ChemEurope.com, website, 2009:
http://www.chemeurope.com/lexikon/e/Reinforced_concrete/

Chang JJ, Yeih W, Huang R, Chen CT, *Suitability of several current used concrete durability indices on evaluating the corrosion hazard for carbonated concrete*, Materials Chemistry and Physics, 84, 71-78, 2004.

Chang CF, Chen JW, *The experimental investigation of concrete carbonation depth,* Cement and Concrete Research, 36, 1760-1767, 2004.

Dhir RK, Hewlett PC, Chan YN, *Near-surface characteristics of concrete: prediction of carbonation resistance,* Magazine of Concrete Research, 41, 137-143, 1989.

Do Lago PR, Castro-Borges P, *A novel method to predict concrete carbonation,* Concreto y Cemento, Investigacion y Desarrollo, 1, 25-35, 2009.

Encyclopaedia Brittanica, website (2009):
http://www.britannica.com/EBchecked/topic/83859/building-construction/60135/Reintroduction-of-concrete#

European Cement Association, website (2009): www.cembureau.be

Fukushima T, Yoshizaki Y, Tomosawa F, Takahashi K, *Relationship between neutralization depth and concentration distribution of $CaCO_3$-$Ca(OH)_2$ in carbonated concrete,* ACI Special Publication, 179, 347-363, 1998.

Glasser FP, Marchand J, Samson E, *Durability of concrete – Degradation phenomena involving detrimental chemical reactions*, Cement and Concrete Research, 38, 226-246, 2008.

Houst YF, Wittmann FH, *Depth profiles of carbonates formed during natural carbonation*, Cement and Concrete Research, 32 1923-1930, 2002.

Hwang KR, Noguchi T, Tomosawa F, *Effects of fine aggregate replacement on the rheology, compressive strenght and carbonation properties of fly ash and mortar,* Proceedings of the 6th International Conference on the Use of Fly Ash, Silica Fume, Slag, and Natural Pozzolans in Concrete, ACI, 178, 401-410, Bangkok, 1998.

Ismail N, Nonaka T, Noda A, Mori T, *Effects of carbonation on microbial corrosion of concrete*, Constructuction Management and Engineering, 20, 133-138, 1993.

Johnson, A., L.J.J. Catalan, S.D. Kinrade, *Characterization and evaluation of fly-ash from co-combustion of lignite and wood pellets for use as cement admixture*, Fuel, 89, 3042-3050, 2010.

Jung WY, Yoon YS, Sohn YM, *Predicting the remaining service life of land concrete by steel corrosion,* Cement and Concrete Research, 65, 663-677, 2004.

Khoury GA and Anderberg Y, *Concrete Spalling Review*, Swedish National Road Administration, Fire Safety Design, p. 9, 2000.

Khunthongkeaw J, Tangtermsirikul S, Leelawat T, *A study on carbonation depth prediction for fly ash concrete*, Construction and Building Materials, 20, 744-753, 2006.

Kosmatka SH, Kerkhoff B, Panarese WC, MacLeod NF, McGrath Rj, *Design and Control of Concrete Mixtures,* 7th Edition, Cement Association of Canada, pp. 57-58, 2002.

Levenspiel, O, *Chemical Reaction Engineering*, 3rd Edition, John Wiley & Sons, pp. 568-586, 1999.

Levi S, Helene P, *Rehabilitation of reinforced concrete schools in the State of Sao Paulom Brazil",* (in Portuguese), Technical Report, Techne, PINI, n. 47, 2000.

Liang MT, Qu W, Liang CH, *Mathematical modeling and prediction method of concrete carbonation and its applications,* Journal of Marine Science and Technology, 10, 128-135, 2002.

Lin XX, Fu Y, *Influence of microstructure on carbonation of concrete containing fly ash,* Proc., 4th Int. Conf. on Durability of Building Materials and Components, pp. 686-693, 1987.

Lo Y, Lee HM, *Curing effects on carbonation of concrete using a phenolphthalein indicator and Fourier-transform infrared spectroscopy*, Building and Environment, 37, 507-514, 2002.

McPolin DO, Basheer PAM, Long AE, Grattan KTV, Sun T, *New test method to obtain pH profiles due to carbonation of concretes containing supplementary cementitious materials,* Journal of Materials in Civil Engineering 19, 936-947, 2007.

Metha PK, *Role of pozzolanic and cementitious material in sustainable development of the concrete industry,* Proceedings of the 6th International Conference on the Use of Fly Ash, Silica Fume, Slag, and Natural Pozzolans in Concrete, ACI SP-178, 1-25, Bangkok, 1998.

Monteiro PJM, Helene P, Kang S, *Designing concrete mixtures for strength, elastic modulus and fracture energy",* Materials and Structures, 26, 443-452, 1993.

Moreno E, Castro-Borges P, Leal J, *Carbonation-induced corrosion of urban concrete buildings in Tucatan, Mexico,* CORROSION/2002, paper 02220, NACE-International, Houston, TX, 2002.

Papadakis VG, *Effect of supplementary cementing material son concrete resistance against carbonation and chloride ingress,* Cement and Concrete Research, 30, 291-299, 2000.

Papadakis VG, Vayenas CG, Fardis MN, AlChE J. 35, 1639, 1989.

Papadakis[1] VG, Vayenas CG, Fardis M, *Fundamental modeling and experimental investigation of concrete carbonation,* ACI Materials Journal 88, 363-373, 1991.

Papadakis[2] VG, Vayenas CG, Fardis M, *Experimental investigation and mathematical modeling of the concrete carbonation problem,* Chemical Engineering Science, 46, 1333-1338, 1991.

Papadakis[3] VG, Vayenas CG, Fardis M, *Physical and chemical characteristics affecting the durability of concrete,* ACI Materials Journal, 8, 186-191, 1991.

Papadakis[1] VG, Fardis MN, Vayenas CG, *Effect of composition, environmental factors and cement-lime mortar coating on concrete carbonation,* Materials and Structures, 25, 293-304, 1992.

Papadakis[2] VG, Fardis MN, Vayenas CG, *Hydration and carbonation of pozzolanic cements,* ACI Materials Journal, 89, 119-130, 1992.

Parrott LJ, *Measurement and modeling of moisture, microstructure and properties in drying concrete*, 1st International RILEM Congress, Versailles, France, pp. 135-142, 1987.

Parrott LJ, *Damage caused by carbonation of reinforced concrete*, RILEM Materials and Structures, Materials and Structures, 23, 230-234, 1990.

Parrott LJ, *Some effects of cement and curing upon carbonation and reinforcement corrosion in concrete*, Materials and Structures, 29, 164-173, 1996.

Portland Cement Association, website (2009):
http://www.cement.org/basics/concretebasics_concretebasics.asp

Portland Cement Association, website (2010):

http://www.cement.org/tech/faq_cracking.asp

RILEM, *Measurement of hardened concrete carbonation depth, Materials and Structures*, 21, 453-455, 1988.

RILEM Technical Commitee 60-CSC, *Corrosion of steel in concrete,* Chapman and Hall, Ed. P. Schiessl, 1988.

Robinson RA and Stokes RH, *Electrolyte Solutions*, 2nd Edition, Butterworths and Co. Publishers, p. 548, 1970.

Rooke W, *What you should know about curing of concrete,* 9th Technical Update, Manitoba Ready Mix Concrete Association, 2007.

Roziere E, Loukili A, Cussigh F, *A performance based approach for durability of concrete exposed to carbonation*, Construction and Building Materials, 23, 190-199, 2008.

Rusell D, Basheer PAM, Rankin GIB, *Long Effect of relative humidity and air permeability on prediction of the rate of carbonation of concrete*, Proceedings of the Institution of Civil Engineers Structures and Buildings, 146, 319-326, 2001.

Saeki N, TAKADA n, Fujita Y, *Influence of carbonation and sea water on corrosion of steel in concrete,* Trans. Japan Concrete Institute, 6, 155-162, 1984.

San Juan MA, Munoz-Martialay R, *Influence of the wáter/cement ratio on the air permeability of concrete,* Journal of Materials Science, 31, 2829-2832, 1996.

Sasatani T, Torii K, Kawamura M, *Five-year exposure test on long-term properties of concretes containing fly ash, blast-furnace slag, and silica fume,* Proceedings of the 5th International Conference on the Use of Fly Ash, Silica Fume, Slag and Natural Pozzolans in Concrete, ACI AP-153, pp. 283-296, Milwaukee, 1995.

Scalny J, *Concrete durability: a multibillion dollar opportunity,* National Materials Advisory Board, National Academy Press, Report NMAB-437, 1987.

Scott A, Thomas MDA, *Evaluation of fly ash from co-combustion of coal and petroleum coke for use in concrete*, ACI Material Journal, American Concrete Institute, 104, 62-70, 2007.

Sisomphon K, Franke L, *Carbonation rates of concretes containing high volume of pozzolanic materials*, Cement and Concrete Research, 37, 1647-1653, 2007.

Smith D, Evans A, *Purple concrete in a Middle East town,* Concrete, 20, 36-41, 1986.

Thomas MDA, Matthews JD, *Carbonation of fly ash concrete,* Magazine of Concrete Research, 44, 217-228, 1992.

Tuutti K, *Service life of structures with regard to corrosion of embedded steel*, in Performance of concrete in marine environment, ACI SP-65, pp. 223-236, 1980.

Webster's Online Dictionary, http://www.websters-online-dictionary.org, 2009.

Zivica V, *Corrosion of reinforcement induced by environment containing chloride and carbon dioxide*, Bulletin of Materials Science, 26, 605–608, 2003.

Zumdahl SS, Zumdahl SA, *Chemistry,* 7th Edition, , Houghton Mifflin Company, Boston, MA, p. 715, 2007.

Appendix A Water Requirement Testing

Water requirement was assessed as the amount of water needed to keep the same diameter increase as that of the control sample in the flow table test. The control sample had a fly ash content of 0 wt%. The formula to calculate the diameter increase is shown next.

$$\text{Diameter Increase (\%)} = \frac{F - 2\left(\frac{\sum_{i=1}^{8} d_i}{8}\right) - M}{M} \cdot 100$$

Where F = diameter of flow table = 25.5 cm; d_i = distance between edge of table and edge of mortar at 8 locations around the flow table after test is done; M = diameter of base of mold = 10 cm

Control mortar diameter increases after the flow table test are shown in Table A1.

Table A1 Flow table results for control mortars.

Sample	Water (mL)	d_1 (cm)	d_2 (cm)	d_3 (cm)	d_4 (cm)	d_5 (cm)	d_6 (cm)	d_7 (cm)	d_8 (cm)	Diameter increase (%)
0% FA[a]	242	5.15	5.10	5.40	5.55	5.20	5.05	4.75	4.95	52.13
0% FA	242	5.45	5.20	5.20	5.30	5.45	5.10	5.05	5.30	49.86
0%FA	242	5.05	5.25	5.00	4.85	4.60	4.70	4.95	5.00	56.50

Diameter increase average = 52.83 %

a. Sample calculation for 0% cement replacement by fly ash

$$\text{Diameter Increase} = \frac{25.5 - 2\left(\frac{5.15 + 5.10 + 5.40 + 5.55 + 5.20 + 5.05 + 4.75 + 4.95}{8}\right) - 10}{10} \cdot 100$$

Diameter Increase = 52.13%

Table A2 Flow table results for mortars containing fly ash.

Sample	Water (mL)	d_1 (cm)	d_2 (cm)	d_3 (cm)	d_4 (cm)	d_5 (cm)	d_6 (cm)	d_7 (cm)	d_8 (cm)	Diameter increase (%)	Pass? Y/N
20% CFA	228	5.15	5.40	5.30	4.95	5.00	5.00	5.10	4.85	53.13	Y
20% BFA	228	5.00	5.25	5.00	4.70	4.70	4.70	4.85	5.00	57.00	Y
40% CFA	206	5.25	5.10	4.95	4.95	4.80	4.80	5.10	5.05	55.00	Y

Appendix B Measurement of CO_2 Concentration in the Carbonation Chamber

B1 Gas Sampling

A hole was drilled on top of the chamber to place the sampling hose down to approximately the center of the carbonation chamber. Two fans were kept inside the chamber at all times to ensure the homogeneity of the gas mixture. A vacuum system was utilized to fill up the hermetically sealed air sampling bags.

The gas samples were analyzed with a gas chromatograph to determine their CO_2 concentration. Gas analysis and subsequent adjustments to the CO_2 flow rate were done on a daily basis to prevent the CO_2 concentration to deviate from the targeted 50 vol%. The CO_2 vol% was allowed to fluctuate between 45 and 55 vol%. The average CO_2 concentration over the 28-day carbonation period was 51.13 ± 2.12 vol%.

B2 GC Calibration Curve

A calibration curve was obtained by running samples of three different CO_2 concentrations: air (0.03 vol%), 50 vol%CO_2 and 100 vol%CO_2. The integrated areas are in a linear relationship with the CO_2 vol%.

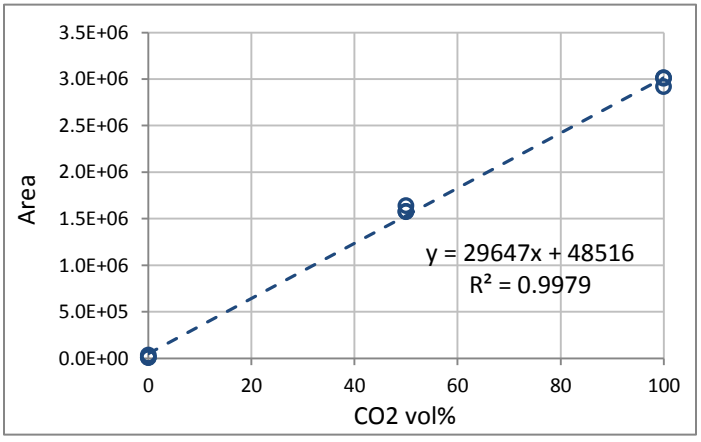

Figure B1 GC calibration curve.

B3 Assessment of CO_2 vol%. Sample Calculations

Since Area = 29647 * CO_2 vol% + 48516; then

CO_2 vol% = (Area + 48516) / 29647

Sample:

Area = 1487220

CO_2 vol% = (1487220 + 48516) / 29647

CO_2 vol% = 51.8007

B4 Summary of GC analyses Over Time

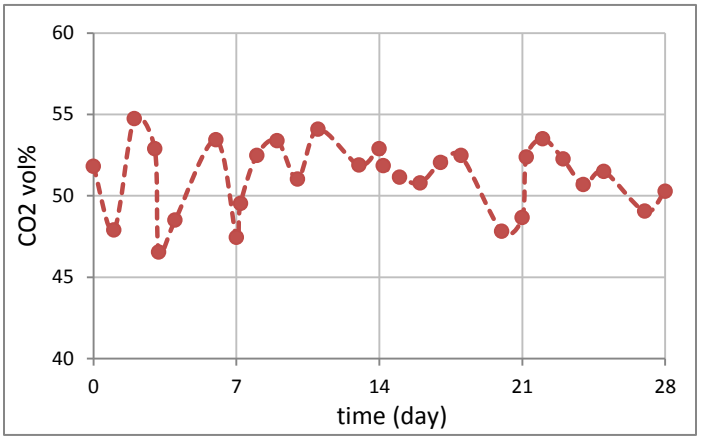

Figure B2 CO_2 vol% over time.

Appendix C FTIR Method

C1 $CaCO_3$-ASTM Sand Calibration Curves

Figure C1 Calibration curve of June 1st, 2009 for peaks at 875 and 1420 cm^{-1}.

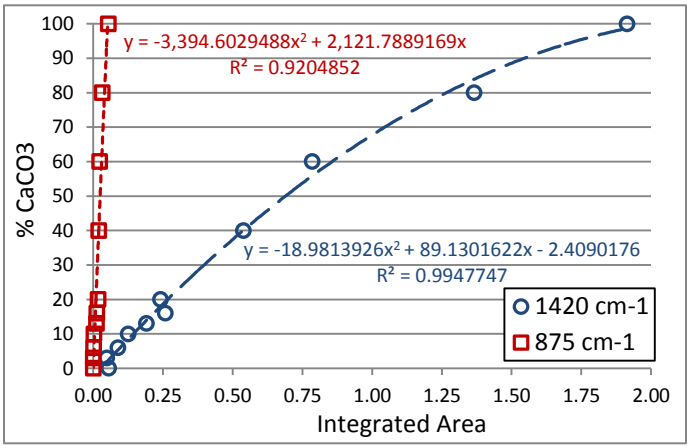

Figure C1.

Figure C2 Calibration curve of July 25th, 2009 for peaks at 875 and 1420 cm^{-1}.

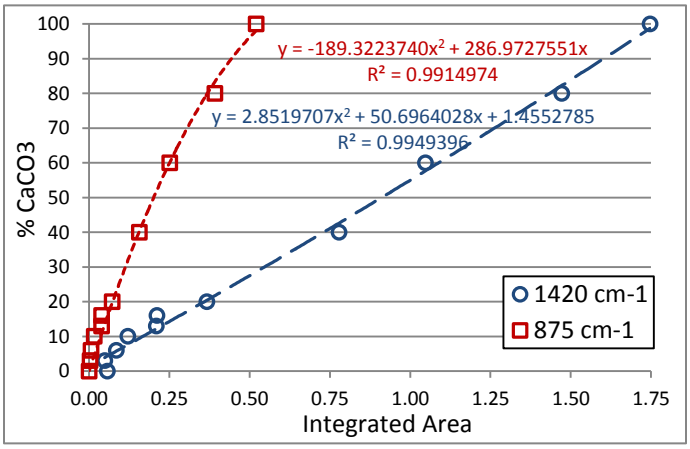

Figure C2.

Figure C3 Calibration curve of August 10th, 2009 for peaks at 875 and 1420 cm^{-1}.

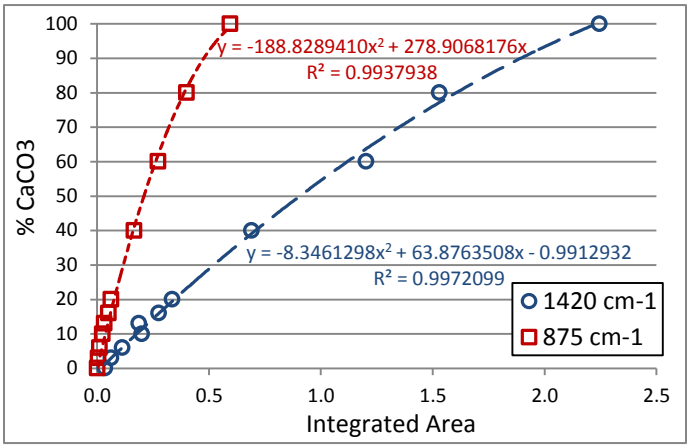

Figure C3.

Figure C4 Calibration curve of August 27th, 2009 for peaks at 875 and 1420 cm^{-1}.

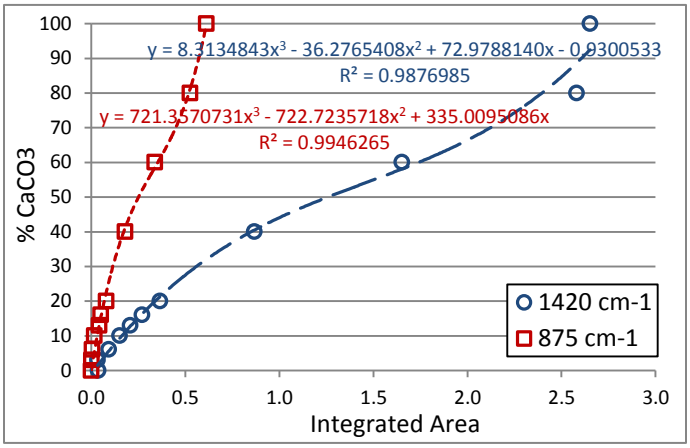

Figure C4.

Figure C5 Calibration curve of September 13th, 2009 for peaks at 875 and 1420 cm^{-1}.

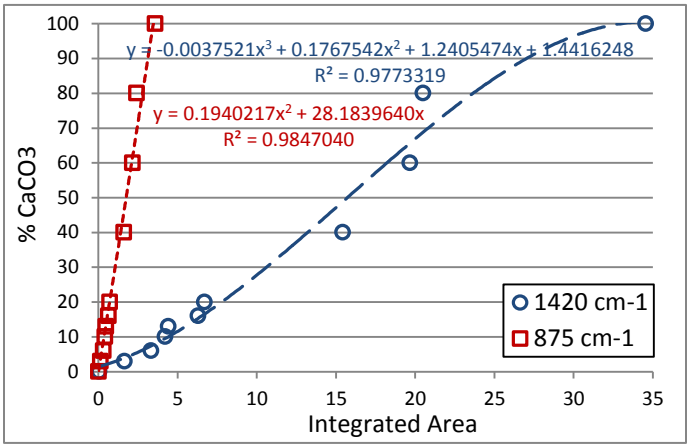

Figure C5.

Figure C6 Calibration curve of October 12th, 2009 for peaks at 875 and 1420 cm^{-1}.

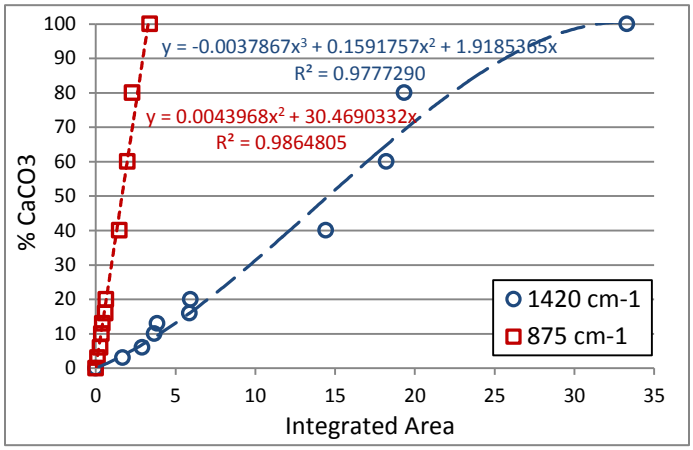

Figure C6.

Figure C7 Calibration curve of November 9th, 2009 for peaks at 875 and 1420 cm^{-1}.

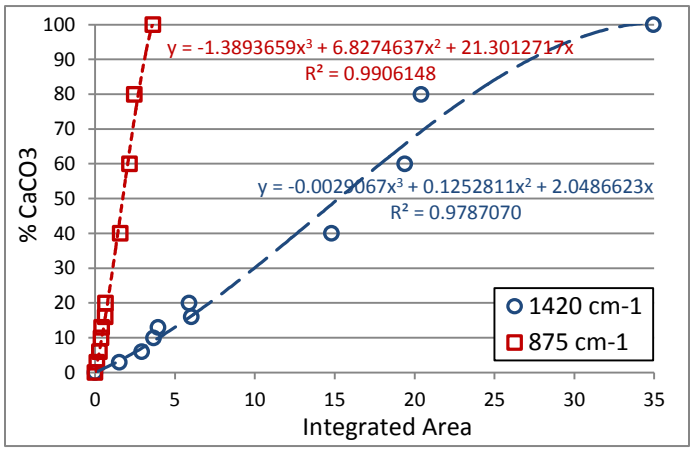

Figure C7.

Figure C8 Calibration curve of December 12th, 2009 for peaks at 875 and 1420 cm^{-1}.

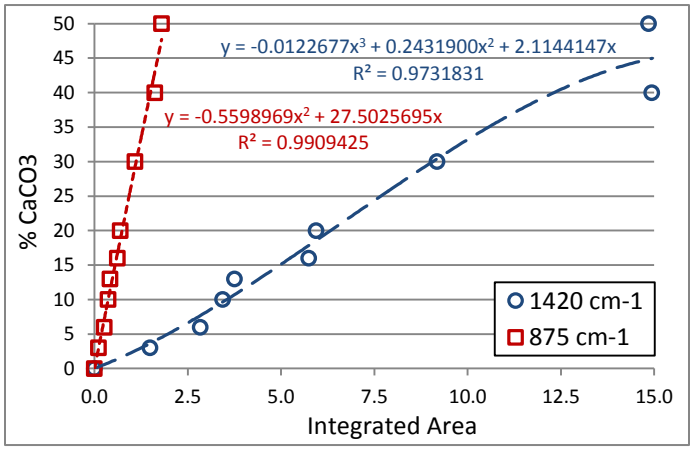

Figure C8.

Figure C9 Calibration curve of January 24th, 2010 for peaks at 875 and 1420 cm^{-1}.

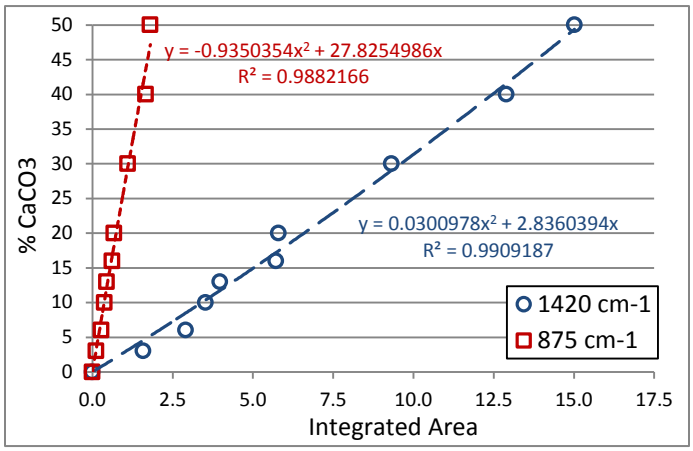

Figure C9.

Figure C10 Calibration curve of February 26th, 2010 for peaks at 875 and 1420 cm^{-1}.

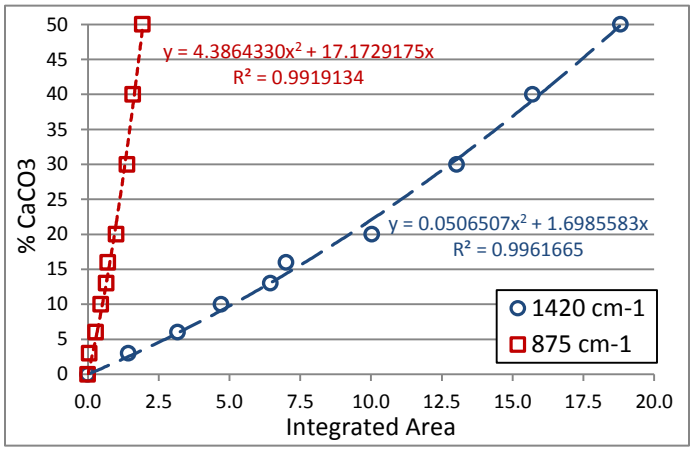

Figure C10.

Figure C11 Calibration curve of April 14th, 2010 for peaks at 875 and 1420 cm^{-1}.

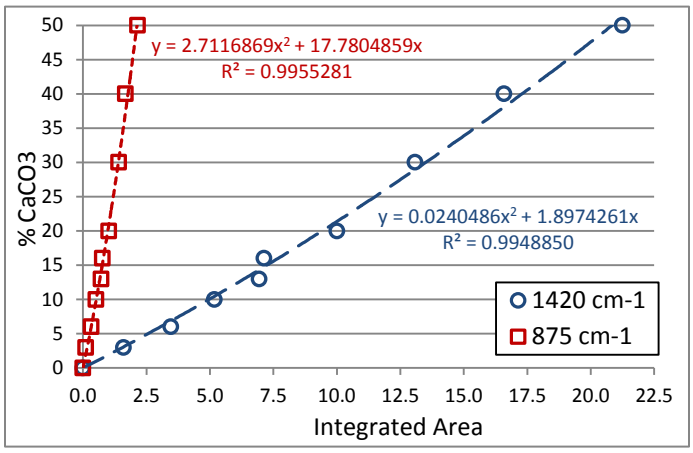

Figure C11.

Figure C12 Calibration curve of May 15th, 2010 for peaks at 875 and 1420 cm^{-1}.

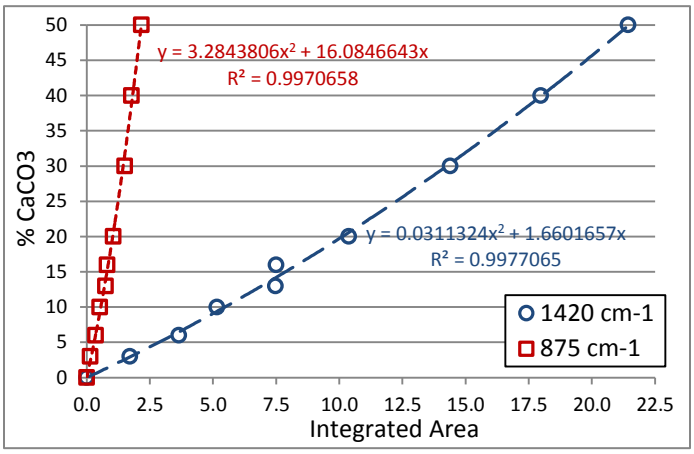

Figure C12.

Figure C13 Calibration curve of July 19th, 2010 for peaks at 875 and 1420 cm^{-1}.

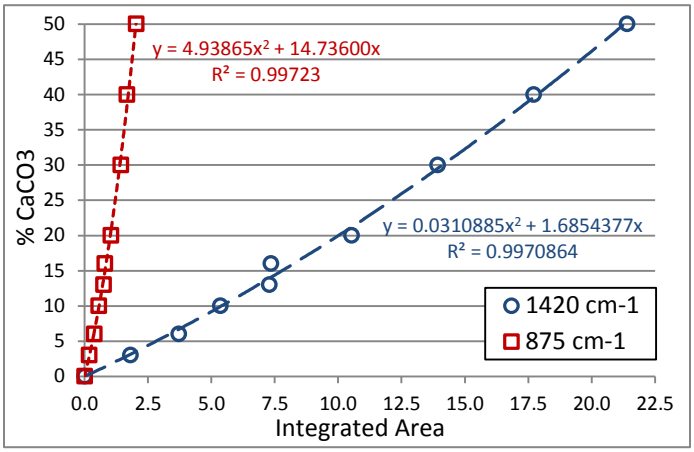

Figure C13.

C2 Assessment of Carbonation Depth. Sample Calculations

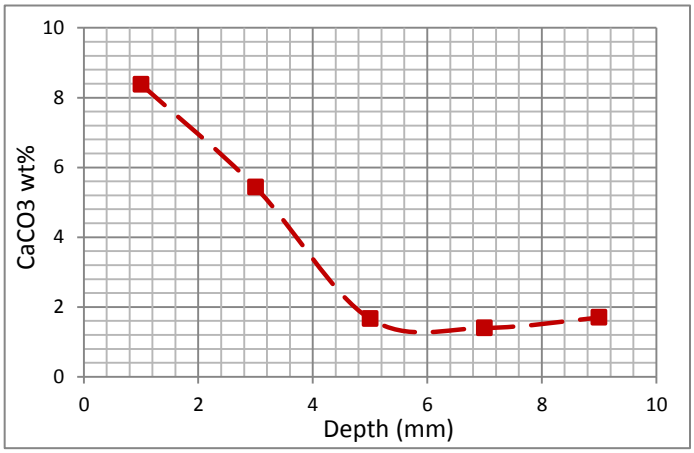

Figure C14 1-day carbonated. 0% cement replacement by FA. Replicate number 1. Calibration curve of November 9th, 2009 was used to calculate $CaCO_3$ concentrations. Estimated carbonation depth = *4.00 mm*.

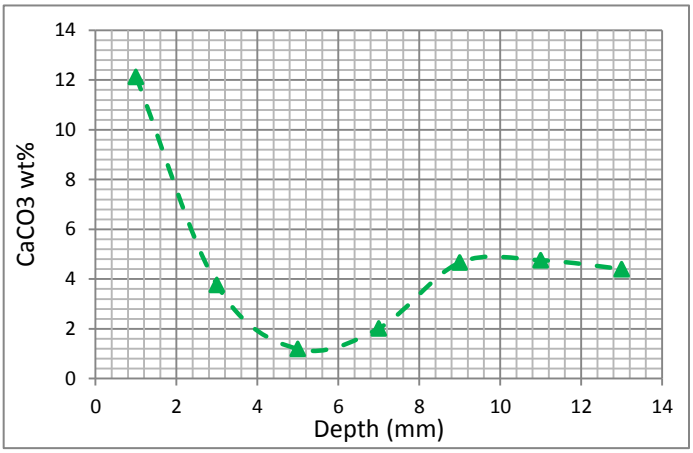

Figure C15 1-day carbonated. 20% cement replacement by FA. Replicate number 1. Calibration curve of February 26th, 2010. Estimated carbonation depth = *2.00 mm*

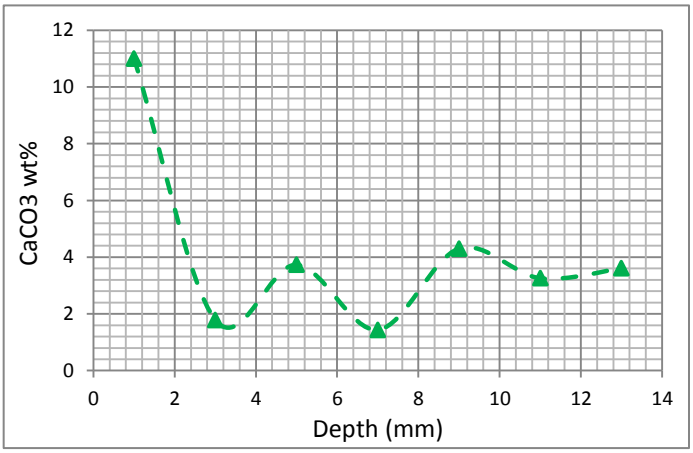

Figure C16 1-day carbonated. 20% cement replacement by FA. Replicate number 2. Calibration curve of February 26th, 2010. Estimated carbonation depth = *2.00 mm*

.

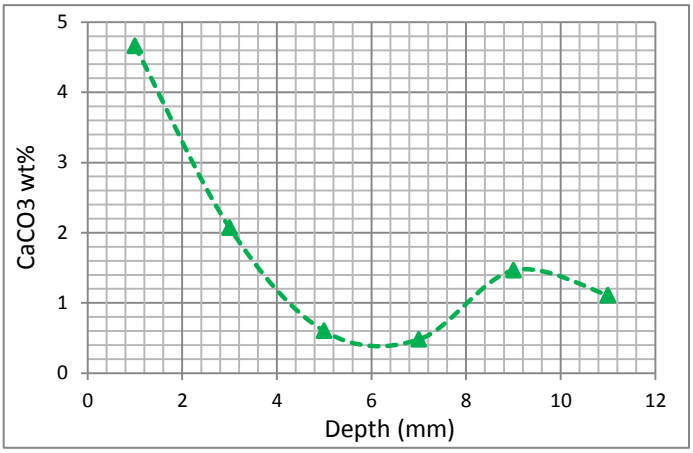

Figure C17 1-day carbonated. 20% cement replacement by FA. Replicate number 3. Calibration curve of May 15th, 2010. Estimated carbonation depth = *3.90 mm*

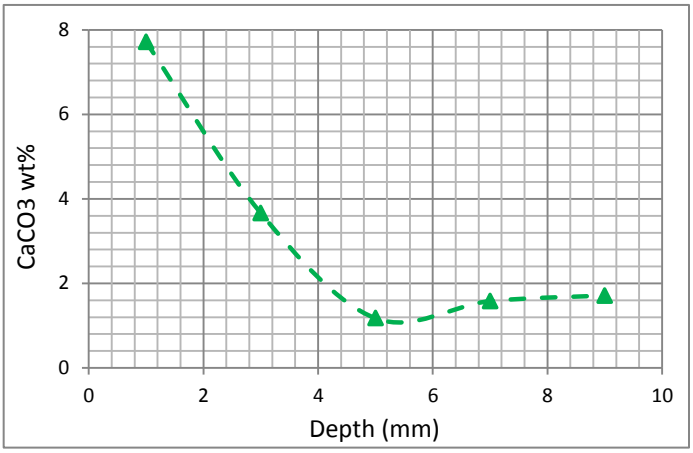

Figure C18 1-day carbonated. 20% cement replacement by FA. Replicate number 4. Calibration curve of November 9th, 2009. Estimated carbonation depth = *4.00 mm*

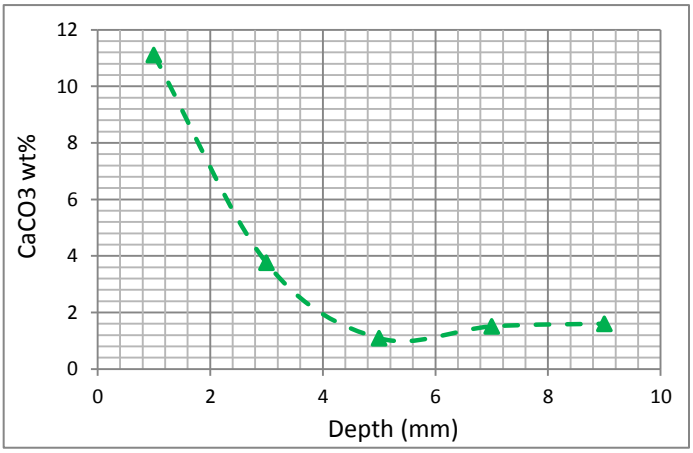

Figure C19 1-day carbonated. 20% cement replacement by FA. Replicate number 5. Calibration curve of November 9th, 2009. Estimated carbonation depth = *3.60 mm*

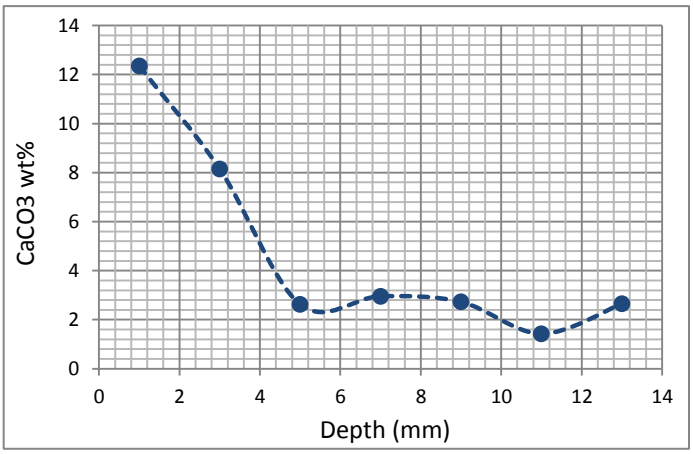

Figure C20 1-day carbonated. 40% cement replacement by FA. Replicate number 1. Calibration curve of December 12th, 2009. Estimated carbonation depth = *4.00 mm*

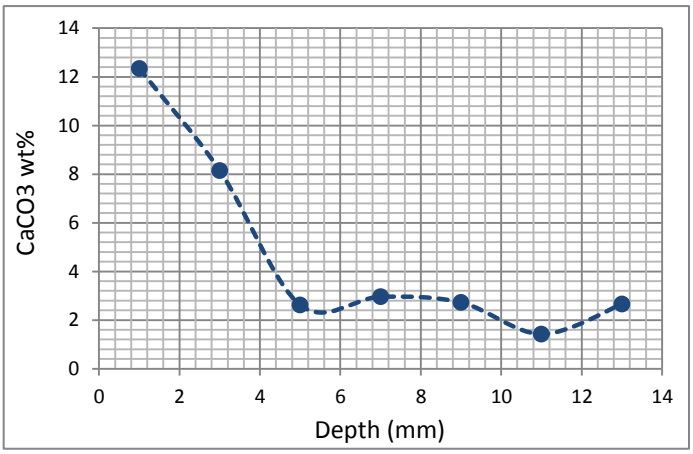

Figure C21 1-day carbonated. 40% cement replacement by FA. Replicate number 2. Calibration curve of December 12th, 2009. Estimated carbonation depth = *4.00 mm*

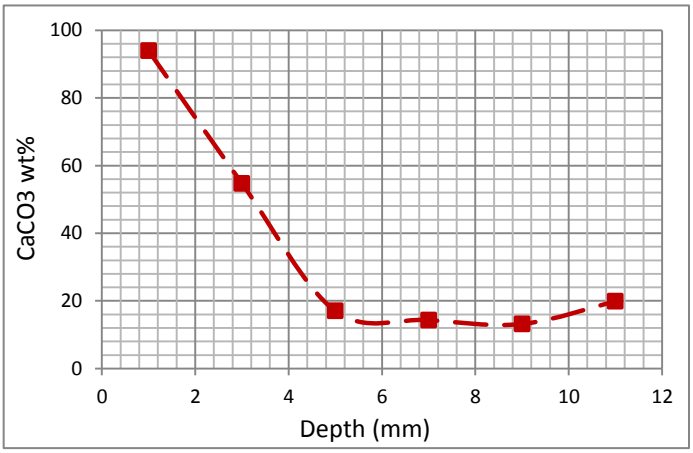

Figure C22 3-day carbonated. 0% cement replacement by FA. Replicate number 1. Calibration curve of July 25th, 2009. Estimated carbonation depth = *4.00 mm*

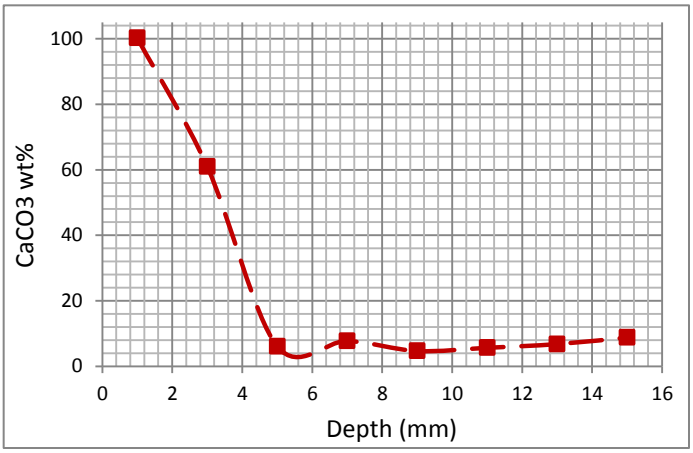

Figure C23 3-day carbonated. 0% cement replacement by FA. Replicate number 2. Calibration curve of June 1st, 2009. Estimated carbonation depth = *4.00 mm*

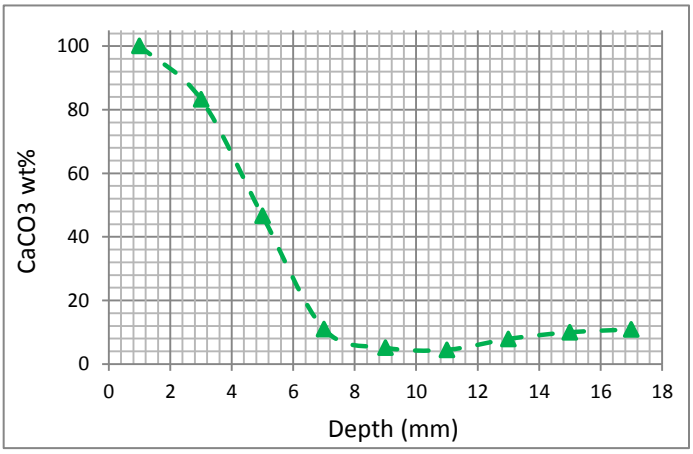

Figure C24 3-day carbonated. 20% cement replacement by FA. Replicate number 1. Calibration curve of June 1st, 2009. Estimated carbonation depth = *7.20 mm*

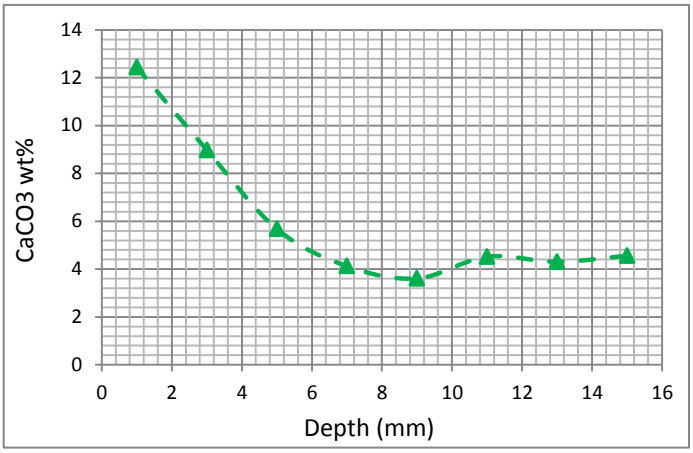

Figure C25 3-day carbonated. 20% cement replacement by FA. Replicate number 2. Calibration curve of April 14th, 2010. Estimated carbonation depth = *5.90 mm*

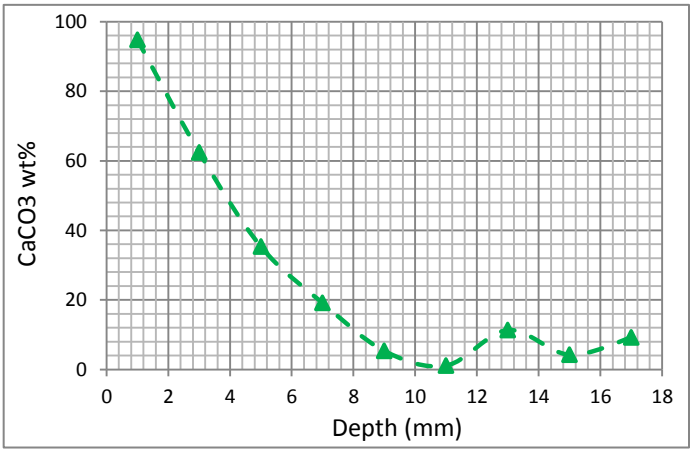

Figure C26 3-day carbonated. 20% cement replacement by FA. Replicate number 3. Calibration curve of June 1st, 2009. Estimated carbonation depth = *8.00 mm*

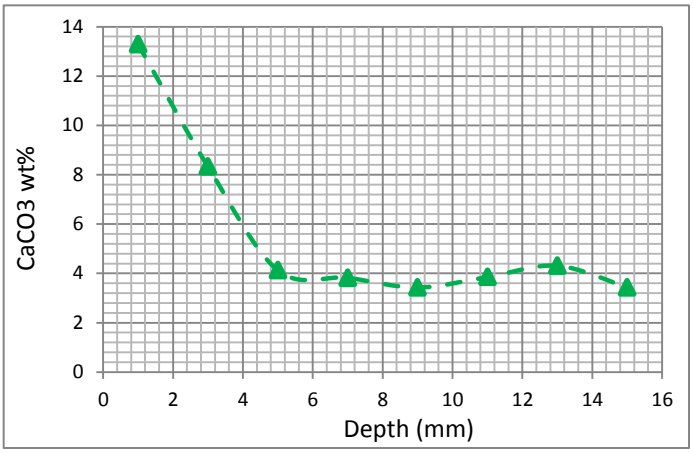

Figure C27 3-day carbonated. 20% cement replacement by FA. Replicate number 4. Calibration curve of April 14th, 2010. Estimated carbonation depth = *5.20 mm*

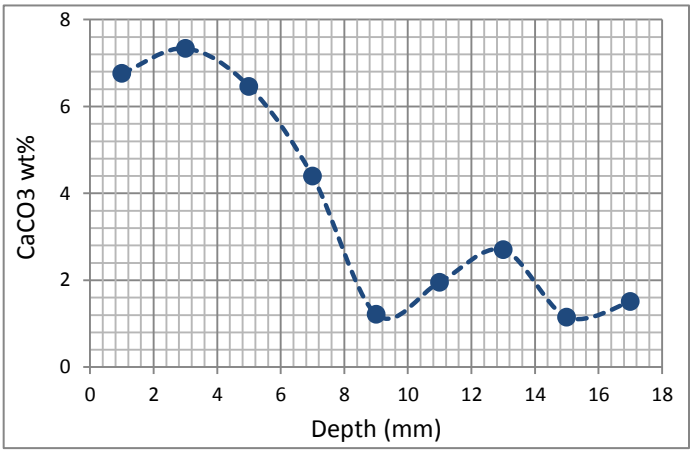

Figure C28 3-day carbonated. 40% cement replacement by FA. Replicate number 1. Calibration curve of May 15th, 2010. Estimated carbonation depth = *8.00 mm*

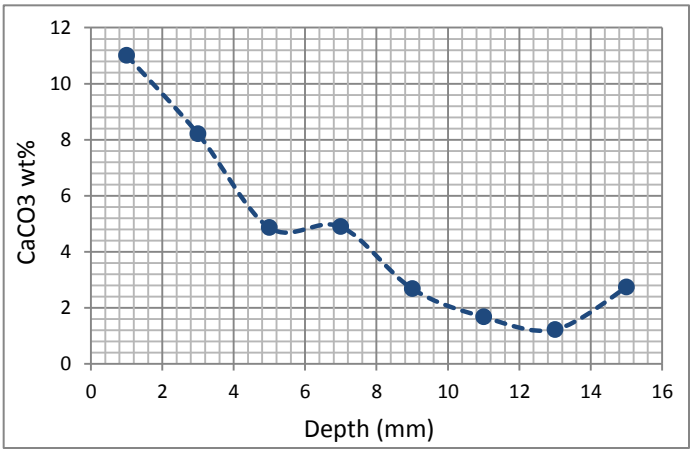

Figure C29 3-day carbonated. 40% cement replacement by FA. Replicate number 2. Calibration curve of December 12th, 2009. Estimated carbonation depth = *8.00 mm*

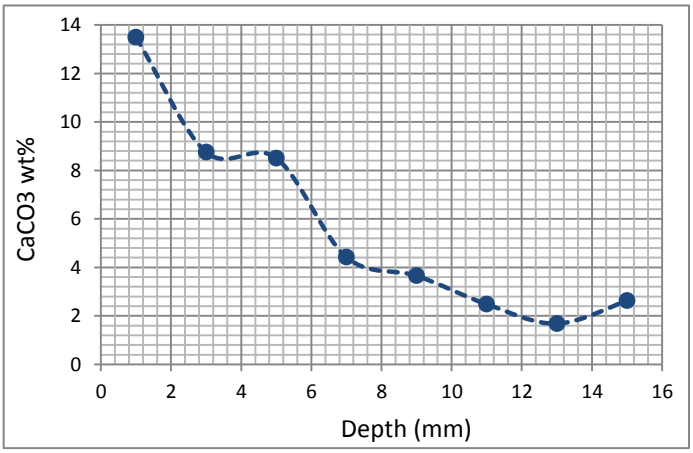

Figure C30 3-day carbonated. 40% cement replacement by FA. Replicate number 3. Calibration curve of December 12th, 2009. Estimated carbonation depth = *10.00 mm*

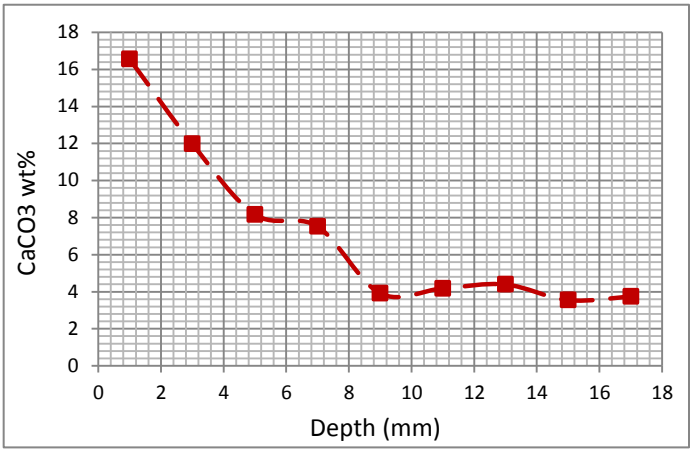

Figure C31 7-day carbonated. 0% cement replacement by FA. Replicate number 1. Calibration curve of April 14th, 2010. Estimated carbonation depth = *8.00 mm*

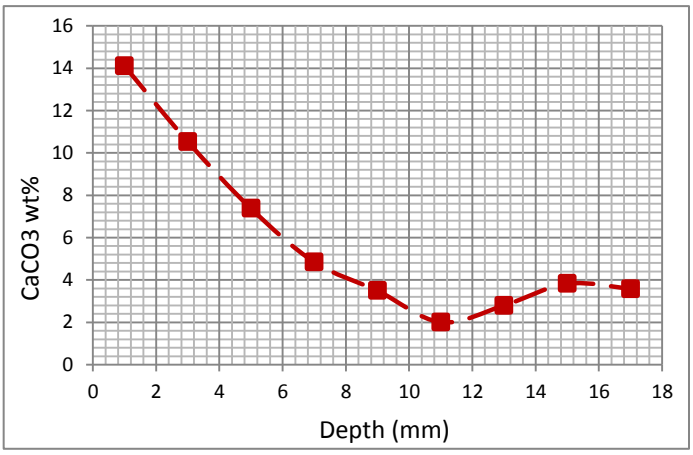

Figure C32 7-day carbonated. 0% cement replacement by FA. Replicate number 2. Calibration curve of May 15th, 2010. Estimated carbonation depth = *8.35 mm*

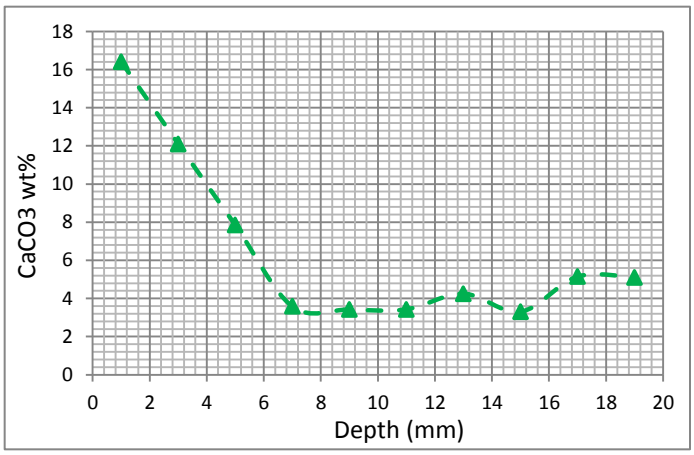

Figure C33 7-day carbonated. 20% cement replacement by FA. Replicate number 1. Calibration curve of April 14th, 2010. Estimated carbonation depth = *6.00 mm*

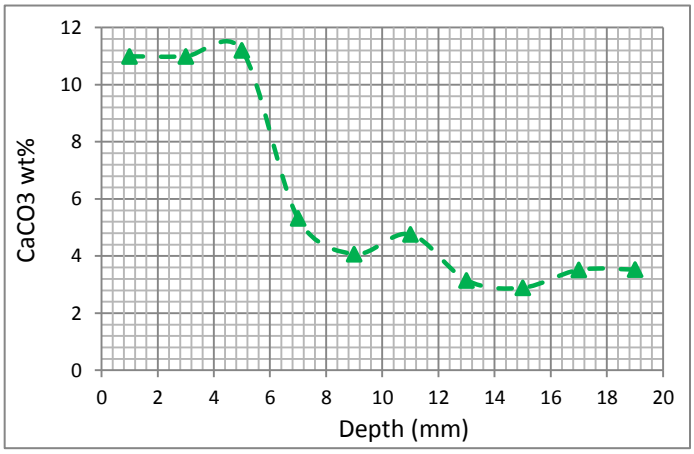

Figure C34 7-day carbonated. 20% cement replacement by FA. Replicate number 2. Calibration curve of April 14th, 2010. Estimated carbonation depth = *11.85 mm*

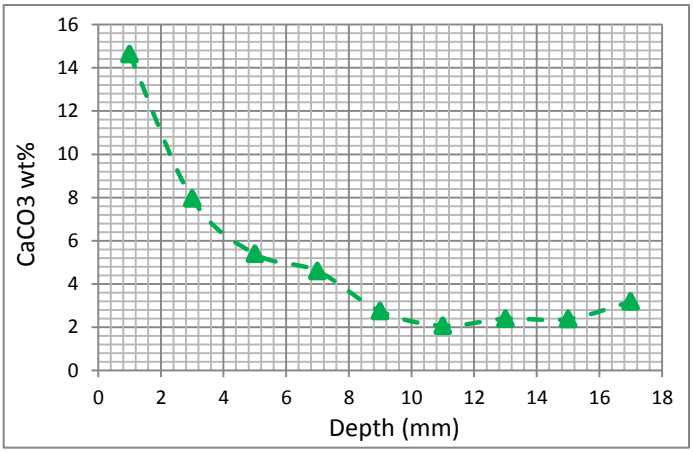

Figure C35 7-day carbonated. 20% cement replacement by FA. Replicate number 3. Calibration curve of May 15th, 2010. Estimated carbonation depth = *8.00 mm*

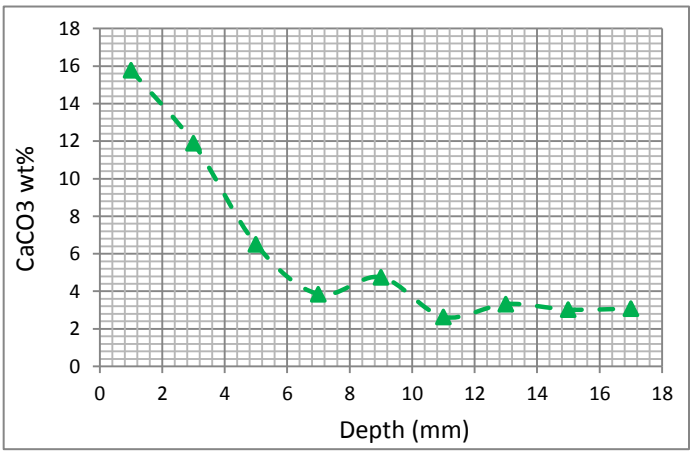

Figure C36 7-day carbonated. 20% cement replacement by FA. Replicate number 4. Calibration curve of April 14th, 2010. Estimated carbonation depth = *10.00* mm

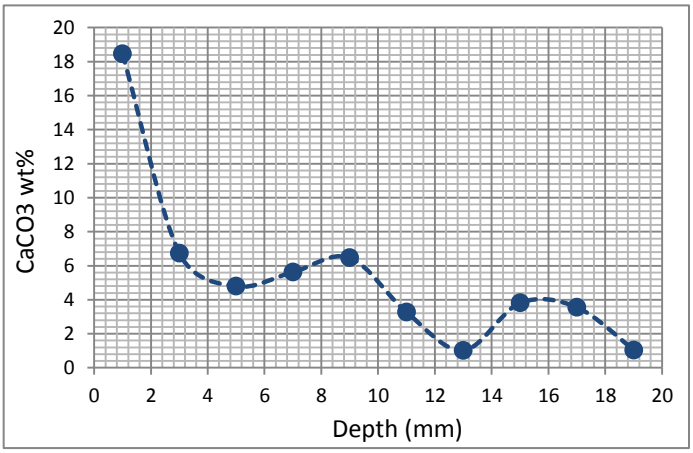

Figure C37 7-day carbonated. 40% cement replacement by FA. Replicate number 1. Calibration curve of May 15th, 2010. Estimated carbonation depth = *10.00 mm*

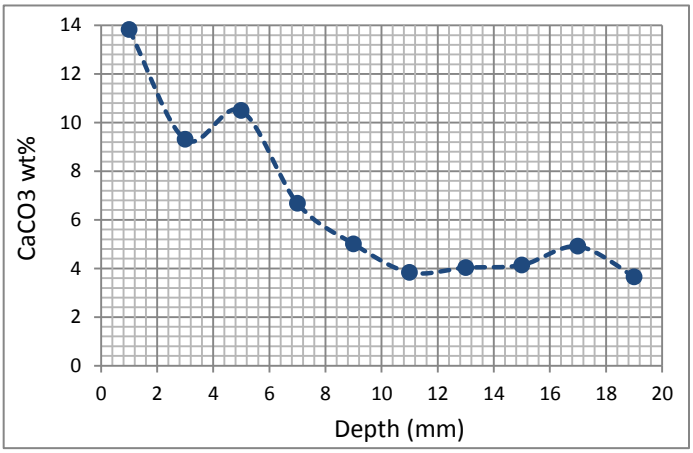

Figure C38 7-day carbonated. 40% cement replacement by FA. Replicate number 2. Calibration curve of May 15th, 2010. Estimated carbonation depth = *9.80 mm*

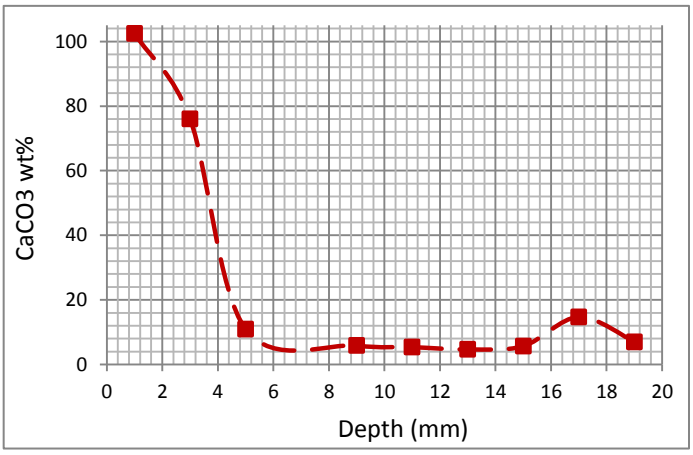

Figure C39 14-day carbonated. 0% cement replacement by FA. Replicate number 1. Calibration curve of July 25th, 2009. Estimated carbonation depth = *7.15 mm*

.

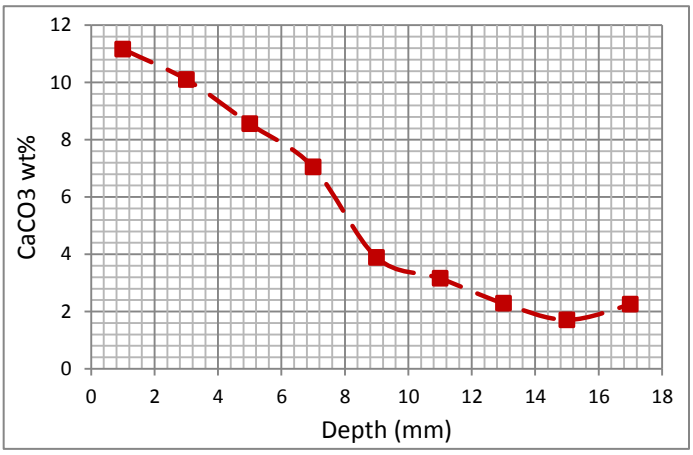

Figure C40 14-day carbonated. 0% cement replacement by FA. Replicate number 2. Calibration curve of July 19th, 2010. Estimated carbonation depth = *12.00 mm*

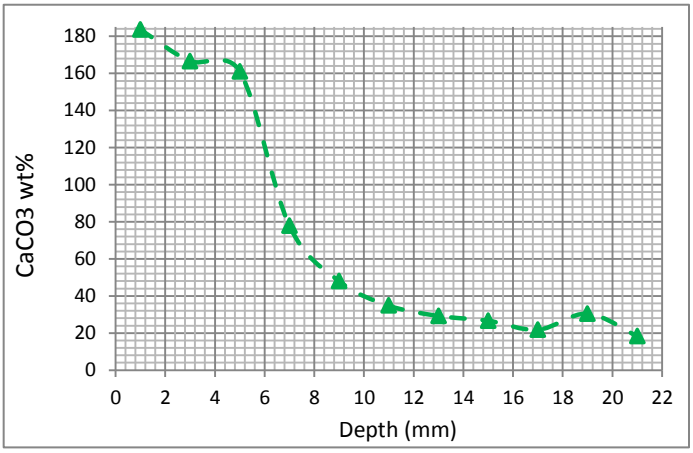

Figure C41 14-day carbonated. 20% cement replacement by FA. Replicate number 1. Calibration curve of August 27th, 2009. Estimated carbonation depth = *12.00 mm*

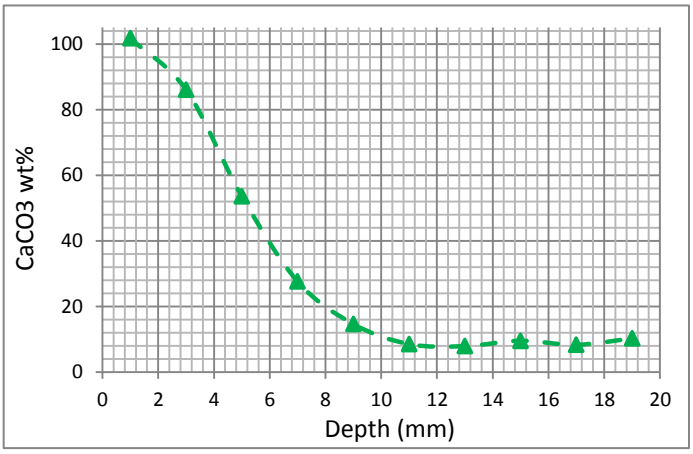

Figure C42 14-day carbonated. 20% cement replacement by FA. Replicate number 2. Calibration curve of June 1st, 2009. Estimated carbonation depth = *9.70 mm*

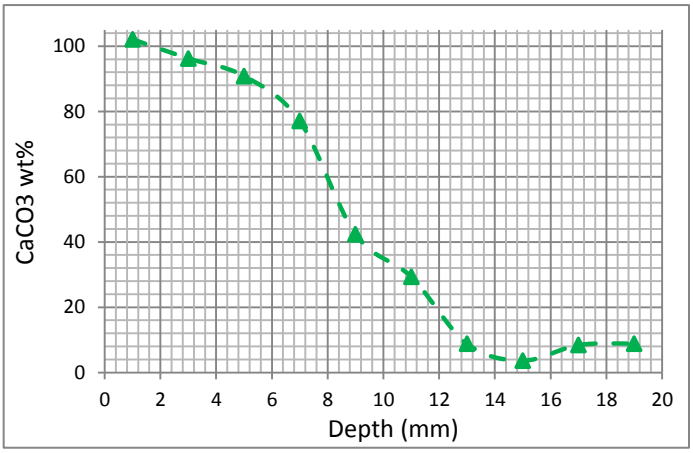

Figure C43 14-day carbonated. 20% cement replacement by FA. Replicate number 3. Calibration curve of June 1st, 2009. Estimated carbonation depth = *12.00 mm*

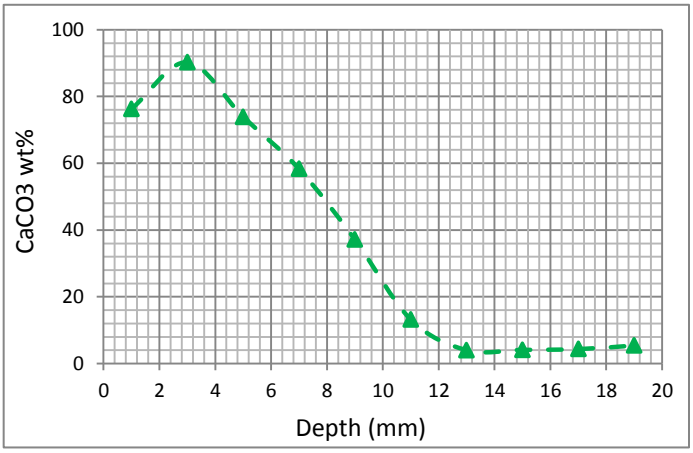

Figure C44 14-day carbonated. 20% cement replacement by FA. Replicate number 4. Calibration curve of August 10th, 2009. Estimated carbonation depth = *11.75 mm*

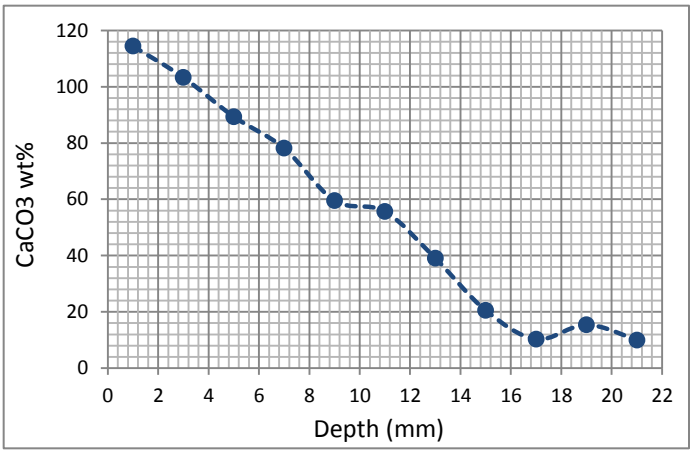

Figure C45 14-day carbonated. 40% cement replacement by FA. Replicate number 1. Calibration curve of July 25th, 2009. Estimated carbonation depth = *15.00 mm*

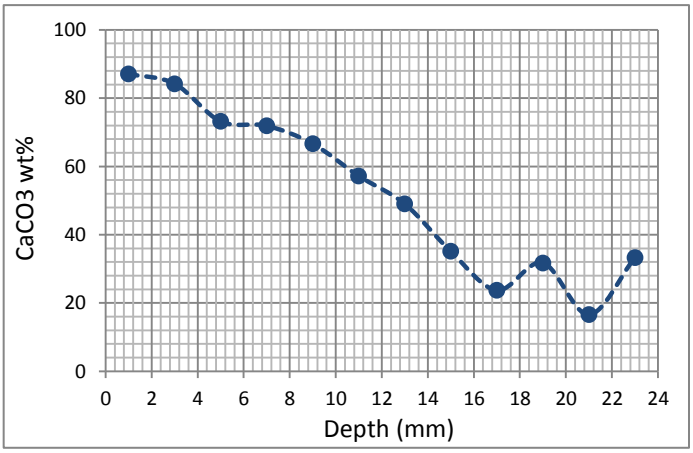

Figure C46 14-day carbonated. 40% cement replacement by FA. Replicate number 2. Calibration curve of August 27th, 2009. Estimated carbonation depth = *16.00 mm*

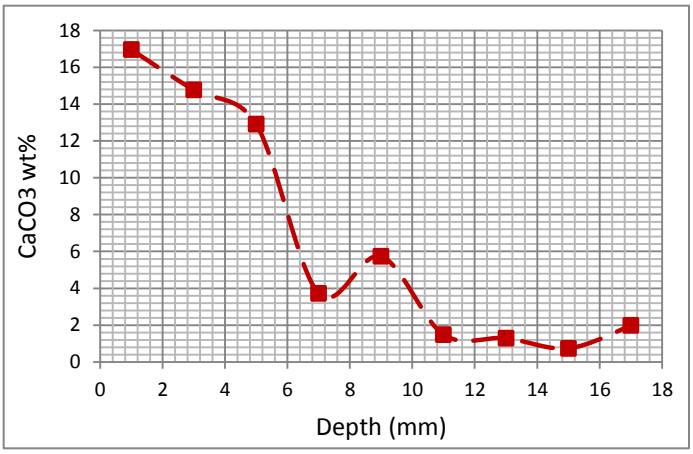

Figure C47 21-day carbonated. 0% cement replacement by FA. Replicate number 1. Calibration curve of February 26th, 2010. Estimated carbonation depth = *10.00 mm*

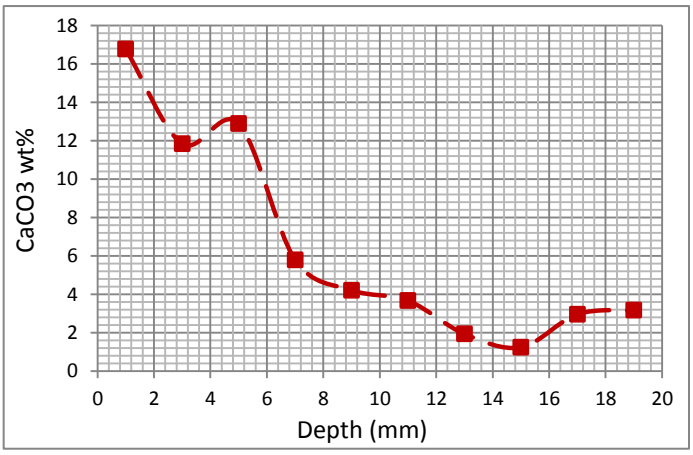

Figure E48 21-day carbonated. 0% cement replacement by FA. Replicate number 2. Calibration curve of February 26th, 2010. Estimated carbonation depth = *12.00 mm*

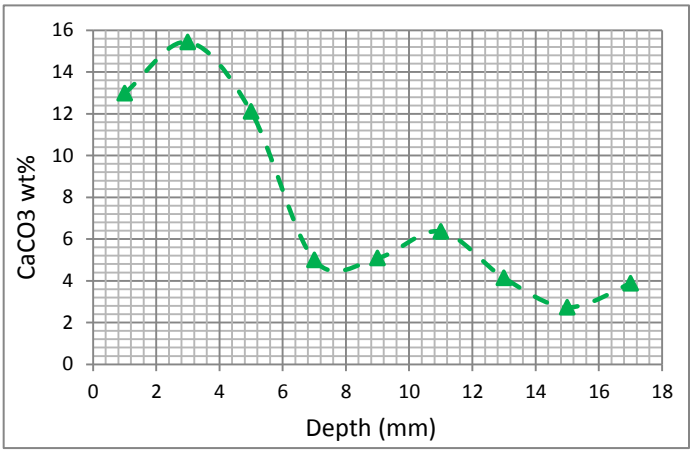

Figure C49 21-day carbonated. 20% cement replacement by FA. Replicate number 1. Calibration curve of February 26th, 2010. Estimated carbonation depth = *14.00 mm*

.

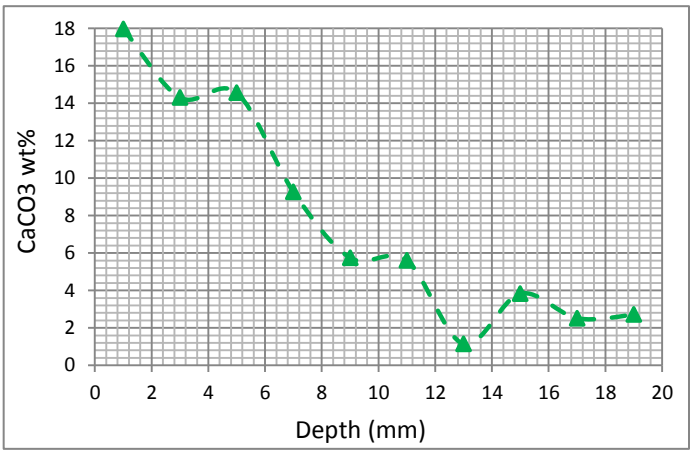

Figure C50 21-day carbonated. 20% cement replacement by FA. Replicate number 2. Calibration curve of February 26th, 2010. Estimated carbonation depth = *12.00 mm*

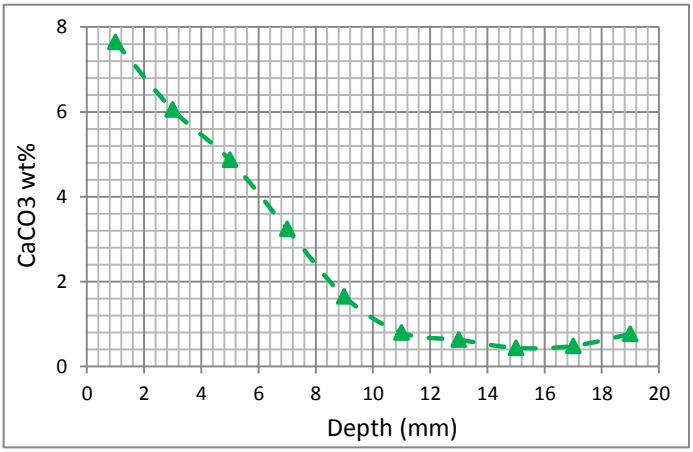

Figure C51 21-day carbonated. 20% cement replacement by FA. Replicate number 3. Calibration curve of July 19th, 2010. Estimated carbonation depth = *11.40 mm*

.

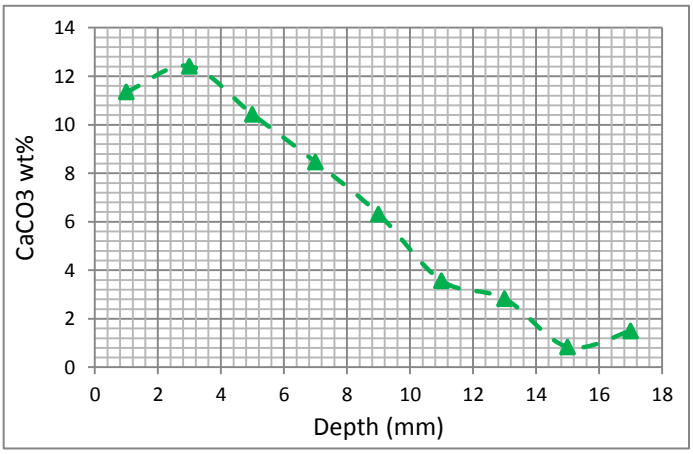

Figure C52 21-day carbonated. 20% cement replacement by FA. Replicate number 4. Calibration curve of February 26th, 2010. Estimated carbonation depth = *14.00 mm*

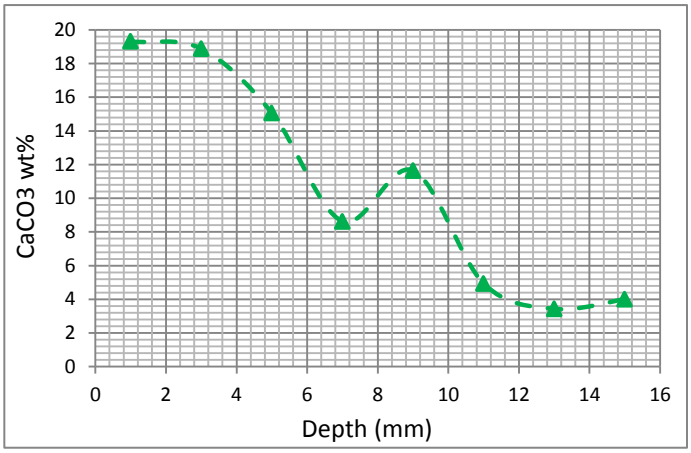

Figure C53 21-day carbonated. 20% cement replacement by FA. Replicate number 5. Calibration curve of January 24th, 2010. Estimated carbonation depth = *11.40 mm*

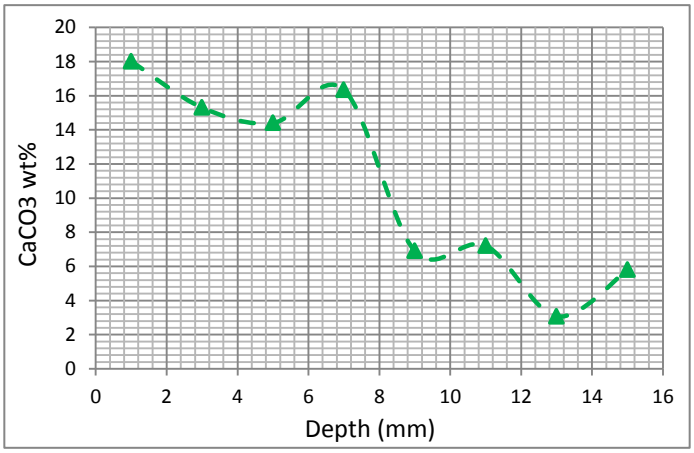

Figure C54 21-day carbonated. 20% cement replacement by FA. Replicate number 6. Calibration curve of January 24th, 2010. Estimated carbonation depth = *12.00 mm*

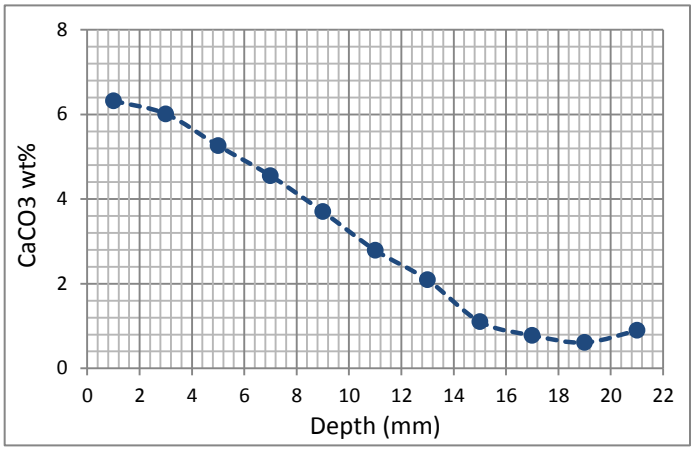

Figure C55 21-day carbonated. 40% cement replacement by FA. Replicate number 1. Calibration curve of July 19th, 2010. Estimated carbonation depth = *16.0 mm*

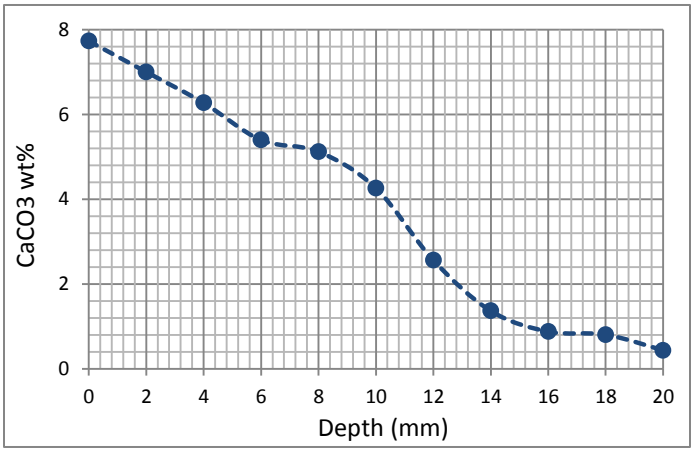

Figure C56 21-day carbonated. 40% cement replacement by FA. Replicate number 2. Calibration curve of July 19th, 2010. Estimated carbonation depth = *15.90 mm*

.

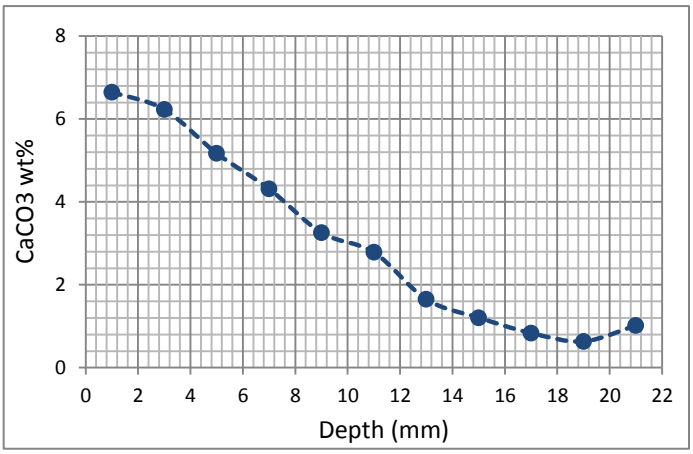

Figure C57 21-day carbonated. 40% cement replacement by FA. Replicate number 3. Calibration curve of July 19th, 2010. Estimated carbonation depth = *15.85 mm*

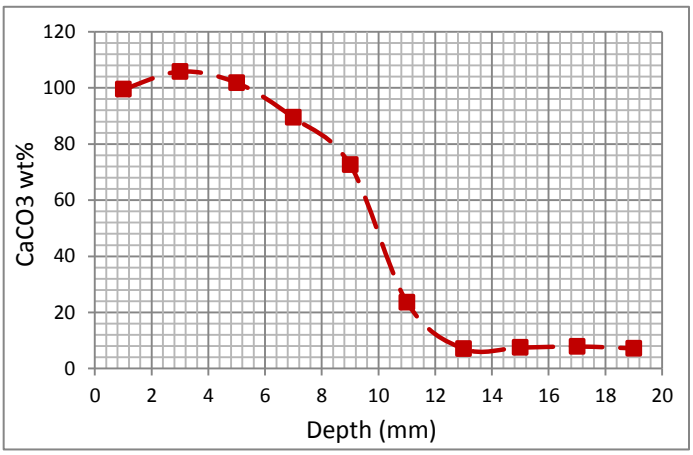

Figure C58 28-day carbonated. 0% cement replacement by FA. Replicate number 1. Calibration curve of August 10th, 2009. Estimated carbonation depth = *11.60 mm*

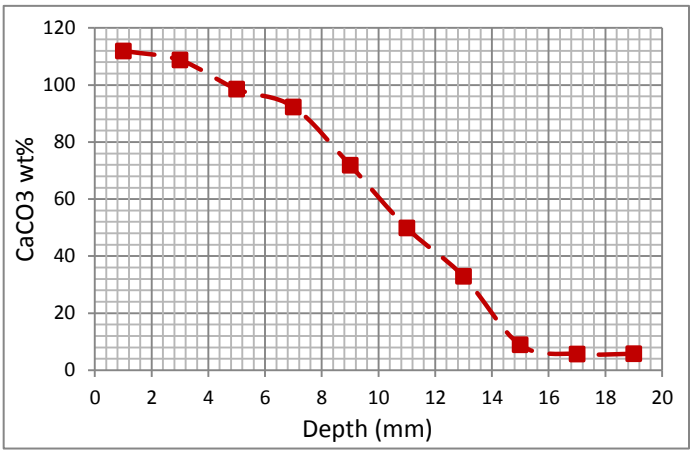

Figure C59 28-day carbonated. 0% cement replacement by FA. Replicate number 2. Calibration curve of August 10th, 2009. Estimated carbonation depth = *15.30 mm*

.

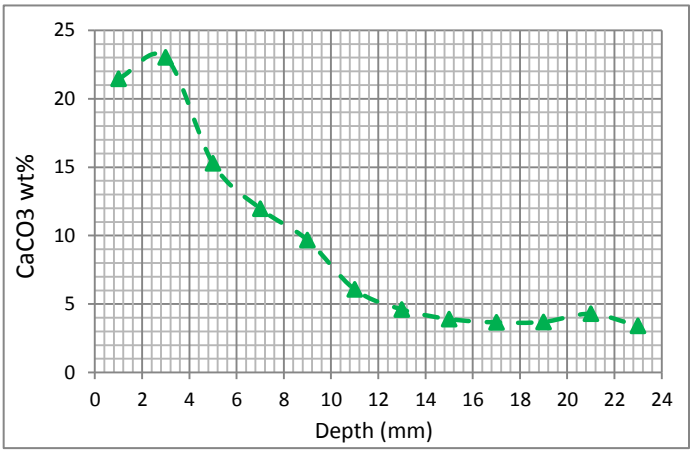

Figure C60 28-day carbonated. 20% cement replacement by FA. Replicate number 1. Calibration curve of September 13th, 2009. Estimated carbonation depth = *13.70 mm*

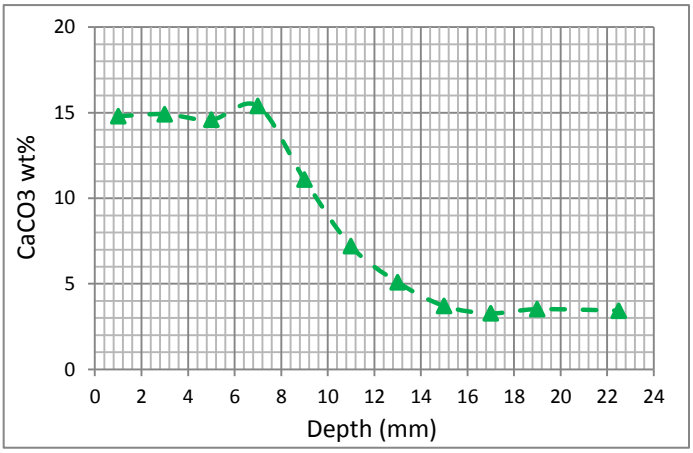

Figure C61 28-day carbonated. 20% cement replacement by FA. Replicate number 2. Calibration curve of September 13th, 2009. Estimated carbonation depth = *15.40 mm*

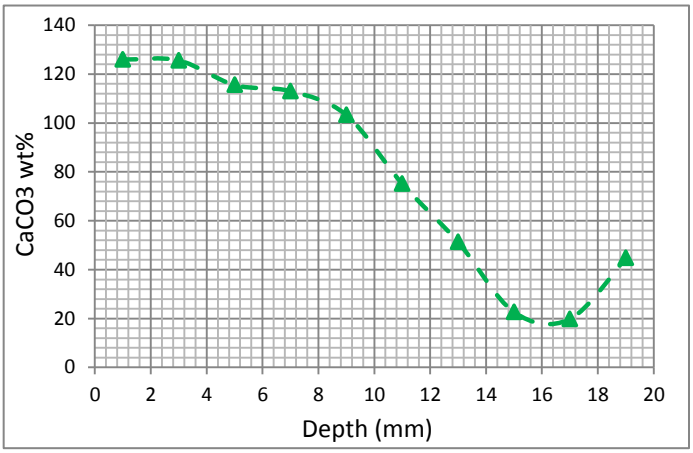

Figure C62 28-day carbonated. 20% cement replacement by FA. Replicate number 3. Calibration curve of August 27th, 2009. Estimated carbonation depth = *14.00 mm*

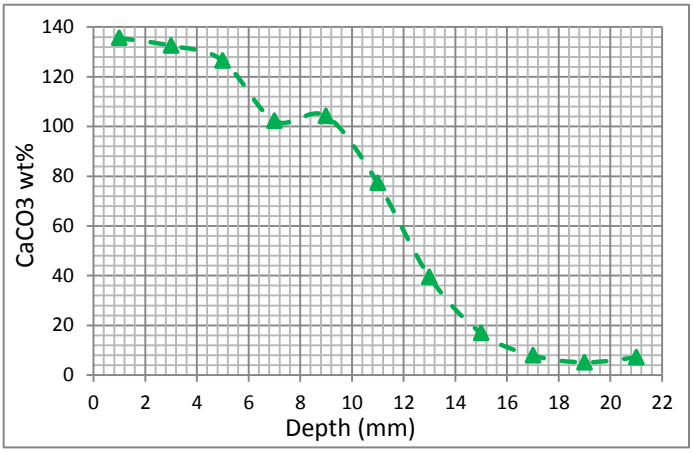

Figure C63 28-day carbonated. 20% cement replacement by FA. Replicate number 4. Calibration curve of July 25th, 2009. Estimated carbonation depth = *16.00 mm*

Appendix D Dust Digestion Method

D1 pH-meter Calibration

Three pH buffers solutions were used to calibrate the instrument to pH 7, 9 and 13. In all cases, the calibration slope of the electrode had a value ranging from 92 to 96%.

D2 Environmental Conditions

A water bath was set up at a constant temperature of 23°C. Samples and buffers were kept inside the water bath for a period of 24 hours before pH measurements.

D3 Assessment of Carbonation Depth. Sample Calculations

A series of steps were followed to determine the carbonation depth based on the mortar powder slurries. First, a baseline had to be established. The baseline represents the uncarbonated material. All slurries made out of uncarbonated mortar had pH values within a small range. As seen in Figure D1, all layers from 6-8 up to 18-20 mm depth had slurry pH averages in the 12.18 – 12.24 range. Once the baseline has been determined, a horizontal average line is drawn (Line a_1 in Figure D1). This line represents all the points of the baseline. For this particular case, the average pH is equal to 12.21. Next, pH measurements away from the baseline are fitted by a line (Line a_2 in Figure D1). The point where lines a_1 and a_2 intercept is the estimated carbonation depth, which is equal to 5.65 mm in this case. It is important to note the location of the first point of the baseline since no estimated carbonation depth can extend beyond the layer corresponding to this point.

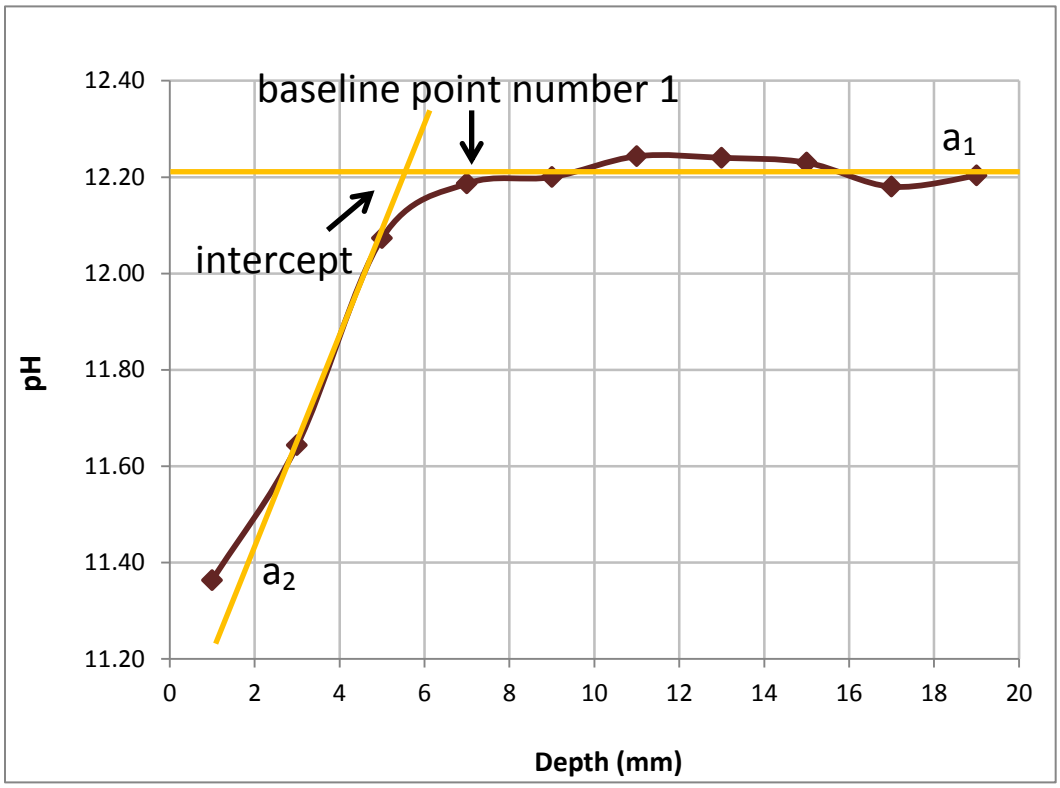

Figure D1 Assessment of the carbonation front.

D4 Experimental Data

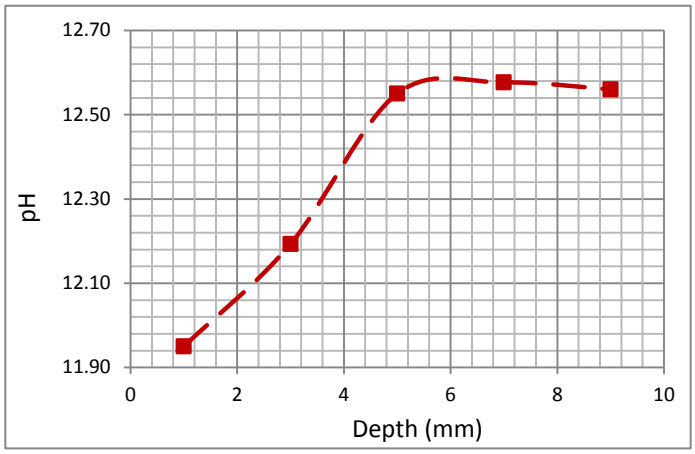

Figure D2 1-day carbonated. 0% cement replacement by FA. Replicate Number 1.

Estimated carbonation depth = *5.10 mm*

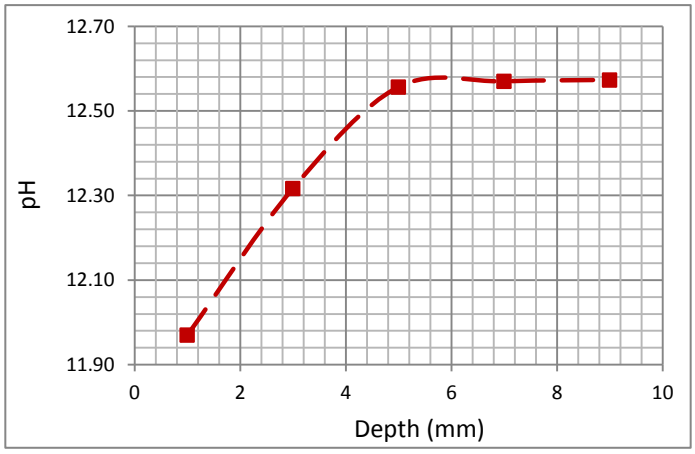

Figure D3 1-day carbonated. 0% cement replacement by FA. Replicate Number 2.

Estimated carbonation depth = *5.10 mm*

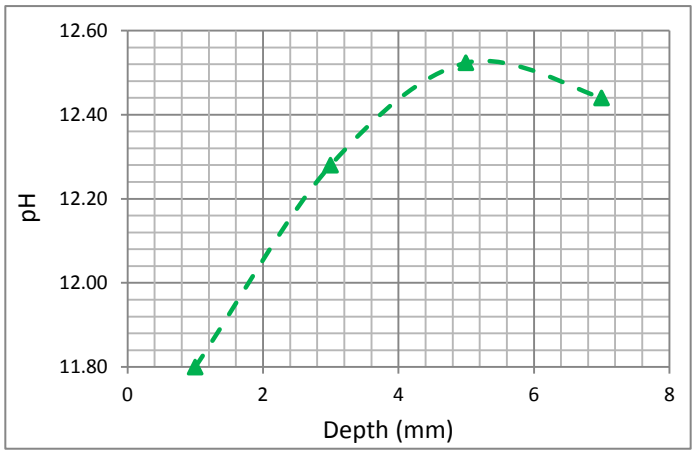

Figure D4 1-day carbonated. 20% cement replacement by FA. Replicate Number 2.

Estimated carbonation depth = *3.80 mm*

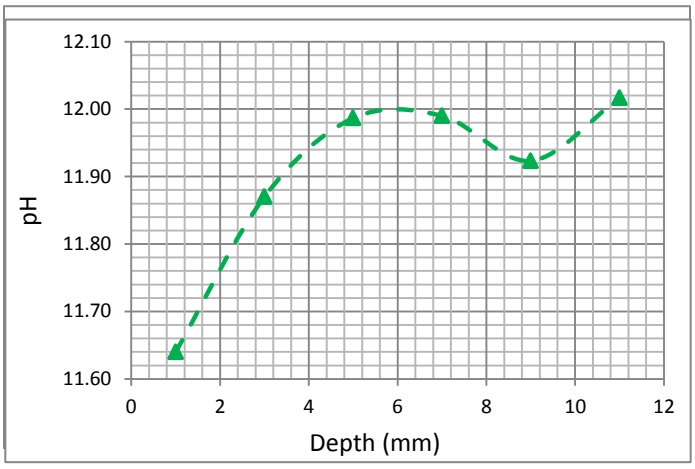

Figure D5 1-day carbonated. 20% cement replacement by FA. Replicate Number 3.

Estimated carbonation depth = *4.00 mm*

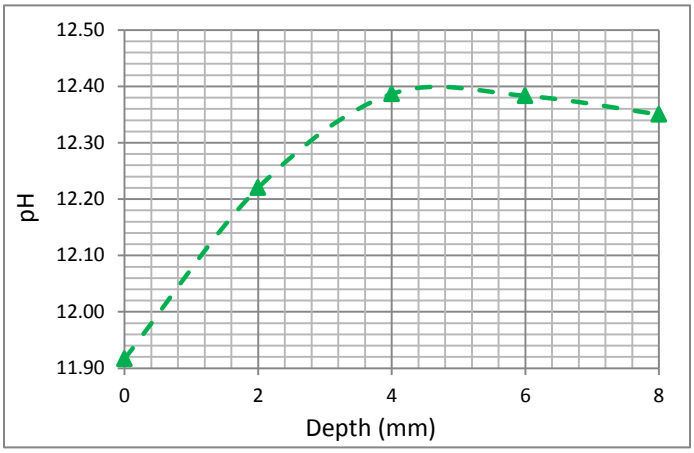

Figure D6 1-day carbonated. 20% cement replacement by FA. Replicate Number 4.

Estimated carbonation depth = *4.00 mm*

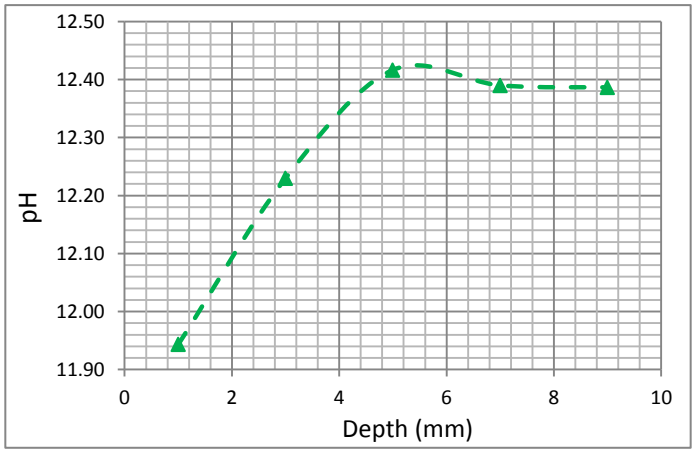

Figure D7 1-day carbonated. 20% cement replacement by FA. Replicate Number 5.

Estimated carbonation depth = *4.00 mm*

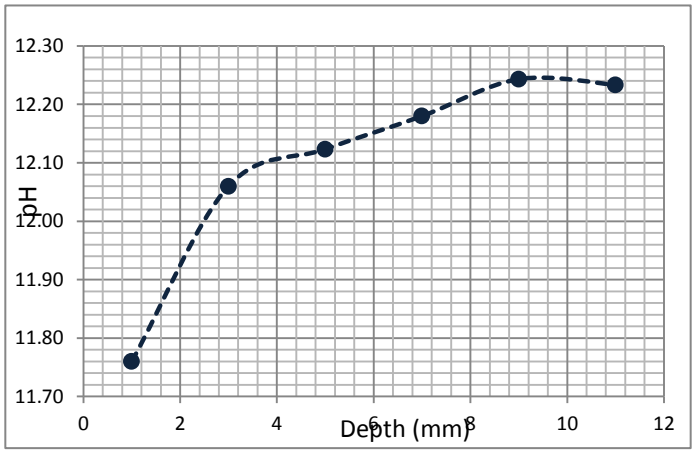

Figure D8 1-day carbonated. 40% cement replacement by FA. Replicate Number 1.

Estimated carbonation depth = *9.00 mm*

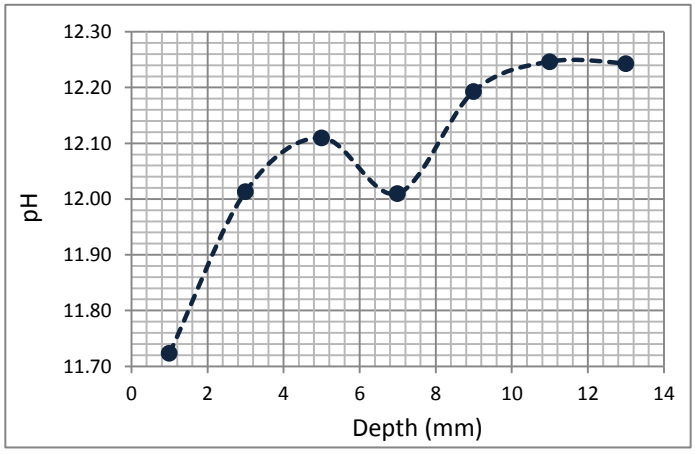

Figure D9 1-day carbonated. 40% cement replacement by FA. Replicate Number 2.

Estimated carbonation depth = *9.50 mm*

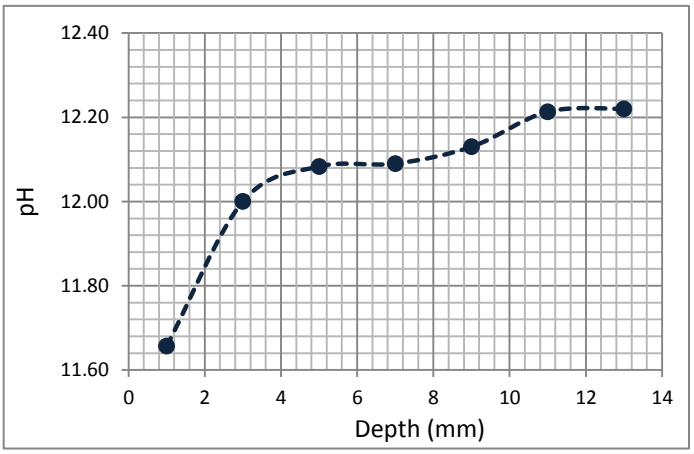

Figure D10 1-day carbonated. 40% cement replacement by FA. Replicate Number 3.

Estimated carbonation depth = *10.00 mm*

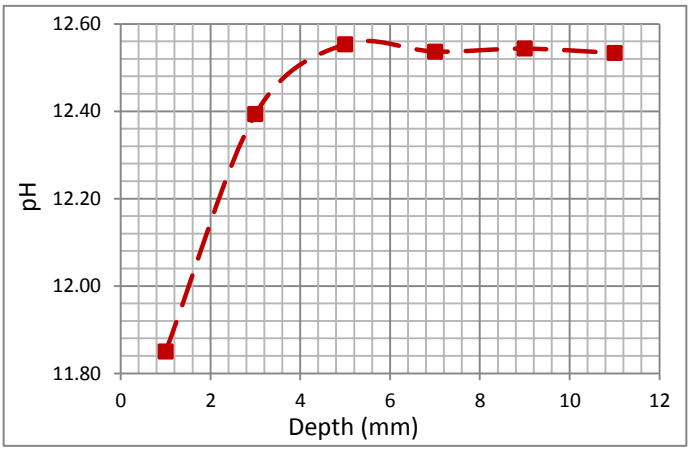

Figure D11 3-day carbonated. 0% cement replacement by FA. Replicate number 1.

Estimated carbonation depth = *3.50 mm*

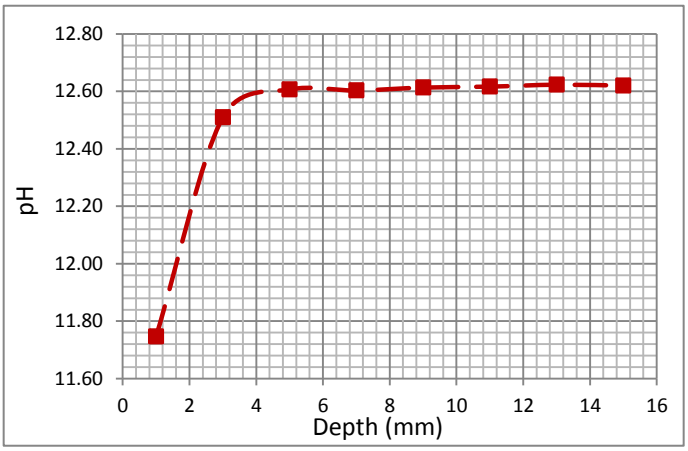

Figure D12 3-day carbonated. 0% cement replacement by FA. Replicate number 2.

Estimated carbonation depth = *3.20 mm*

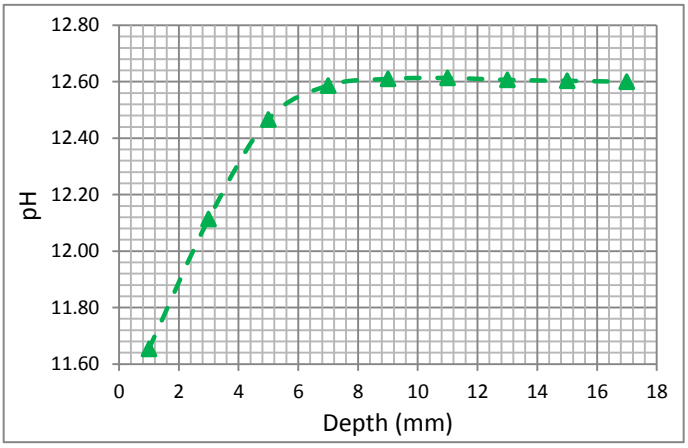

Figure D13 3-day carbonated. 20% cement replacement by FA. Replicate number 1.

Estimated carbonation depth = *7.30 mm*

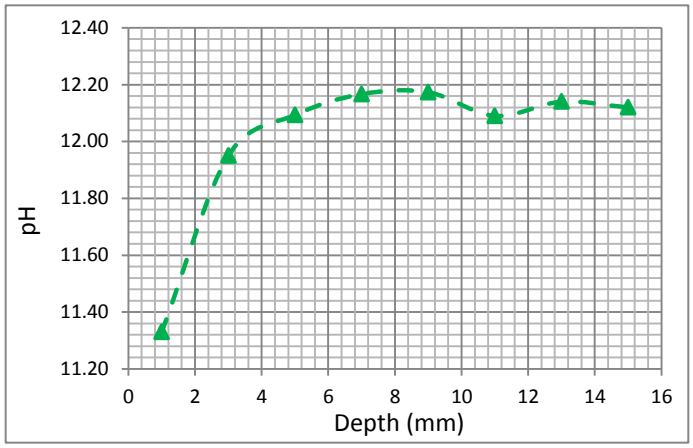

Figure D14 3-day carbonated. 20% cement replacement by FA. Replicate number 2.

Estimated carbonation depth = *3.60 mm*

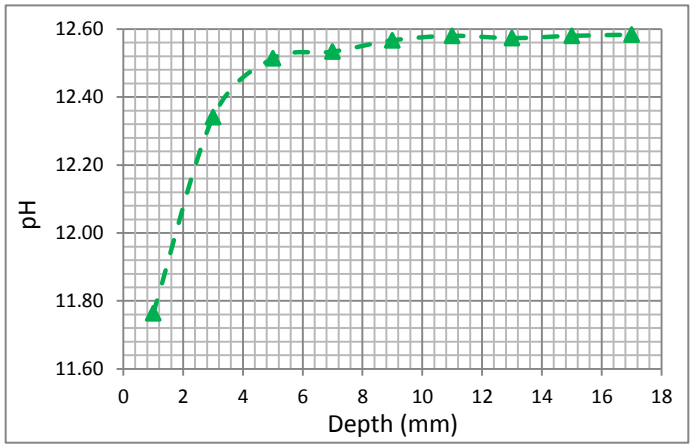

Figure D15 3-day carbonated. 20% cement replacement by FA. Replicate number 3.

Estimated carbonation depth = *8.00 mm*

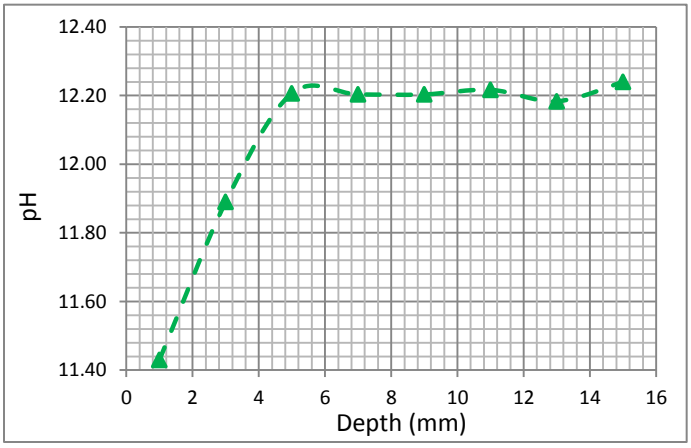

Figure D16 3-day carbonated. 20% cement replacement by FA. Replicate number 4.

Estimated carbonation depth = *4.00 mm*

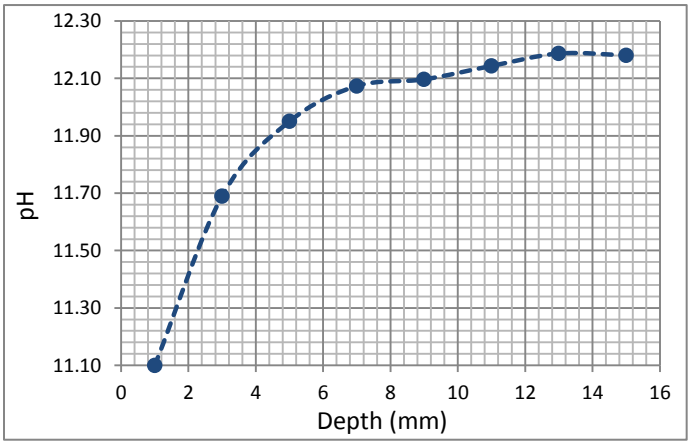

Figure D17 3-day carbonated. 40% cement replacement by FA. Replicate number 1.

Estimated carbonation depth = *12.00 mm*

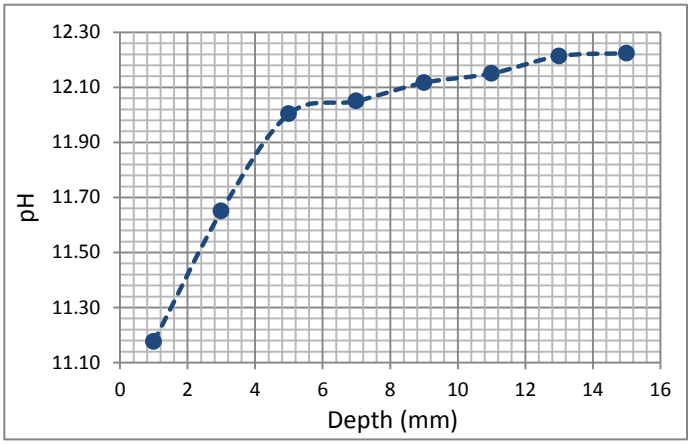

Figure D18 3-day carbonated. 40% cement replacement by FA. Replicate number 2.

Estimated carbonation depth = *12.00 mm*

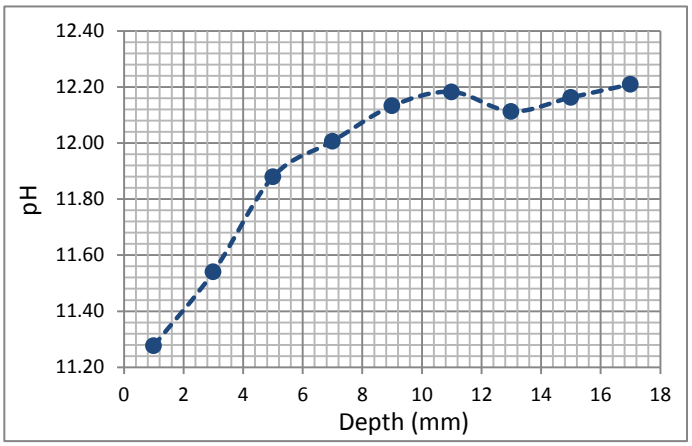

Figure D19 3-day carbonated. 40% cement replacement by FA. Replicate number 3.

Estimated carbonation depth = *8.00 mm*

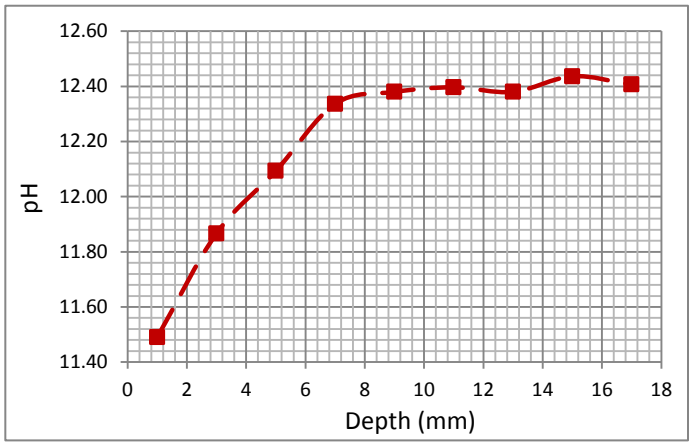

Figure D20 7-day carbonated. 0% cement replacement by FA. Replicate number 1.

Estimated carbonation depth = *7.50 mm*

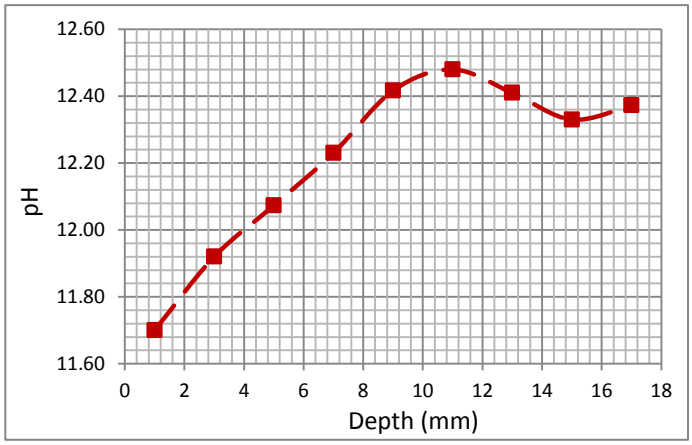

Figure D21 7-day carbonated. 0% cement replacement by FA. Replicate number 2.

Estimated carbonation depth = *8.00 mm*

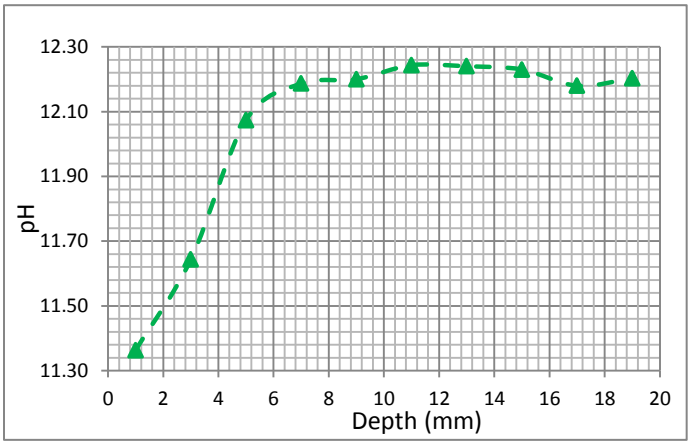

Figure D22 7-day carbonated. 20% cement replacement by FA. Replicate number 1.

Estimated carbonation depth = *5.65 mm*

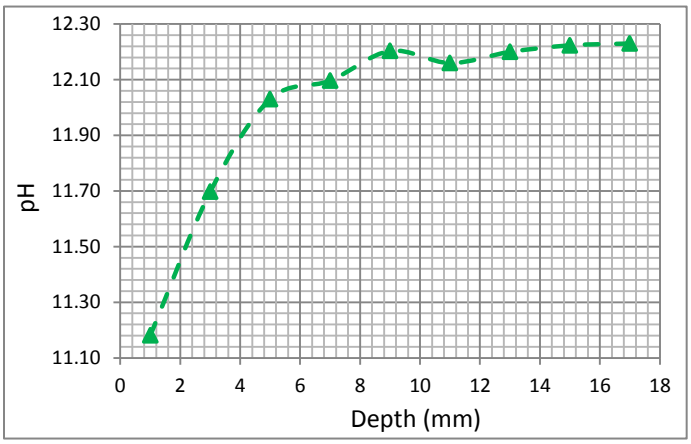

Figure D23 7-day carbonated. 20% cement replacement by FA. Replicate number 2.

Estimated carbonation depth = *8.00 mm*

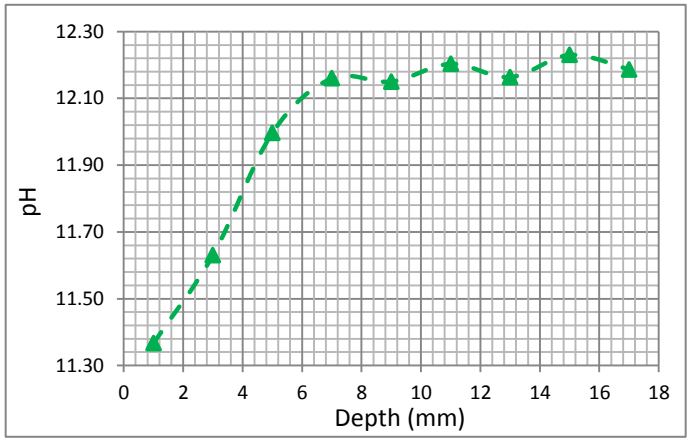

Figure D24 7-day carbonated. 20% cement replacement by FA. Replicate number 3.

Estimated carbonation depth = *6.00 mm*

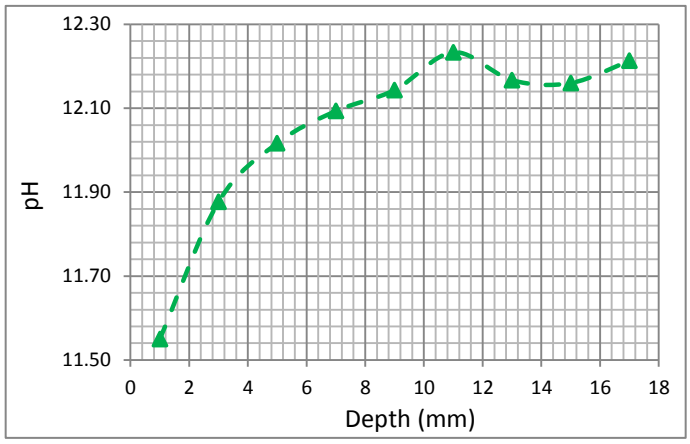

Figure D25 7-day carbonated. 20% cement replacement by FA. Replicate number 4.

Estimated carbonation depth = *10.00 mm*

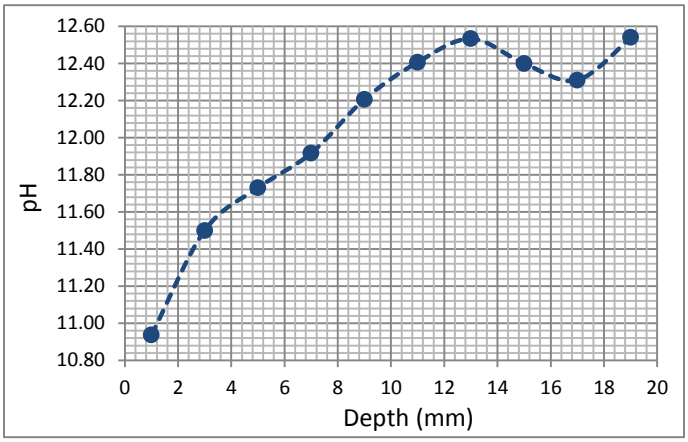

Figure D26 7-day carbonated. 40% cement replacement by FA. Replicate number 1.

Estimated carbonation depth = *10.00 mm*

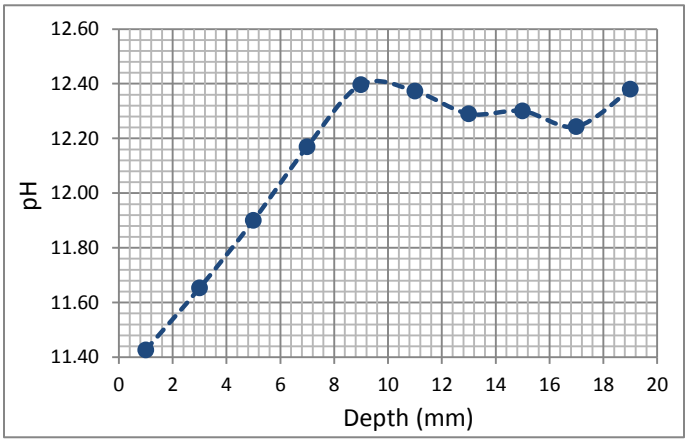

Figure D27 7-day carbonated. 40% cement replacement by FA. Replicate number 2.

Estimated carbonation depth = *8.00 mm*

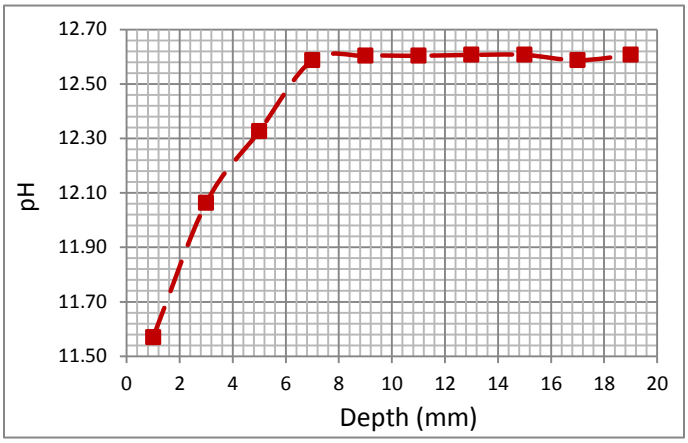

Figure D28 14-day carbonated. 0% cement replacement by FA. Replicate number 1.

Estimated carbonation depth = *6.00 mm*

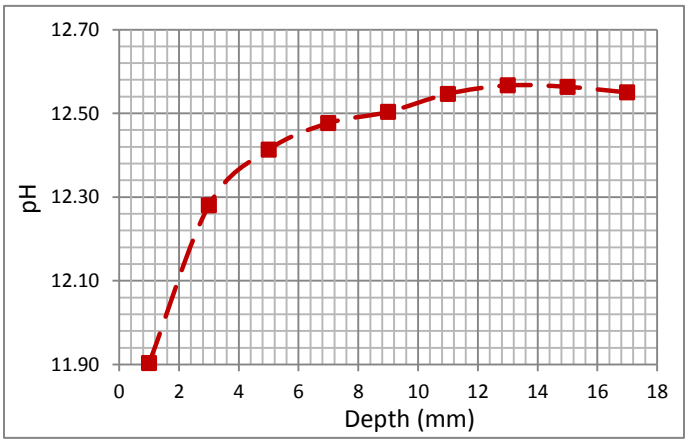

Figure D29 14-day carbonated. 0% cement replacement by FA. Replicate number 2.

Estimated carbonation depth = *10.00 mm*

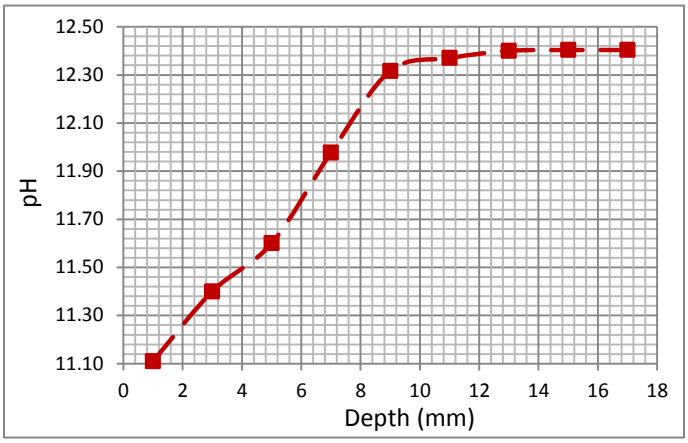

Figure D30 14-day carbonated. 0% cement replacement by FA. Replicate number 3.

Estimated carbonation depth = *11.70 mm*

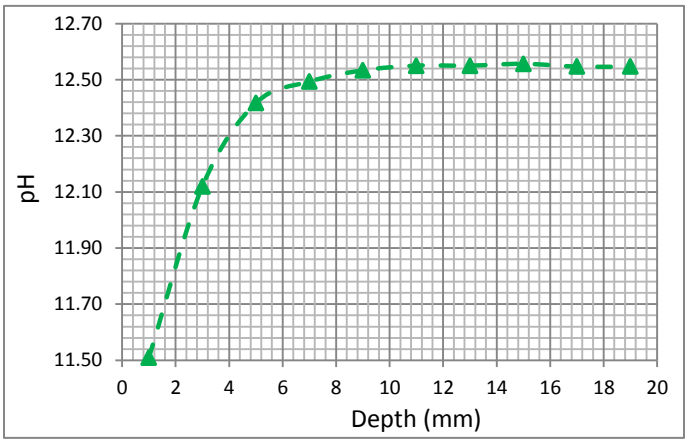

Figure D31 14-day carbonated. 20% cement replacement by FA. Replicate number 1.

Estimated carbonation depth = *9.60 mm*

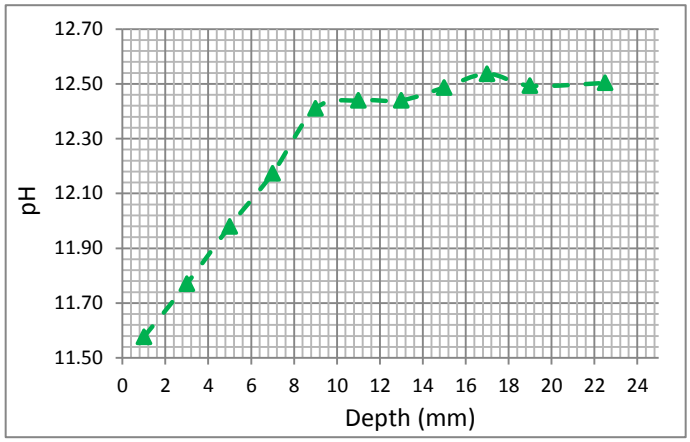

Figure D32 14-day carbonated. 20% cement replacement by FA. Replicate number 2.

Estimated carbonation depth = *14.00 mm*

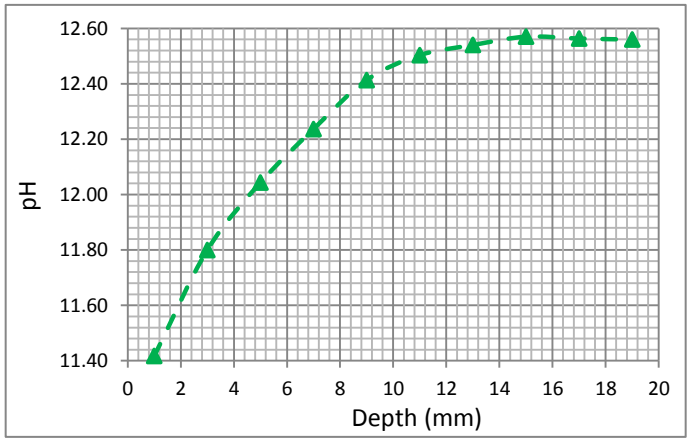

Figure D33 14-day carbonated. 20% cement replacement by FA. Replicate number 3.

Estimated carbonation depth = *13.70 mm*

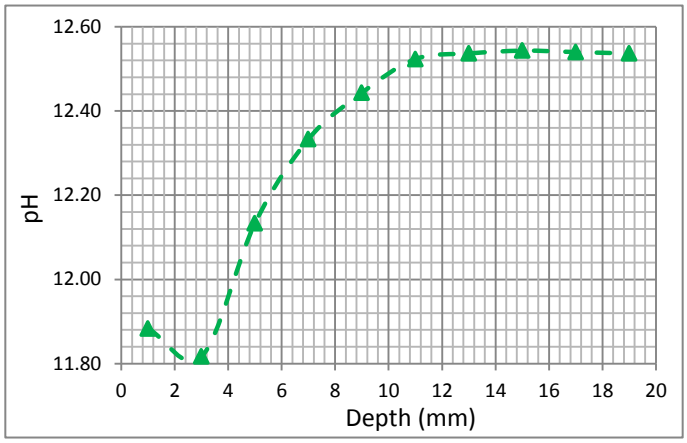

Figure D34 14-day carbonated. 20% cement replacement by FA. Replicate number 4.

Estimated carbonation depth = *11.35 mm*

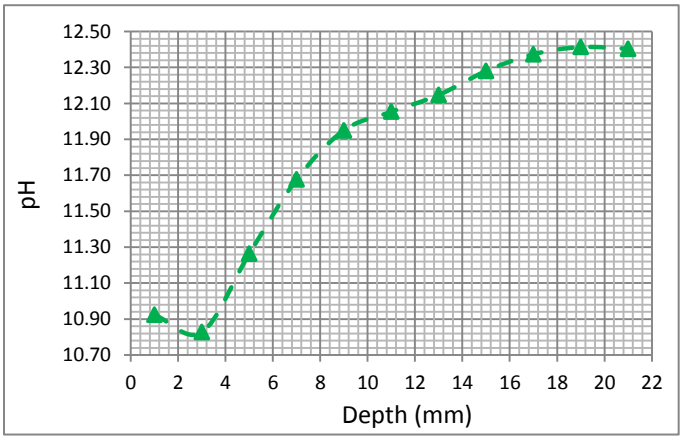

Figure D35 14-day carbonated. 40% cement replacement by FA. Replicate number 1.

Estimated carbonation depth = *17.60 mm*

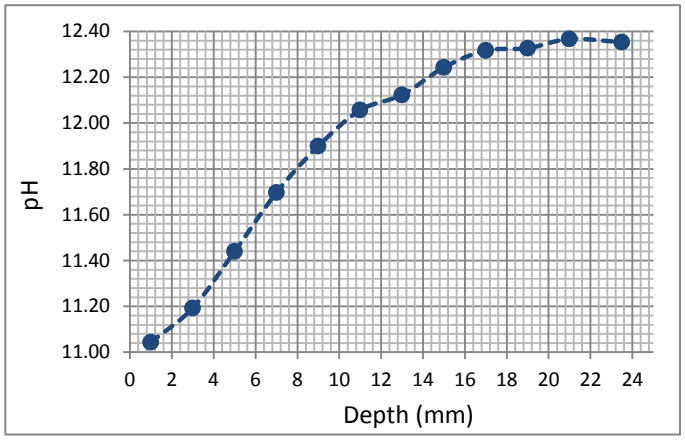

Figure D36 14-day carbonated. 40% cement replacement by FA. Replicate number 2.

Estimated carbonation depth = *20.00 mm*

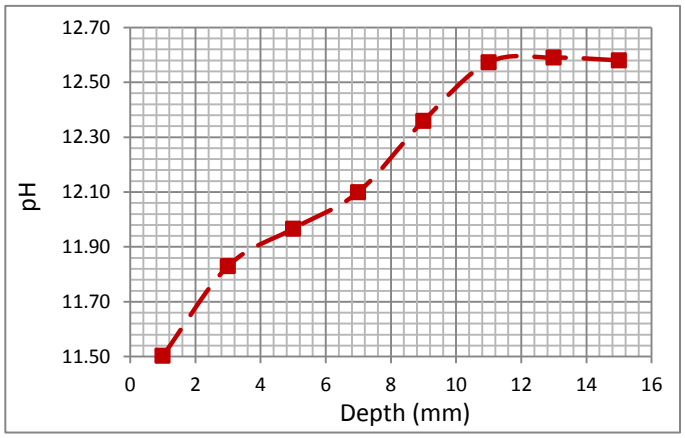

Figure D37 21-day carbonated. 0% cement replacement by FA. Replicate number 1.

Estimated carbonation depth = *11.10 mm*

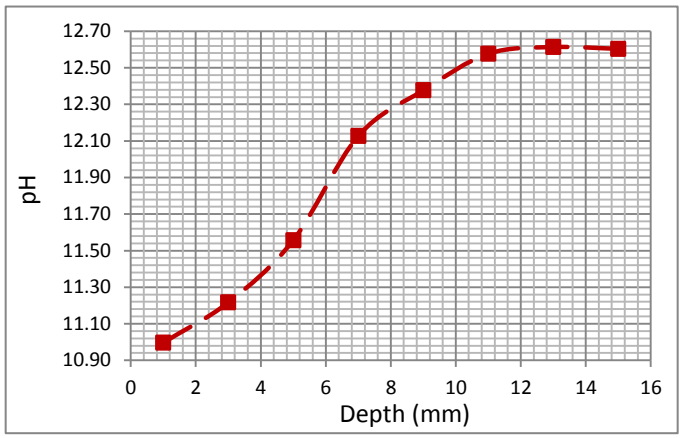

Figure D38 21-day carbonated. 0% cement replacement by FA. Replicate number 2.

Estimated carbonation depth = *11.25 mm*

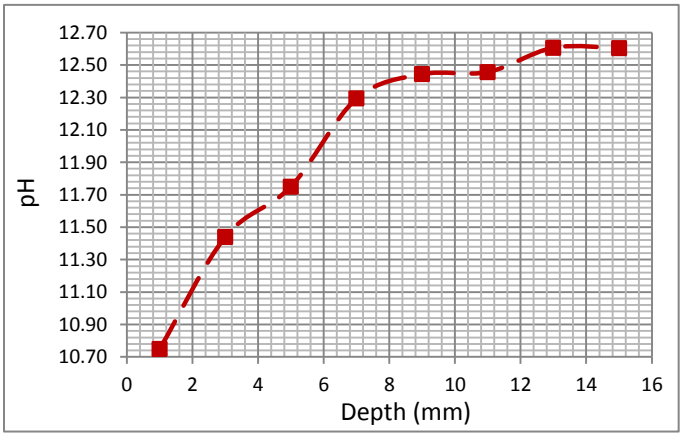

Figure D39 21-day carbonated. 0% cement replacement by FA. Replicate number 3.

Estimated carbonation depth = *12.00 mm*

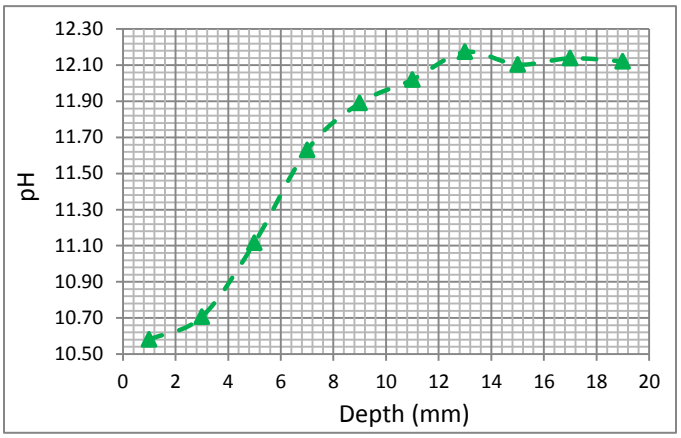

Figure D40 21-day carbonated. 20% cement replacement by FA. Replicate number 2.

Estimated carbonation depth = *12.00 mm*

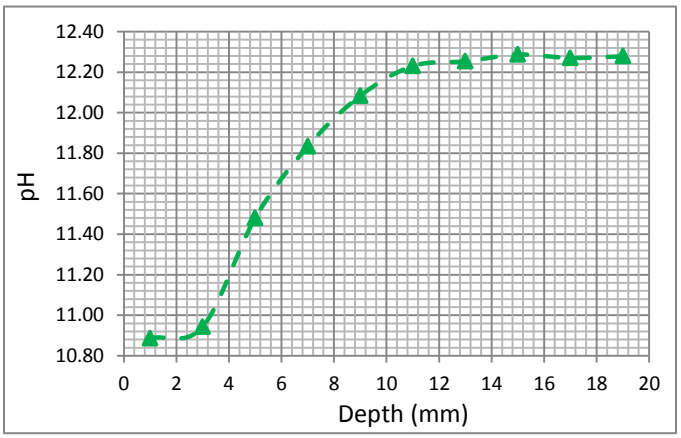

Figure D41 21-day carbonated. 20% cement replacement by FA. Replicate number 3.

Estimated carbonation depth = *13.80 mm*

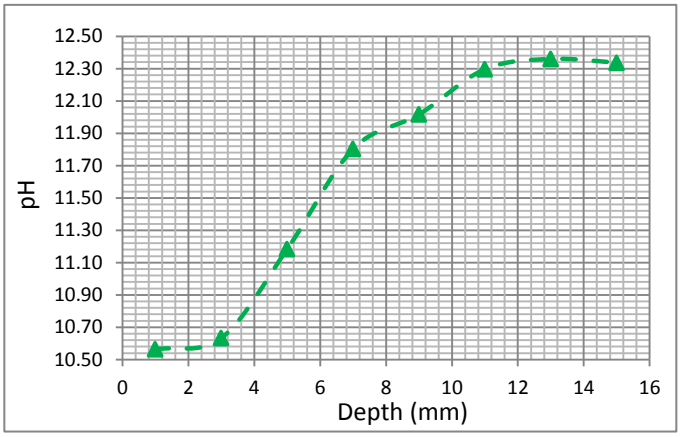

Figure D42 21-day carbonated. 20% cement replacement by FA. Replicate number 4.

Estimated carbonation depth = *11.40 mm*

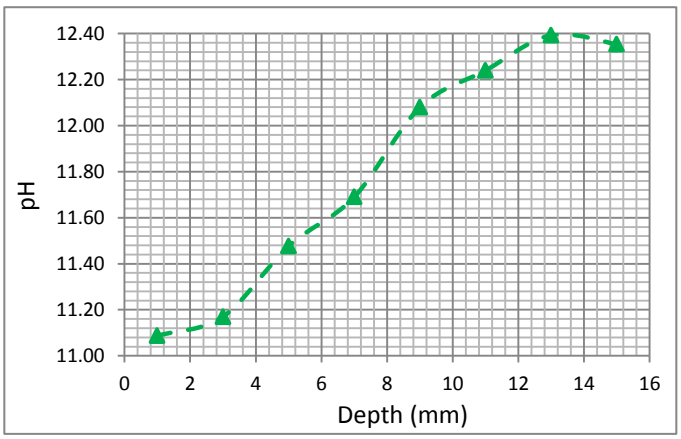

Figure D43 21-day carbonated. 20% cement replacement by FA. Replicate number 5.

Estimated carbonation depth = *12.00 mm*

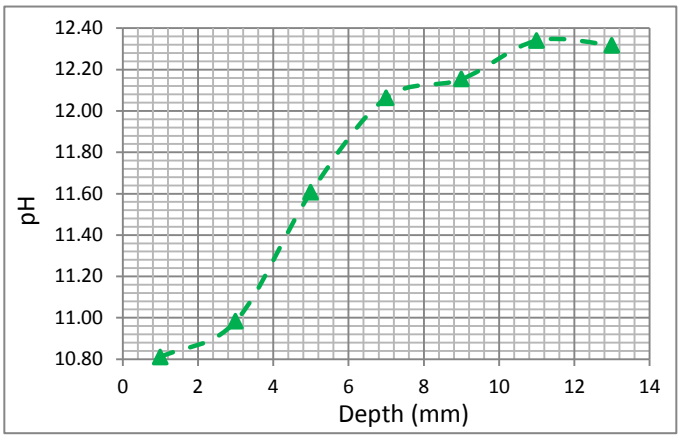

Figure D44 21-day carbonated. 20% cement replacement by FA. Replicate number 6.

Estimated carbonation depth = *10.00 mm*

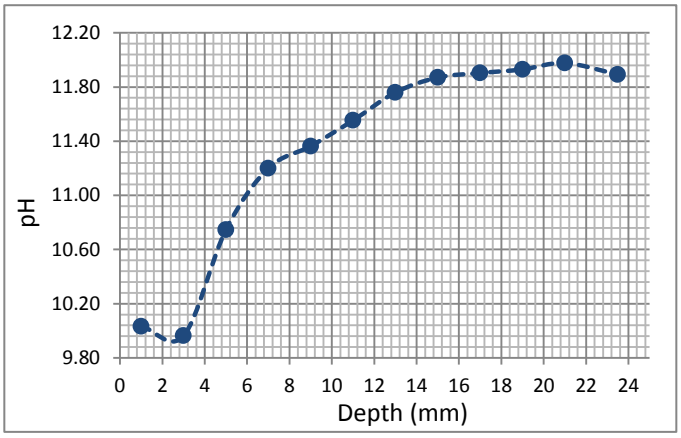

Figure D45 21-day carbonated. 40% cement replacement by FA. Replicate number 1.

Estimated carbonation depth = *16.00 mm*

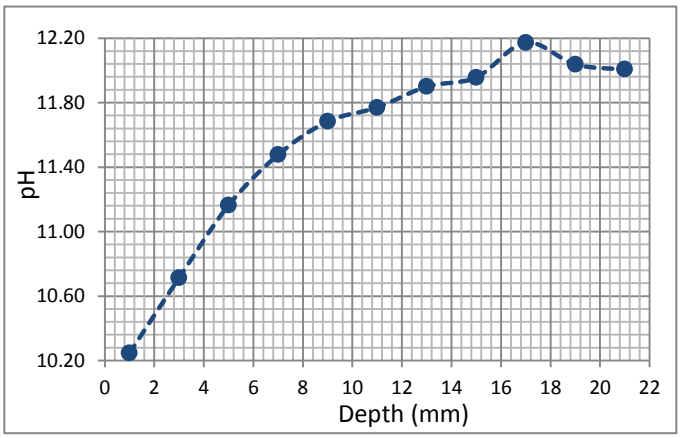

Figure D46 21-day carbonated. 40% cement replacement by FA. Replicate number 2.

Estimated carbonation depth = *16.00 mm*

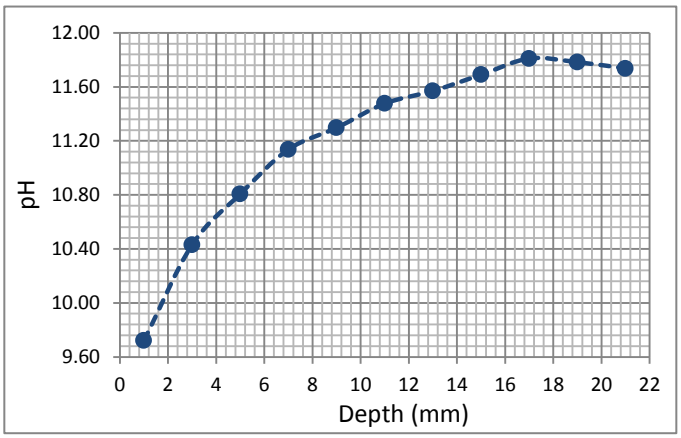

Figure D47 21-day carbonated. 40% cement replacement by FA. Replicate number 3.

Estimated carbonation depth = *16.00 mm*

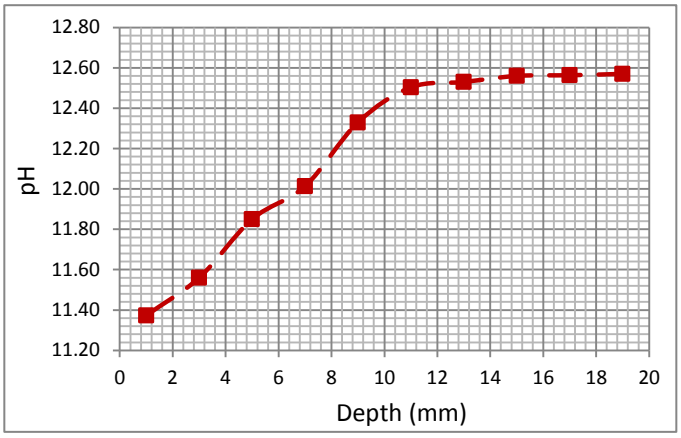

Figure D48 28-day carbonated. 0% cement replacement by FA. Replicate number 1.

Estimated carbonation depth = *14.00 mm*

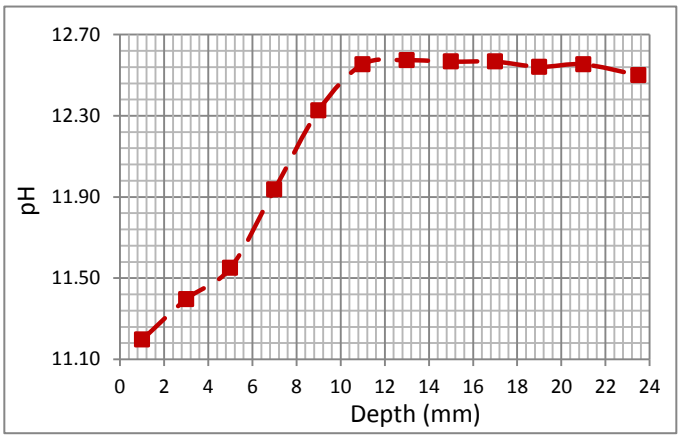

Figure D49 28-day carbonated. 0% cement replacement by FA. Replicate number 2.

Estimated carbonation depth = *10.00 mm*

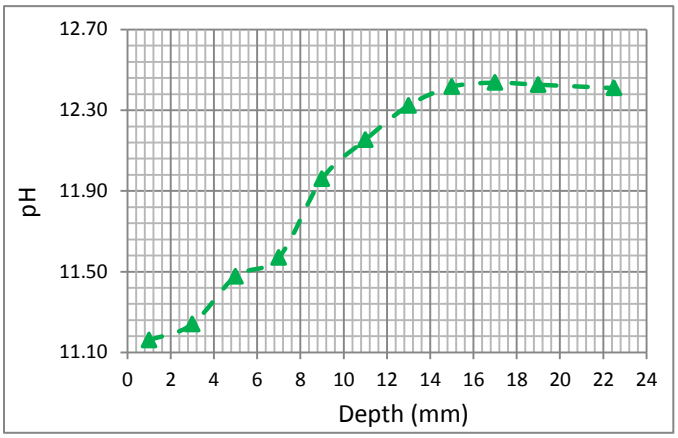

Figure D50 28-day carbonated. 20% cement replacement by FA. Replicate number 1.

Estimated carbonation depth = *14.00 mm*

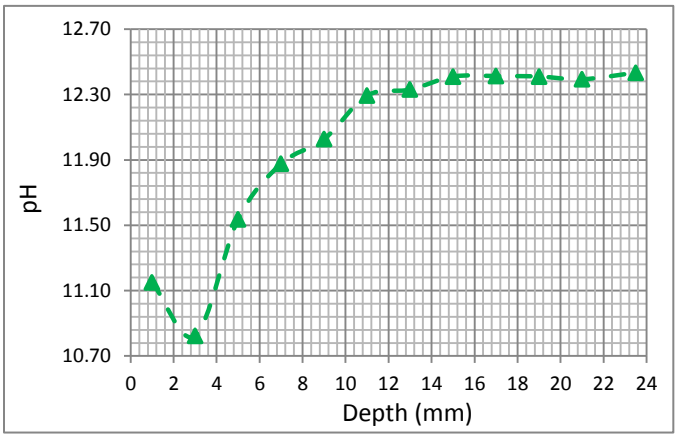

Figure D51 28-day carbonated. 20% cement replacement by FA. Replicate number 2.

Estimated carbonation depth = *14.00 mm*

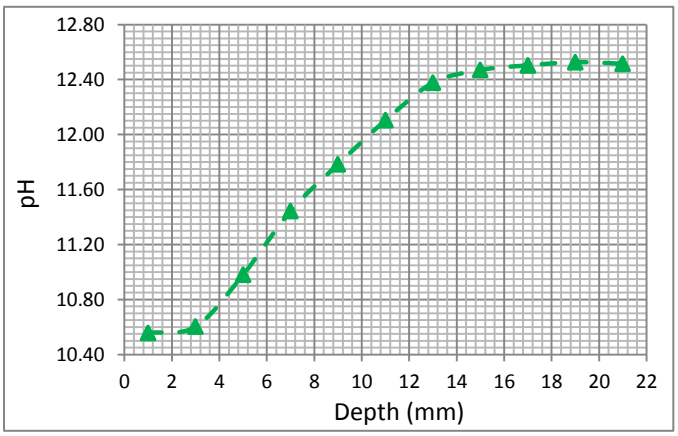

Figure D52 28-day carbonated. 20% cement replacement by FA. Replicate number 3.

Estimated carbonation depth = *16.00 mm*

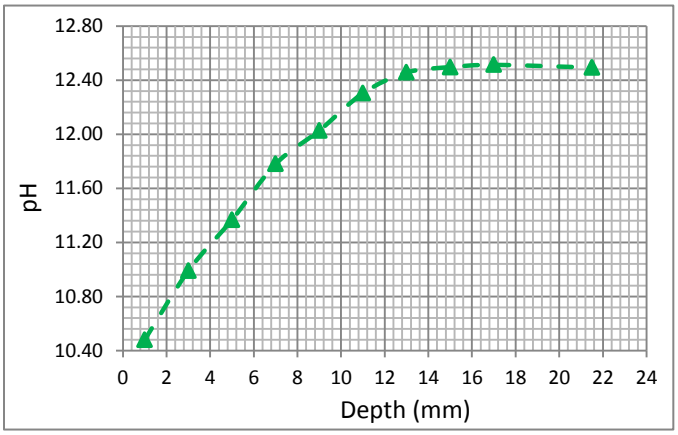

Figure D53 28-day carbonated. 20% cement replacement by FA. Replicate number 4.

Estimated carbonation depth = *13.45 mm*

Appendix E Traditional Phenolphthalein Method (Trad-P)

The carbonation depth was determined by averaging eight individual measurements. The measurements were done every two centimeters along the edge of the sample towards the location of the visible carbonation front as shown in Figure E1. Four carbonation depth measurements *D* were done on each side of the specimen.

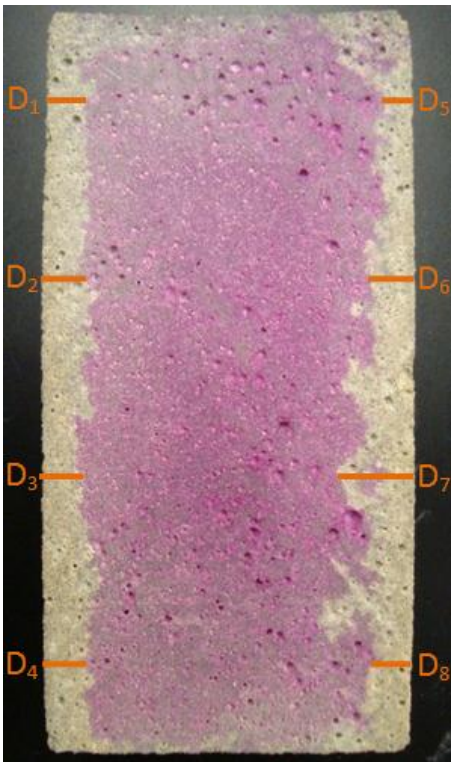

Figure E1 Phenolphthalein-sprayed mortar sample. Assessment of the carbonation depth.

$$\text{Carbonation Depth (mm)} = \frac{\sum_{i=1}^{8} D_i}{8}$$

Appendix F Image Processing Methods

F1 Image Processing Method on Unsprayed Samples (IM-U). Sample calculation.

The imaging method addresses changes in color intensity due to the carbonation reaction. The method is a multi-step process that requires the image analysis software MaxIm-DL and the data analysis software Microsoft Excel. For the sake of clarity, a sample calculation is shown below.

Sample characteristics:

Wt% cement replacement by fly ash: 20

Carbonation time (day): 28

A digital picture of the sample was taken and analysed with the software MaxIm-DL, as seen in Figure F1. The intensity of all blue, green and red pixels in the rectangular section "a" was measured. An average of color intensity along x-axis is reported graphically in Figure F2. The raw color intensity data are imported to Microsoft Excel for further calculations. A Blue-Red color intensity profile is shown in Figure F3. This profile accounts for significant changes in color intensity regardless of some other factors such as room illumination and mortar matrix heterogeneity.

Figure F1 Image of an unsprayed carbonated sample.

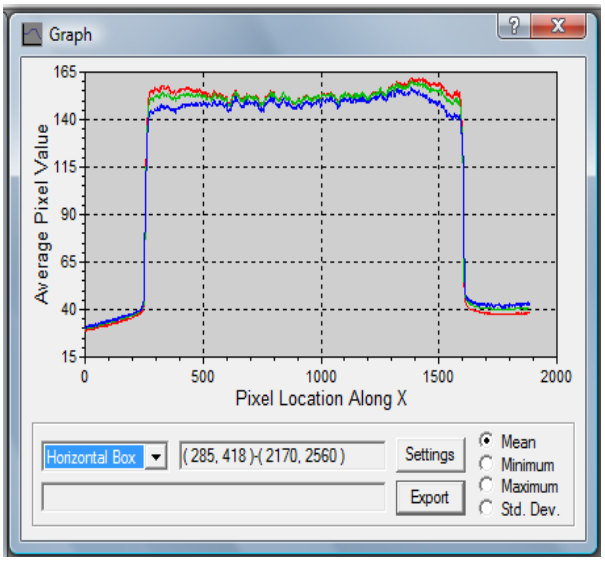

Figure F2 Profile of average pixel values along the width of the sample.

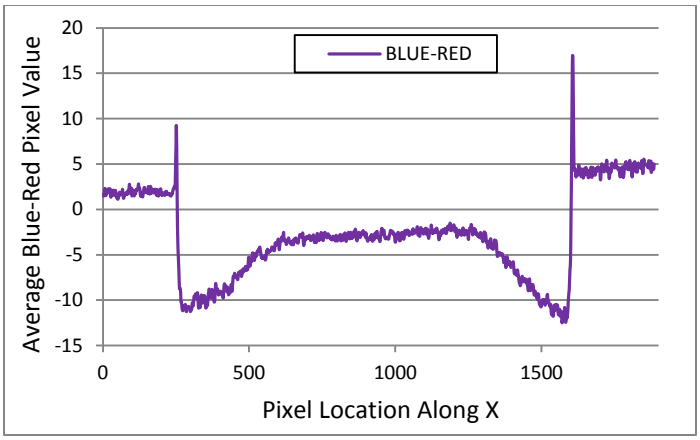

Figure F3 Difference between blue and red average pixel values versus pixel location along the width of the sample.

The carbonation depth can be assessed by looking at changes in the Blue-Red color intensity profile in Figure F3. In Figure F4, the corresponding edges of the sample have been designated as middle points m_1 and m_2, while the carbonation extends to the depths corresponding to the maxima a_3 and a_4. The distance between a_3 and a_4 represents the noncarbonated section of the mortar.

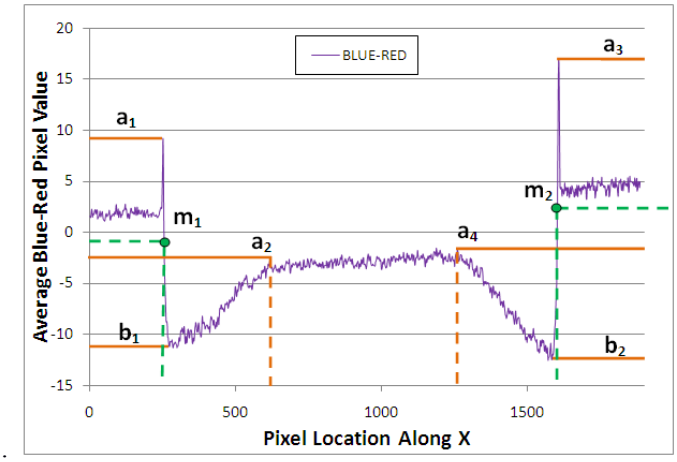

Figure F4 Location of the reference points.

The detailed calculations for this particular sample are shown below.

Blue-Red profile. Left-hand side.

a_1 (local maximum): 9.2506 value on the y-axis

b_1 (local minimum): -11.102 value on the y-axis

m_1 (middle point): -0.9257 value on the y-axis → **254.7 pixel location on the x-axis**

a_2 (local maximum) → **617 pixel location on the x-axis**

Blue-Red profile. Right-hand side.

a_3 (local maximum): 16.9668 value on the y-axis

b_2 (local minimum): -12.194 value on the y-axis

m_2 (middle point): -2.3864 value on the y-axis → **1601.8 pixel location on the x-axis**

a_4 (local maximum) → **1259 pixel location on the x-axis**

Sample width: 1601.8 – 254.7 = 1347.1 pixels = 50.8 mm

Carbonation depth (left-hand side): 617 – 254.7 = 362.3 pixels = 13.6626 mm

Carbonation depth (right-hand side): 1601.8 – 1259 = 342.8 pixels = 12.9272 mm

Ave. Carbonation depth = (13.6626+12.9272) / 2 mm

Ave. Carbonation depth = 13.2949 mm

F2 Image Processing Method for Phenolphthalein, Thymolphthalein and Alizarin pH Indicators

The principle of analysis for IM-U can be extended to the cases where pH indicators (i.e. phenolphthalein, thymolphthalein and alizarin) were sprayed on the split carbonated mortar cylinders. Similar steps can be followed to assess the carbonation depth. Since the color

intensities vary with the pH indicator that is employed, different elementary color subtractions should be applied according to the particular case. It is always desirable to pair the two elementary colors with the most different intensity values. For phenolphthalein, it was Red-Blue, while for thymolphthalein it was Blue-Red. Finally, it was determined that a Red-Green profile should be used for the case of the alizarin indicator.

Appendix G Reaction-limited UR-core Modelling

In this section, we evaluate how well the chemical reaction-limited UR-core model fits the carbonation depth versus time data provided by each analytical method. Also, we compare the methods with respect to the predicted time for complete carbonation of the cylindrical mortar samples.

G1 Model equations

The model equations describing the radial position of the carbonation front, *r*, are as follows:

$$X_s = 1 - \left(\frac{r}{R}\right)^2 \qquad (1)$$

$$\frac{t}{\tau} = 1 - (1 - X_s)^{0.5} \qquad (3)$$

where R is the radius of the cylinder, X_s is the fractional conversion of the solid reactant, t is carbonation time, and τ is the time required for complete conversion of the reactant.

G2 Calculation of τ

Similarly to what was previously shown in Section 4, the time for complete carbonation, τ, can be estimated by plotting the right hand side of equation 3 as a function of t. The inverse of the slope of the best fit line is τ. Experimental values of X_s are obtained from measured carbonation depths, D, noting that $r = R - D$. Figures G1a to g show the fit of equation 3 to carbonation data

obtained with various experimental methods and mortars. The corresponding values of τ are given in Table G1.

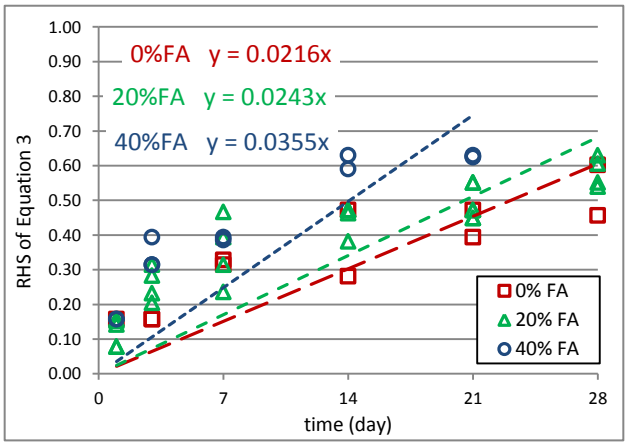

a)

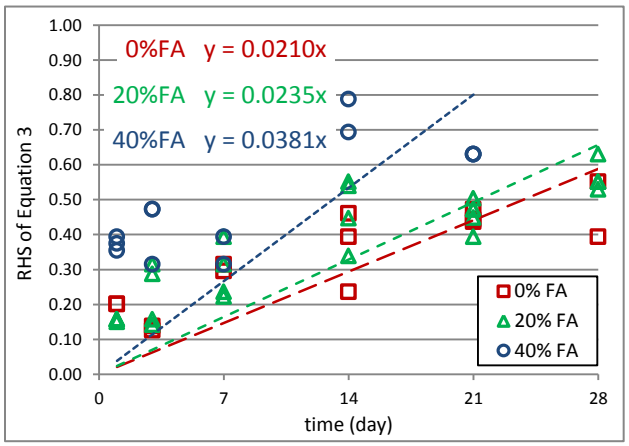

b)

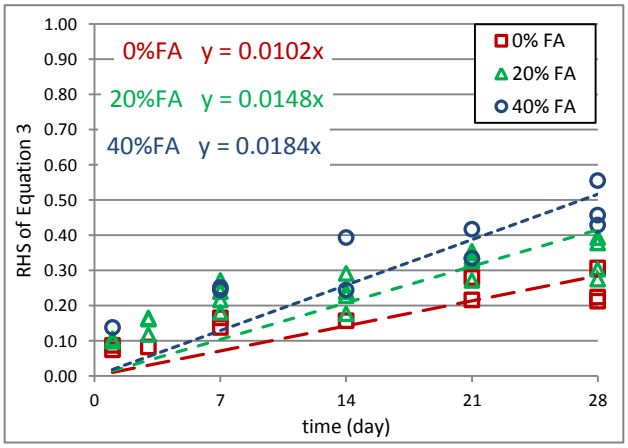

c)

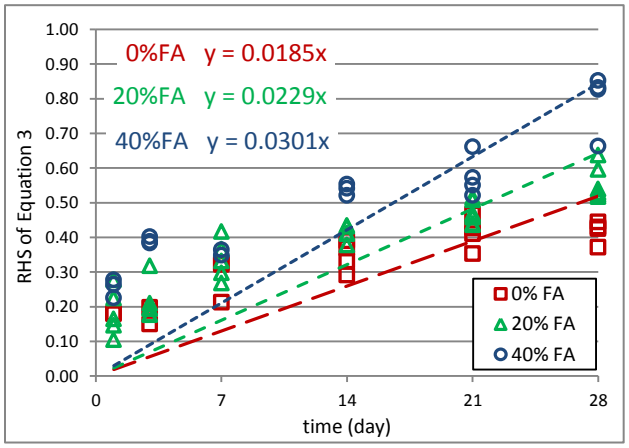

d)

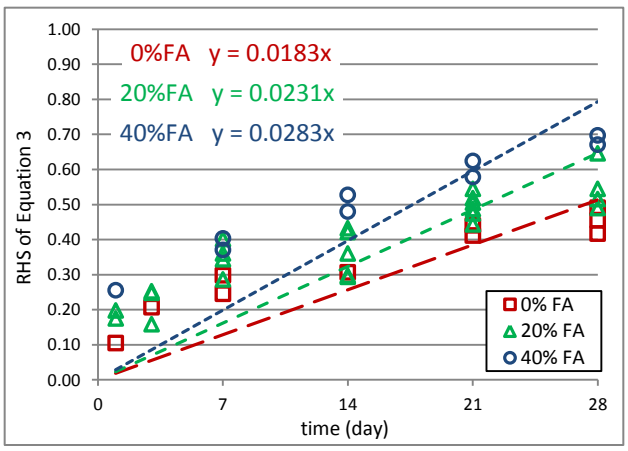

e)

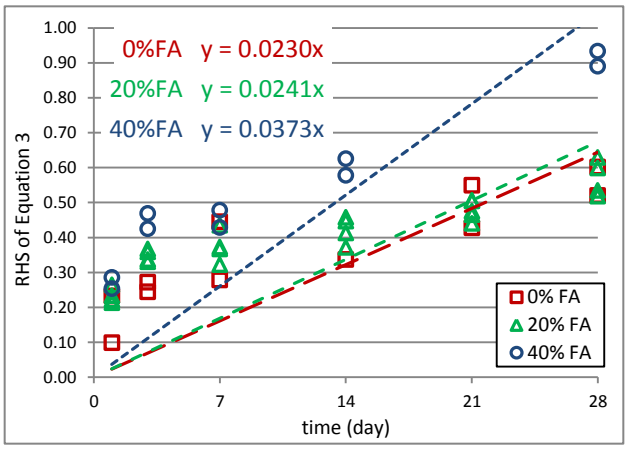

f)

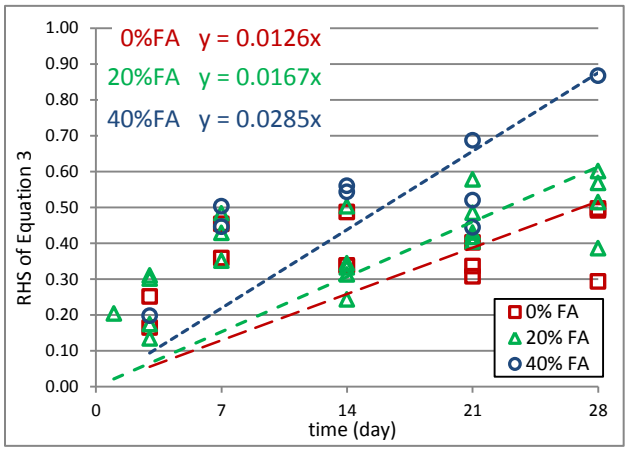

g)

Figure G1 RHS of equation 3 versus time and best fit lines for a) FTIR; b) DD; c) Trad-P; d) IM-U; e) IM-P; f) IM-T; g) IM-A carbonation data.

Table G1 Estimated times for total carbonation using the chemical reaction-limited UR-Core model.

Method	*FA content (%)*	*Time for total carbonation τ (day)*
Trad-P	*0*	*98.3 ± 10.3*
	20	*67.4 ± 4.6*
	40	*54.2 ± 4.5*
FTIR	*0*	*46.2 ± 4.8*
	20	*41.1 ± 2.8*
	40	*28.2 ± 3.1*
DD	*0*	*47.6 ± 4.8*
	20	*42.6 ± 3.1*
	40	*26.2 ± 4.2*
IM-U	*0*	*54.0 ± 4.5*
	20	*43.6 ± 2.6*
	40	*33.2 ± 2.6*
IM-P	*0*	*54.5 ± 5.1*
	20	*43.3 ± 2.8*
	40	*35.3 ± 3.4*
IM-T	*0*	*43.5 ± 5.6*
	20	*41.5 ± 3.8*
	40	*26.8 ± 3.6*
IM-A	*0*	*54.1 ± 7.4*
	20	*45.7 ± 4.1*
	40	*32.0 ± 3.4*

As seen in Table G1, regardless of method, the value of τ consistently decreases as a function of increasing cement replacement by fly ash. The τ values obtained with the Trad-P method were, in average, twice as long as those obtained with the other methods. All the other methods provide similar values of τ when considering statistical uncertainty.

Figure G2 shows the best fit lines to the experimental data using the chemical reaction-limited UC model. It is clear that the diffusion-limited UR-core model has a better fit with the experimental data (compare Figure G2 to Figures 3-1, 3-2, 3-4 and 3-6). Therefore, the chemical reaction-limited model was no longer considered.

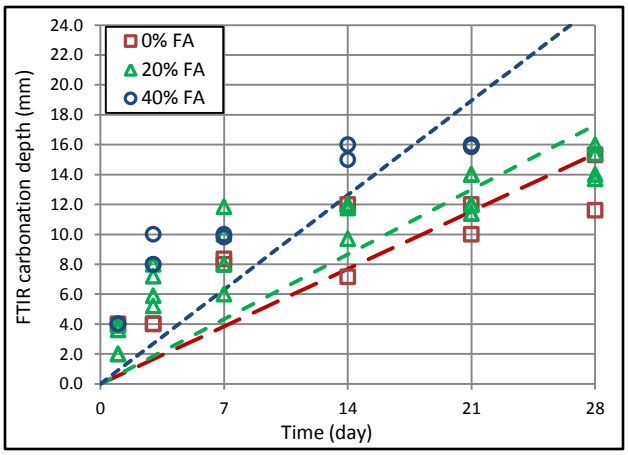
0% FA
20% FA
40% FA
FTIR carbonation depth (mm)
Time (day)

a)

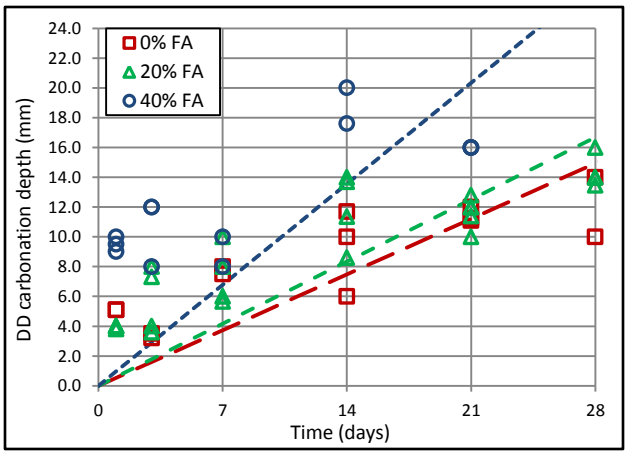
0% FA
20% FA
40% FA
DD carbonation depth (mm)
Time (days)

b)

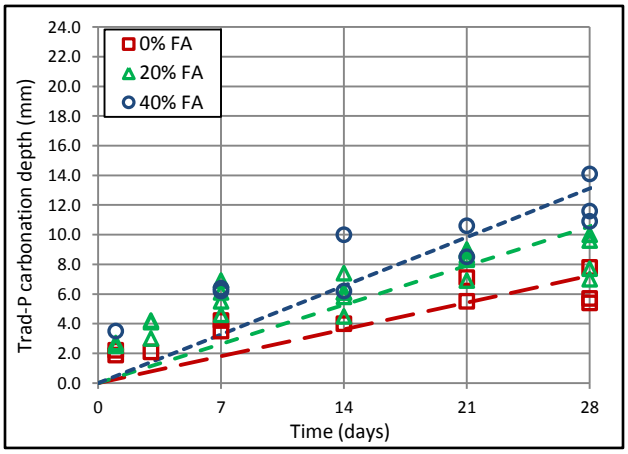
0% FA
20% FA
40% FA
Trad-P carbonation depth (mm)
Time (days)

c)

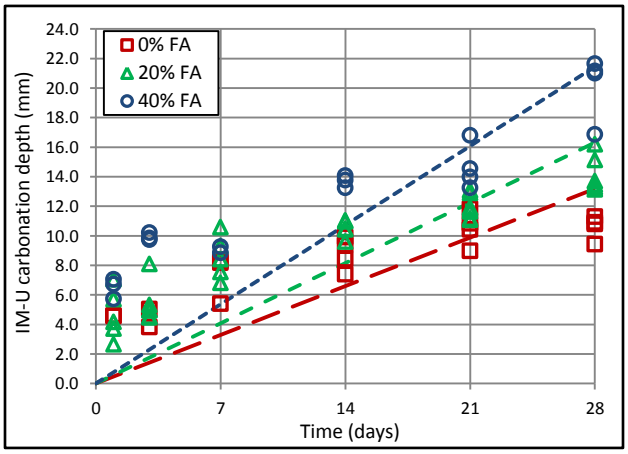
0% FA
20% FA
40% FA
IM-U carbonation depth (mm)
Time (days)

d)

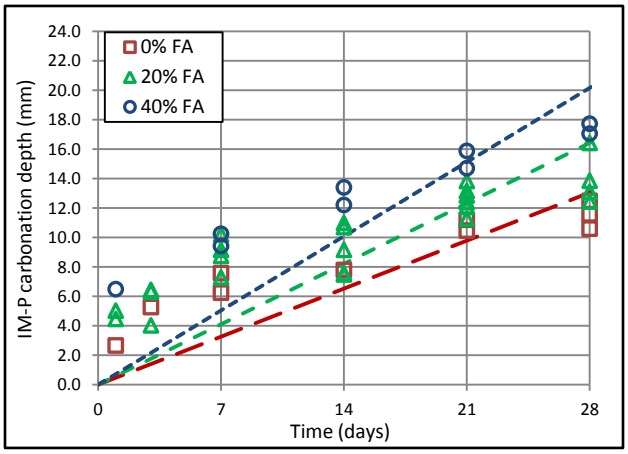
0% FA
20% FA
40% FA
IM-P carbonation depth (mm)
Time (days)

e)

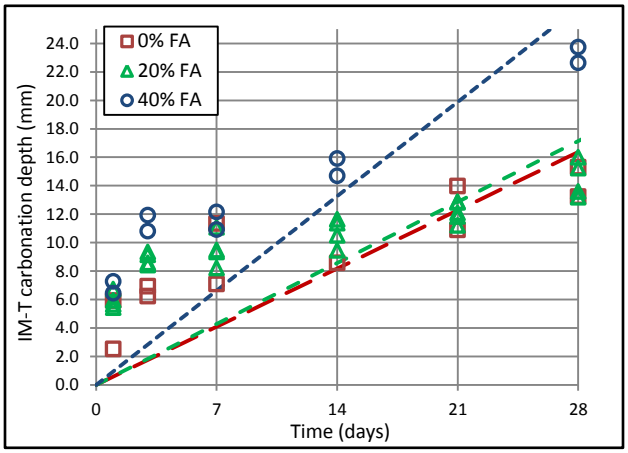
0% FA
20% FA
40% FA
IM-T carbonation depth (mm)
Time (days)

f)

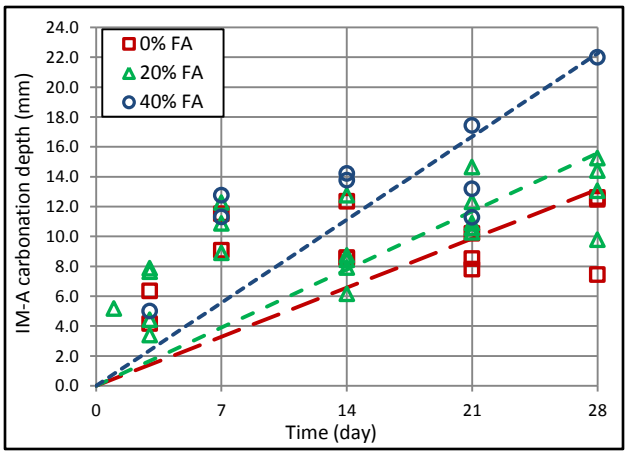

g)

Figure G2 Carbonation depths versus carbonation time determined by: a) FTIR; b) dust digestion; c) traditional phenolphthalein method; d) unsprayed mortar samples; e) phenolphthalein; f) thymolphthalein; g) alizarin. Best fit lines were determined using the chemical reaction-limited UR-Core model.